The principle and operation of an induction stepping motor

Mestha, Lingappa Keshav

Award date:
1986

Awarding institution:
University of Bath

THE PRINCIPLE AND OPERATION OF AN INDUCTION STEPPING MOTOR

Submitted by Lingappa Keshav Mestha, B.E.,
for the degree of Ph.D. of the
University of Bath
1986

COPYRIGHT

[L. K. Mestha]

ProQuest LLC
789 East Eisenhower Parkway
P.O. Box 1346
Ann Arbor, MI 48106-1346

ACKNOWLEDGEMENTS

The author wishes to thank and express his deepest gratitude to Dr. M. L. Fryett, the Project Supervisor, for his encouragement and many helpful suggestions. The author is grateful to Prof. J. F. Eastham for providing the excellent facilities at Electrical Engineering Laboratories. He is also indebted to the University of Bath for an award from the Research Funds and the ORS committee of the CVCP for their financial support.

Furthermore, gratitude is expressed to Dr. P. D. Evans from the School of Electrical Engineering for his guidance with the theoretical aspects of the work. The assistance given by the colleagues and the related University staff in various technical discussion is also acknowledged.

Finally, the author is grateful to his wife, Mrs. Veena Mestha, for her efforts in typing the manuscript and for staff at the computer center for their help throughout the project.

SUMMARY

A new induction stepping motor has been developed for a.c. applications. In this thesis its basic characteristics including the principles of operation are discussed.

Chapter 1 contains a brief survey of stepping motors with attention focussed on a.c. stepping motors.

One particularly interesting model was chosen for detailed investigation in Chapter 2. The steady state static performance of this existing model has been predicted and was found to have good agreement with the measured results. A method for calculating the machine inductances, including harmonic effects is also presented here.

In Chapter 3 a new model has been proposed and the analysis has been extended to predict its steady state performance characteristics. The theoretical study showed that this new model produced torque due to the combined effect of the harmonics in the mutual inductance distribution between stator and rotor windings.

Chapter 4 describes the steady state static performance when more than one stator phase is excited simultaneously. From the analysis and experiments it was found that of the different conditions tested the best results were obtained when the stator phases were excited sequentially in pairs.

Chapter 5 includes the description of a numerical step-by-step prediction technique to simulate both the steady state and transient behaviour of the machine operation. Single step transient responses were predicted and compared with measurements.

Chapter 6 describes briefly the power electronics and microprocessor equipment which was developed to provide the controlled stepping operation of the prototype machines.

CONTENTS

LIST OF PRINCIPAL SYMBOLS

SYMBOLS	DESCRIPTIONS
N_s	Number of stator winding turns
N_r	Number of rotor winding turns
l_s	Stator length
l_r	Rotor length
r_s	Radius of the stator bore
r_r	Radius of the rotor
p	Number of pole pairs
H	Field intensity
g	Actual airgap length
g'	Effective airgap length
B	Flux density
B_{00}, B_{11}, B_{22}	Flux densities due to coils 00, 11 and 22
L_{AA}, L_{BB}, L_{CC}	Magnetising component of the stator self inductances
$L_{\alpha\alpha m}$	Magnetising component of the rotor self inductance
L_{aa}	Self inductance of the A phase stator windings
L_{bb}	Self inductance of the B phase stator windings
L_{cc}	Self inductance of the C phase stator windings
$L_{\alpha\alpha}$	Self inductance of the α-axis rotor windings
$L_{\beta\beta}$	Self inductance of the β-axis rotor windings
V_a, V_b, V_c	Supply voltages, rms values
R_a, R_b, R_c	Stator winding resistances
R_α, R_β	Rotor winding resistances
T_i	Instantaneous electromagnetic torque
θ	Rotor position in mechanical degrees
J	Rotor inertia
T_f	Frictional torque
I_a, I_b, I_c	Steady state stator winding currents, rms values
I_α, I_β	Steady state rotor winding currents, rms values
v_a, v_b, v_c	Instantaneous supply voltages

i_a , i_b , i_c	Instantaneous stator winding currents
i_α, i_β	Instantaneous rotor winding currents
j	Imaginary quantity
I^*	Conjugate of I
$\hat{I}$	Peak value of I
$\hat{v}$	Peak value of v
ω	Supply frequency in rad/sec
n , m	Harmonic numbers
T_a , T_{ab} , T_{abc}	Average static torques
T_{po} , $T_{\alpha\beta}$	Pull-out torques
$M_{\alpha a}$, $M_{\alpha b}$, $M_{\alpha c}$	Mutual inductances between stator and α-axis rotor windings
$M_{\beta a}$, $M_{\beta b}$, $M_{\beta c}$	Mutual inductances between stator and β-axis rotor windings
M_{ab}	Mutual inductance between stator phase windings
$\hat{M}$	Peak value of mutual inductances
a	Suffix used to represent A phase stator winding
b	Suffix used to represent B phase stator winding
c	Suffix used to represent C phase stator winding
α	Suffix used to represent α-axis rotor winding
β	Suffix used to represent β-axis rotor winding
X_{la}	Reactance due to leakage inductance in the stator windings
X_{lr}	Reactance due to leakage inductance in the rotor windings
Z_{oa} , Z_{sa}	Impedances
ϕ_{oa} , ϕ_{sa}	Phase angle between current and voltages

CHAPTER 1

INTRODUCTION

1.1 CLASSIFICATION OF STEPPER MOTOR DRIVES

Development of stepper motor drives has become the focus of much research activity (1,2) in recent times, and there are now several variants available on the market. The two most common types of drive use either a Variable-Reluctance (V.R) motor or a Hybrid which is a combination of a permanent magnet motor and V.R. motor. The electrical supplies to these motors are relatively complex and expensive. They generally use rectified a.c. which is conditioned in a suitable way by chopper circuits. The sequential control of the d.c. supply to the windings of the motor can be provided by specialised integrated circuits.

The work presented in this thesis concerns an a.c. stepping motor. The motor itself is very similar in construction to an induction motor and is therefore likely to be inexpensive and reliable. It requires a supply from an a.c. source, and the control of this supply can be achieved by means of low cost naturally commutated circuits employing back-to-back thyrister pairs, or triacs.

The basic arrangement of the V.R. stepping motor (1) is shown in figure 1.1. Two diametrically opposite windings located on projecting poles form a stator phase. In the example shown, the stator thus has three phases on six poles. The rotor has a different number of poles, in this case four, which carry no windings. When phase A winding is excited, the magnetic field produced attracts the rotor in such a way that the rotor becomes aligned in the minimum reluctance position as shown. When phase B winding is switched on and phase A winding is switched off, the rotor "steps" clockwise through an angle equal to the mechanical angular displacement of the stator poles - in this case 30 degrees. Similarly, excitation of the phase C winding with A phase and B phase windings off, causes the rotor to "step" another 30 degrees clockwise. Thus continuous rotation can be obtained by following the phased winding excitation sequence A, B, C, A, . . etc. The principal observation during the operation is

the repetitive movement of the rotor in discrete steps on suitable command.

A similar stepping action was described by Hassan *et al* (2) in their study of a modified induction motor operating as a stepping motor. They used a conventional three phase stator of an induction motor and various slotted rotors. The slotted rotors were of four different types such as single stack, double stack, salient pole single stack, and slotted pole face without any rotor windings. They observed that the peak static torque obtained with these variants was lower than the conventional doubly salient construction. The stator was connected in star but excited with d.c. The torque which aligns the rotor in the maximum permeance position is then simply a 'reluctance torque'. In other words it resembles the V.R. stepping motors in its operation including the type of excitation required.

Two other authors Dawson and Bolton (3) have examined a doubly excited, doubly salient concentrated windings type rotory actuator structure. Their discussion was mainly focussed on achieving a constant static torque/angle characteristic over a limited range of actuating angle typically less than 90 degrees. The analysis, they present, incorporates both linear and non-linear conditions in the magnetic circuit, and the normal operation of the device is by constant rotor current and switched stator supply (d.c.).

A d.c. excited toroidal-stator, permanent-magnet rotor has also been used as a limited motion rotory actuator (4). The presence of a permanent magnet on the rotor, in practice, provides a small 'detent' torque even after the stator windings are de-energised (5). This is sometimes useful, yet demagnetisation owing to stator excitation is a set back, particularly when required to be designed for high torque applications.

Fenton (6) describes a high-torque axial flux V.R. type step motor in which half of each winding is excited from a d.c. source and the other half with a.c. A polyphase a.c. motor with salient pole rotor structure has been realised (7) to obtain a satisfactory stepping motor performance for industrial applications. The shape of the torque/angle characteristic, however, shows lack of restoring torque at the stable equilibrium position mainly due to the rotor winding disposition.

One form of a.c. stepping motor has been described by Michio Nakano *et al* (8). They suggested an alternating-magnetic-field type stepping motor which is a wound rotor type induction motor with two or three stator phase windings and one or two rotor phase windings, each set being equally spaced. The analytical treatment does not present the static torque/rotor position expression per stator phase excitation, which would have been interesting. Further, even with one winding on the rotor no performance characteristic have been predicted. The second winding on the rotor, although placed in quadrature with the other one mentioned above, is used only for detecting mechanical error in high-precision servo applications. No attempt has been made to observe the performance either experimentally or analytically when the two rotor windings are shorted independently. However, their configuration involved the continuous excitation of one rotor winding by a.c. and switching an a.c. supply to the stator windings in sequence. Clearly, having to supply both the stator and the rotor increases the cost of manufacture and maintenance of this type of motor.

The principle of the a.c. stepper motor of the type under consideration in this thesis apparently dates from the patents of Hore (9). These patents show short circuited winding loops which are arranged symmetrically in parallel and electrically isolated from one another as shown in Fig. 1.2. All short circuited loops are aranged on one axis. The stator is of the polyphase induction motor type without necessarily any special design. An alternating magnetic field set up in the machine due to a.c. excitation of one stator phase induce voltages in the rotor windings which drive currents through them. The rotor current produces mmf which interacts with the stator mmf and develops torque. This torque is pulsating due to the type of excitation and its average value is different at different rotor positions. For example in figure 1.2, the rotor mmf is zero because of zero flux linkage with the rotor windings, and hence zero average torque. When the short circuited loops are perpendicular to the instantaneous stator flux, there is maximum flux linkage with the rotor windings. At this position, eventhough the stator and rotor mmfs are at their maximum values, the "torque-angle" between the two mmfs is zero, and hence there is zero average torque. In between these two torque-zero positions there is maximum average torque as shown in the experimental curve, figure 1.3, reproduced here from reference (9).

It appears from figure 1.3 that the average torque has substantially deteriorated towards the stable torque-zero position- i.e., around the minimum flux linkage position. This property is generally not suitable for a good stepper motor due to the slow progressive build up of the restoring torque when the rotor tries to settle after completing the step. Further development which improves the torque/angle characteristic is therefore needed.

The present work establishes a method of analysing the type of motor proposed by Hore (9). Alternative versions of the machine are also proposed and the analysis is extended to handle them. The theoretical results agree well with measurements and show that improved torque characteristics are feasible.

CHAPTER 2

STUDY OF EXISTING INDUCTION STEPPER MOTOR

2.1 INTRODUCTION

Some information on the behaviour of the existing induction stepper motor can be obtained by observing the torque developed by the machine. This chapter lays a general foundation for the studies related to this aspect of the machine, and further it demonstrates that the existing induction stepper motor model can be improved to provide better performance.

To support the investigation, work is initiated and carried out in the following order:

(i) A description of the existing induction stepper motor model is presented. A test machine was built along the same lines as that of an existing induction stepper motor (9) and hence its configuration has been fully explained.

(ii) The main equivalent circuit parameters of the machine are predicted from which the torque can be calculated. A description of the prediction technique is given.

(iii) A detailed analysis of the existing stepping motor with respect to torque development is presented and the validity of the technique is supported by the good agreement seen with the measurements.

2.2 DESCRIPTION OF THE MODEL

2.2.1 HORE'S MODEL

The induction stepper motor is not as familiar as the d.c. stepper motors. Of the work published so far, the concept of a.c. excitation and a truely a.c. stepping motor seems to have been introduced by Hore (9). He published

various models with particular design modifications on the rotor to give the motor a wide range of different characteristics. Some of the models were used as variable reactors and others for limited motion rotory actuation.

Out of the various models, particularly interesting one is a rotor with short circuited winding loops, all loops are arranged geometrically in parallel and electrically isolated from one another as shown in figure 2.1. The stator is a polyphase induction machine type without any special design. There were three or more stator phases and only three such phases with usual displacement is shown in the figure. The stator phase windings are although called phases in the conventional sense, do not mean the same here. This is because, they are used to excite the machine for a specific period only in order to achieve the rotor movement in discrete steps. In doing so, there exists no definite relationship between the time when one phase is switched on and the other is switched off. Hence, they are designated by phase A, B and C instead of usual R, Y and B for red, yellow and blue phases respectively.

Figure 2.2. represents the rotor by a winding which is concentrated on one axis. Let the new concentrated rotor winding be called the α-axis winding and the magnetic axis of this winding is the same as the magnetic axis of the stator winding when the rotor displacement angle, $p\theta$, is equal to zero. A test machine is constructed on the similar features as Hore's model and is described below.

2.2.2 TEST MODEL

An experimental model was made from a standard 4-pole 3-phase and 200-volts induction motor stator with a modified rotor. All 3-phase stator windings are arranged in 36 slots and the distribution of one of such stator phase windings in these slots is shown in the developed diagram of the test machine, figure 2.3.

The rotor windings are arranged with two parallel coils on α-axis as shown in figure 2.3. They were connected in series. The rotor is of standard slip ring induction motor form and has 24 slots with one slot pitch skewing (15°). Slots 2, 5, 8, 11, 14, 17, 20 and 23 were not required. A set of coils identical to the α-axis coils, but positioned in quadrature to them (slots 3, 4, 9, 10, 15, 16, 21, 22) was also provided in the test machine and the use of these is described in

chapter 3. The ends of these rotor windings were brought out to the sliprings to facilitate measurement of parameters.

Particulars of the test machine used in the investigation are shown in table 2.1 below.

TABLE 2.1

Particulars of the Test Machine		
Particulars	Stator	Rotor
Number of slots	36	24
Number of layers/slot	1	2
Number of turns/layer	56	50
Length in mm	53	51
Slot depth in mm	15.7	21.2
Voltage rating	200	
Number of Poles	4	
Number of phases	3	
Airgap length, g in mm	0.33	

2.3 CALCULATION OF MACHINE PARAMETERS

The induction stepper motor described so far has an equivalent circuit very similar to that of a conventional induction motor at standstill. Hence, the parameters fundamental to the machine analysis are well known.

Conventional techniques for calculating the machine parameters for the present model were therefore adopted as for example described by Evans (10). The problem is relatively simple in the present type of induction stepping machine because of its uniform airgap. The actual calculations were made for the self and mutual magnetising inductance components for the various coils.

Measured values of leakage inductances were used in subsequent analysis. The slot conductors were assumed to have zero cross sectional area and to be situated on the surface of the stator at the centre of the slot opening.

2.3.1 STATOR SELF INDUCTANCE

In view of the fact that the analysis concerns an unusual machine, the simplification often used in conventional machines, such as the assumption that the windings are sinusoidally distributed in space, were not made. Instead, the precise winding configuration was used and the total flux linkage with the set of coils connected in series for one stator phase was calculated. This was done for the flux linkage due to the main magnetic circuit. The flux density in the uniform airgap due to one amp flowing in one stator coil was calculated. The total flux density due to all the stator coils was then calculated by summation. The inductance was then obtained by calculating the total flux linkage due to these total flux density distributions with all the stator coils. This technique for the stator winding, is described in detail below.

The stator winding configuration in the test machine is shown in figure 2.3 and the flux density wave due to each coil, 0-0', 1-1' and 2-2' are shown in figure 2.4. Consider coil 1-1' in figure 2.4, then Ampere's Law can be applied in the usual way, i.e.,

$$N_s I_s = \int H dl \qquad \ldots 2.1$$

$$= \frac{B_{g1}}{\mu_0} g' + \frac{B_{g2}}{\mu_0} g' \qquad \ldots 2.2$$

with B_{g1} and B_{g2} as the flux densities in the airgap. The effective gap length g' is assumed here to include slotting effects via Carter's coefficient and approximate allowance for the iron path. This is considered in more detail in section 2.3.3 below.

Further from Maxwell's equations it is well known that

$$divB = 0$$

That is, from figure 2.4

$$B_{g1}A_1 - B_{g2}A_2 = 0$$

or

$$B_{g2} = B_{g1}\frac{A_1}{A_2} \qquad \text{... 2.3}$$

Substituting equation 2.3 in equation 2.2

$$N_s I_s = \frac{B_{g1}g'}{\mu_0}\left|1+\frac{A_1}{A_2}\right| \qquad \text{... 2.4}$$

Hence

$$B_{g1} = \frac{\mu_0 N_s I_s}{g'}\left[\frac{A_2}{A_1+A_2}\right] \qquad \text{... 2.5}$$

and

$$B_{g2} = \frac{\mu_0 N_s I_s}{g'}\left[\frac{A_1}{A_1+A_2}\right] \qquad \text{... 2.6}$$

Clearly for a full pitched coil, $B_{g1}=B_{g2}$. These equations can be applied to each of the stator coils 0-0', 1-1', 2-2', in turn so that the resulting flux density due to all of them, which has the shape shown in figure 2.4(b) can be calculated by summation.

One period length of this resultant flux density wave is divided into 360 points, for convenience in computation, each point hence corresponds to one electrical degree. Thus, by substituting the appropriate limits for individual components, the resultant flux density waves due to all three stator phase windings may be written as

$$\begin{aligned}
B_A(N)\Big|_1^{360} &= B_{22}(N)\Big|_1^{360} + B_{00}(N)\Big|_1^{360} + B_{11}(N)\Big|_1^{360} \\
B_B(N)\Big|_1^{360} &= B_{22}(N)\Big|_{+121}^{-120} + B_{00}(N)\Big|_{+121}^{-120} + B_{11}(N)\Big|_{+121}^{-120} \\
B_C(N)\Big|_1^{360} &= B_{22}(N)\Big|_{+61}^{-60} + B_{00}(N)\Big|_{+61}^{-60} + B_{11}(N)\Big|_{+61}^{-60}
\end{aligned} \qquad \text{... 2.7}$$

The lower and upper limits in the above series corespond to the start and finish of the operations. The magnitudes of B_{00}, B_{11} and B_{22} are selected

conveniently depending on which side the summation falls within its limits.

These set of equations are used to determine the total flux which is linking with each stator phase windings. The 'total flux linkage', in this case, is obtained by summing the resultant flux between the upper and lower limits of each coils associate with the corresponding phases. Using this total flux linkage the magnetising component of stator self inductance for all three phases are obtained. This in mathematical terms become

$$L_{AA} = \left[\sum_{-21}^{180} B_A(N) + \sum_{1}^{200} B_A(N) + \sum_{21}^{160} B_A(N)\right] \frac{N_s l_s r_s \frac{\pi}{2} p}{180}$$

$$L_{BB} = \left[\sum_{101}^{300} B_B(N) + \sum_{121}^{320} B_B(N) + \sum_{141}^{280} B_B(N)\right] \frac{N_s l_s r_s \frac{\pi}{2} p}{180}$$

$$L_{CC} = \left[\sum_{221}^{-60} B_C(N) + \sum_{241}^{-80} B_C(N) + \sum_{261}^{-40} B_C(N)\right] \frac{N_s l_s r_s \frac{\pi}{2} p}{180} \quad \text{... 2.8}$$

Since all three stator phases are identical, L_{AA}, L_{BB} and L_{CC} turn out to be equal.

The procedure in prediction of the magnetising component of rotor self inductance also, closely parallels that followed hithertoo, except that in this case there are only two coils on one axis. This is described in the following subsection.

2.3.2 ROTOR SELF INDUCTANCE

Figure 2.5 shows the resultant flux density waveform due to individual rotor winding loops for α-axis winding. Here also the coils are not connected in full pitch form. However, the expression for the resultant flux density waveform can be obtained by using the general equation 2.4. This is done after knowing the magnitudes of the flux densities due to coils 0-0' and 1-1' on the rotor. From equations above they are equal to

$$B_{00} = \frac{\mu_0 N_r I_r}{g'\left(1 + \frac{A_1}{A_2}\right)} \quad \text{... 2.9}$$

and

$$B_{11}=\frac{\mu_0 N_r I_r}{g'(1+\frac{A_2}{A_1})} \qquad \text{... 2.10}$$

By summing the magnitudes of the flux densities between appropriate limits, the resultant flux density wave due to all the α-axis windings is given by

$$B_\alpha(N)\Big|_1^{360} = B_{00}(N)\Big|_1^{360} + B_{11}(N)\Big|_1^{360} \qquad \text{... 2.11}$$

The limits in the above equation are selected by dividing the period of the resultant waveform into 360 degrees each division is corresponding to one electrical degree as was the case with stator flux density waveform.

Now, with the usual substitution the magnetising component of rotor self inductance is calculated below. The mathematical representation of this is given by

$$L_{\alpha\alpha m}=\left|\sum_{15}^{165} B_\alpha(N)+\sum_{-15}^{195} B_\alpha(N)\right|\frac{2N_r l_r r_r \frac{\pi}{2}p}{180} \qquad \text{... 2.12}$$

The number of turns are doubled in equation 2.12 above, because in the test machine they are twice as much as for a single layer winding per slot.

Clearly, what has been shown in the hithertoo discussion is only to predict the stator and rotor self inductance by considering the actual machine winding layout. Results obtained from this techniques are compared with the measured values later in this section. Before this, the mutual inductance between the stator and rotor windings is calculated. The discussion of which follows next.

2.3.3 MUTUAL INDUCTANCE

Prediction of the mutual inductance between the stator and the rotor windings is rather more difficult than that discussed so far. This is mainly due to the influence of two more constraints such as the rotor position and the rotor skewing. In order to consider rotor skew, the rotor was imagined as a whole block in 3D form. It was subdivided into fifteen notional sub-stacks each 51/15

mm long as shown in figure 2.6. These sub-stacks are displaced circumferentially in one degree (mechanical) steps to give a close approximation to skew.

At first the mutual inductance is calculated for one such sub-stack at any arbitrary position θ, and then the summation is extended for the 15 sub-stacks so that the entire length of the rotor winding is thus covered and allows for the effect of skew. This is shown below in mathematical form where the flux density due to A phase stator is linked with the windings of the α-axis coils on the rotor. That is

$$M_{\alpha a}(\theta)\Big|_{At\ position\ \theta} = \Bigg\{ \sum_{\theta+15+1}^{165} B_A(N) + \sum_{\theta-15+1}^{195} B_A(N) + \sum_{\theta+15+2}^{165} B_A(N) + \sum_{\theta-15+2}^{195} B_A(N) + \ldots\ldots + \ldots\ldots + \ldots\ldots + \ldots\ldots + \sum_{\theta+15+15}^{165} B_A(N) + \sum_{\theta-15+15}^{195} B_A(N) \Bigg\} \frac{2l_r N_r r_r \frac{\pi}{2} p}{15 \times 180} \qquad \ldots 2.13$$

The actual airgap length, 'g', shown in table 2.1 is increased due to slot effects (11) as well as the type of iron used in the machine. It is done by allowing approximately for the ampere turns absorbed by the iron in the usual way and assuming the average relative permeability of the iron as 1000. With this approximation the physical airgap used in the prediction equations was increased by 31% due to Carter's coefficient and 35% due to the iron path, giving an overall increase of 66%.

The leakage inductances were not calculated separately due to the complexities in accurate predictions. Instead, the values were obtained by measurement. A method describing the measurement of leakage, self and mutual inductances is shown in appendix A. The measured and predicted values of the stator and rotor winding parameters are shown in table 2.2 for 75 volts, excitation voltage. The self inductance of stator and rotor windings are the total inductances which include both leakage and magnetising components. In figure 2.7 the measured and predicted values of the mutual inductances are

plotted against rotor position. They are observed to be in good agreement. In the same figure, fundamental component of the predicted mutual inductance values is shown. Also, amplitudes of the predominant harmonic contents of the predicted space mutuals are shown in table 2.3. The percentage figures show that the 1st and the 3rd harmonics are the most dominant ones.

Measured					Predicted	
V_a	R_a	R_α	L_{aa}	$L_{\alpha\alpha}$	L_{aa}	$L_{\alpha\alpha}$
75 V	4.3 Ω	8.0 Ω	0.23 H	0.32 H	0.237 H	0.326 H

TABLE 2.3

Harmonic Number	Harmonic Amplitude	Percentage of the Peak Mutual Inductance
1	0.23364	95.5
3	0.0129	5.273
5	0.00053	0.217
7	0.00021	0.086
9	0.00058	0.237
11	0.00025	0.102
13	-0.00019	0.078
15	-0.00025	0.102
17	-0.00008	0.033
19	0.00004	0.016
21	0.00004	0.016

2.4 STEADY STATE ANALYSIS

When the stator winding is excited with an alternating emf, the interaction of the mmf of the rotor winding with that of the stator winding magnetic field, produces a torque. As a result the rotor tries to move to a position of equilibrium. If the external torque is zero, the electromagnetic torque is also zero and this is known as the null position. The average torque at any position during steady non-switched excitation is known as the average static torque.

An equation for the static torque can be derived by the application of the principle of virtual work. It is desired to start from the very basics of the principle of energy conversion because of the special nature of the machine.

In the virtual displacement, the mechanical work done against force is expressed by the relation(12)

$$f = \frac{dW_{mech}}{dx}$$

but, from principle of conservation of energy

$$dW_{elec} = dW_{mech} + dW_{fld}$$

Therefore

$$f\,dx = dW_{elec} - dW_{fld}$$

That is,

$$f\frac{dx}{dt} = \left[\Sigma V_i I_i - \Sigma I_i^2 R_i\right] - \left[\frac{1}{2}\Sigma I_i \frac{d\psi_i}{dt}\right]$$

$$= \Sigma I_i \frac{d\psi_i}{dt} - \frac{1}{2}\Sigma I_i \frac{d\psi_i}{dt}$$

$$= \frac{1}{2}\Sigma I_i \frac{d\psi_i}{dt} \qquad \textit{by neglecting copper losses}$$

$$f = \frac{dW_{fld}}{dx} \qquad \textit{at constant current} \qquad \text{... 2.14}$$

Based on the similar principle the electrical torque T_i can be derived for a set of mutually coupled circuits. For uniform airgap machines such as the one

considered in this discussion, the reluctance of the magnetic circuit is independent of the rotor angular position. If the effect of the slots is also neglected, the self-inductances of the windings are therefore independent of the rotor position, θ, and the reluctance torques are zero (13). This method assumes that each coil can be considered in turn, the overall result being obtained by summing the effects of all the coils. This also assumes that the system is linear, which in this case requires that the effects of saturation are neglected. Thus, the instantaneous energy stored in the magnetic field of k mutually coupled circuits is given by the expression (12)

$$W_{fld} = \frac{1}{2}L_{11}i_1^2 + \frac{1}{2}L_{22}i_2^2 + ... + \frac{1}{2}L_{kk}i_k^2 + \left\{ M_{12}i_1i_2 + M_{13}i_1i_3 + M_{14}i_1i_4 + ... + M_{1k}i_1i_k + M_{21}i_1i_2 + M_{23}i_2i_3 + M_{24}i_2i_4 + ... + M_{2k}i_2i_k \right\} \times \frac{1}{2} \qquad \text{... 2.15}$$

which can be written in matrix form as

$$W_{fld} = \frac{1}{2}[i_1 \;\; i_2 \;\; \ldots i_k] \begin{bmatrix} L_{11} & M_{12} & M_{13} & . & . & M_{1k} \\ M_{21} & L_{22} & M_{23} & . & . & M_{2k} \\ . & . & . & . & . & . \\ . & . & . & . & . & . \\ . & . & . & . & . & L_{kk} \end{bmatrix} \begin{bmatrix} i_1 \\ i_2 \\ . \\ . \\ i_k \end{bmatrix} \qquad \text{... 2.16}$$

From equations 2.14 and 2.16 the instantaneous electrical torque is given in the usual form

$$T_i = \frac{1}{2}[I_t]\left[\frac{dM}{d\theta}\right][I] \qquad \text{... 2.17}$$

where $[I_t]$ is the transpose of the matrix for $[I]$. In view of the assumption of uniform airgap made above the differential of the self inductance terms in $\left[\frac{dM}{d\theta}\right]$ are zero.

In general, the current and inductance matrices include all the windings which are active for the process of energy conversion. In the present case, there are only two coupled windings which are one stator and one rotor winding. The instantaneous voltage equations for such a coupled circuit is written in matrix

form as

$$\begin{bmatrix} v_a \\ 0 \end{bmatrix} = \begin{bmatrix} R_a + L_{aa}\frac{d}{dt} & M_{\alpha a}\frac{d}{dt} \\ M_{\alpha a}\frac{d}{dt} & R_\alpha + L_{\alpha\alpha}\frac{d}{dt} \end{bmatrix} \begin{bmatrix} i_a \\ i_\alpha \end{bmatrix} \qquad \text{... 2.18(a)}$$

For sinusoidal voltage excitation, the instantaneous values of the currents and voltages assume the following form

$$\begin{aligned} v_a &= \hat{V}_a \cos\omega t \quad = \mathrm{Re}\, \hat{V}_a e^{j\omega t} \\ i_a &= \hat{I}_a \cos(\omega t - s) = \mathrm{Re}\, \hat{I}_a e^{-js} e^{j\omega t} \\ i_\alpha &= \hat{I}_\alpha \cos(\omega t - \alpha) = \mathrm{Re}\, \hat{I}_\alpha e^{-j\alpha} e^{j\omega t} \end{aligned} \qquad \text{... 2.19}$$

Substituting equation 2.19 in equation 2.18 the voltage equations for sinusoidal excitations become

$$\begin{bmatrix} V_a \\ 0 \end{bmatrix} = \begin{bmatrix} R_a + j\omega L_{aa} & j\omega M_{\alpha a} \\ j\omega M_{\alpha a} & R_\alpha + j\omega L_{\alpha\alpha} \end{bmatrix} \begin{bmatrix} I_a \\ I_\alpha \end{bmatrix} \qquad \text{... 2.18(b)}$$

where,

$$\begin{aligned} V_a &= \frac{1}{\sqrt{2}} \hat{V}_a e^{j0} \\ I_a &= \frac{1}{\sqrt{2}} \hat{I}_a e^{-ja} \\ I_\alpha &= \frac{1}{\sqrt{2}} \hat{I}_\alpha e^{-j\alpha} \end{aligned} \qquad \text{... 2.20}$$

solving for I_a and I_α,

$$I_a = \frac{V_a (R_\alpha + j\omega L_{\alpha\alpha})}{A' + jB'} \qquad \text{... 2.21}$$

$$I_\alpha = \frac{-j\omega M_{\alpha a} I_a}{R_\alpha + j\omega L_{\alpha\alpha}} \qquad \text{... 2.22}$$

with,

$$\begin{aligned} A' &= R_a R_\alpha - \omega^2 L_{aa} L_{\alpha\alpha} + \omega^2 M_{\alpha a}^2 \\ B' &= \omega (L_{aa} R_\alpha + L_{\alpha\alpha} R_a) \end{aligned} \qquad \text{... 2.23}$$

The mutual inductance, $M_{\alpha a}$, varies with rotor position as seen earlier, as

the alignment of the coils on the stator and rotor varies. It is often assumed that this variation is sinusoidal as the space distributions of the windings are themselves very nearly sinusoidal. For the present case however, where the analysis of an unusual machine is being undertaken this assumption has not been made, and the already established actual variation of mutual inductance has been used. From the calculated values of the mutual linductances, the variation with respect to position have been expressed in the form of a Fourier series in the usual way, i.e.,

$$M_{\alpha a} = \sum_{n=1}^{\infty} \hat{M}_n \cos np\,\theta \qquad \ldots 2.24$$

where

$$\hat{M}_n = \frac{1}{\pi} \int_0^{2\pi} M_{\alpha a}(p\,\theta) \cos np\,\theta \; d(p\,\theta) \qquad \ldots 2.25$$

The function $M_{\alpha a}(p\,\theta)$ is the actual mutual inductance, θ the, mechanical angle and $p\,\theta$ represents the electrical angle and the integration to calculate the harmonic coefficients is taken from one pair of poles.

Further, for convenience, substituting equation 2.25 in equation 2.18 and the results thus obtained in equation 2.17 the instantaneous torque is reduced to the following form

$$T_i = \frac{1}{2}[i_a \quad i_\alpha] \begin{vmatrix} 0 & -p\sum_{n=1}^{\infty} n\hat{M}_n \sin np\,\theta \\ -p\sum_{n=1}^{\infty} n\hat{M}_n \sin np\,\theta & 0 \end{vmatrix} \begin{bmatrix} i_a \\ i_\alpha \end{bmatrix} \qquad \ldots 2.26$$

which becomes,

$$T_i = -p i_a i_\alpha \sum_{n=1}^{\infty} n\hat{M}_n \sin np\,\theta \qquad \ldots 2.27$$

The time average torque produced with sinusoidal voltage excitation on the primary, for any fixed rotor position is therefore given by

$$T_a = \mathrm{Re}\, \overset{*}{I}_a p\,[-I_\alpha \sum_{n=1}^{\infty} n\hat{M}_n \sin np\,\theta] \qquad \ldots 2.28$$

Substituting for I_α from equations 2.22 and equation 2.24 above gives

$$T_a = \mathrm{Re}\left| I_a \right|^2 \frac{pj\omega}{R_\alpha + j\omega L_{\alpha\alpha}} \left| \sum_{n=1}^{\infty} \sum_{m=1}^{\infty} n\hat{M}_n \hat{M}_m \sin np\theta \cos mp\theta \right| \quad \ldots 2.29$$

where subscripts 'm' and 'n' have been used for clarity to distinguish the harmonic coefficients of $M_{\alpha a}$ and $\frac{dM_{\alpha a}}{d\theta}$.

Further simplification of equation 2.29 is possible by substituting for the stator current from equations 2.21 and 2.24. Thus

$$T_a = \frac{p\omega^2 L_{\alpha\alpha} V_a^2}{A'^2 + B'^2} \left| \sum_{n=1}^{\infty} \sum_{m=1}^{\infty} n\hat{M}_n \hat{M}_m \sin np\theta \cos mp\theta \right| \quad \ldots 2.30$$

with

$$A' = R_a R_\alpha - \omega^2 L_{aa} L_{\alpha\alpha} + \omega^2 \left| \sum_{n=1}^{\infty} \sum_{m=1}^{\infty} \hat{M}_n \hat{M}_m \cos np\theta \cos mp\theta \right| \quad \ldots 2.31$$

The steady state torque described by equation 2.30 is thus a complicated function of rotor position. More discussion about its variation hence requires the torque values for different rotor positions and is done by comparing them with the measured values in the following section.

2.5 COMPARISON OF THE PREDICTED AND EXPERIMENTAL RESULTS

In figure 2.8 the predicted values of static torque is plotted against rotor position at constant stator excitation voltage. Measured values are also shown in the same figure. Measurement of torque is done by using two spring balances and a clamp to hold the rotor at a particular rotor position. In this figure the stable torque-zero position is at 90° and an unstable torque-zero position at 0° and 180° electrical. The unstable torque-zero position is at position when the stator and rotor magnetic axes are coincident with each other.

Figures 2.9 and 2.10 represent the corresponding theoretical and measured values of rms currents I_a and $I_{\alpha\alpha}$ respectively. It can be seen that the stator and rotor currents are at their maximum values at the unstable torque-zero positions. At this position the magnetic coupling between the stator and rotor

windings is at its maximum. When the rotor is displaced away from its unstable torque-zero position currents start falling and so does the torque after reaching its peak. The peak static torque occurs very close to the unstable torque-zero position. At the stable torque-zero position, since all the flux lines are aligned to the short circuited rotor coils there is no flux linking with them and hence no torque. Thus torque changes from unstable-zero to positive peak and then to stable-zero to negative peak and then back to unstable-zero, completing one cycle between 0 and 180 electrical degrees. The general shape of this torque therefore shows symmetry about the null position and the inherent presence of negative torque implies that there is a tendency to restore the rotor to its null position when disturbed from it. This torque symmetry is believed to be due to the symmetry of the coil distribution in the rotor.

In addition to the observation noted above the shape of the torque-displacement curve is not particularly encouraging, since the torque is low over a considerable range either side of the stable torque-zero point. The torque capability has deteriorated due to the decline in flux linkage as the rotor moves towards this position.

The behaviour of the machine with ideal sinusoidally distributed windings, that is to say with n=m=1 in equation 2.30 above, is illustrated in figures 2.11 to 2.13. It can be seen that there is a significant change in characteristic eventhough the harmonic content of $M_{\alpha a}$ is found to be small as shown in table 2.3 above. The peak value of the static torque has diminished by more than 50% although there is some 'flattening' of the characteristic, and hence the torque/angle characteristic has not become more favourable.

These defficiencies in torque/angle distribution need to be resolved in order to achieve a useful motor. This can be done by modifying the windings on both the stator and rotor. For the stator, the use of a polyphase winding in which coils are switched in turn, one or multiple phases at a time, as the rotor moves will allow continuous operation this is understood in subsequent chapters below. For the rotor, additional coils might also improve the torque/angle characteristic and a particular interesting configuration is investigated below.

CHAPTER 3

STUDY OF THE MODIFIED INDUCTION STEPPING MOTOR

3.1 INTRODUCTION

The shape of the static torque/angle characteristic of a stepper motor is particularly important in influencing the overall motor performance. It gives the maximum torque capability of the machine, which is sometimes called the 'holding torque', since it is the greatest applied load the motor can hold stationary. It also permits the designer to select the appropriate excitation sequence for continuous stepping operation (5).

Ideally, the static torque/angle characteristic should perhaps have a constant torque between the stable and unstable torque-zero positions as shown in figure 3.1. With such a characteristic the rotor comes to rest on completing a sequence of steps at a known position, for all loads between no load and full load. Furthermore, the average torque is equal to the maximum torque and this clearly is desirable from the dynamic performance point of view. This latter aspect of performance is discussed more fully later, but let it suffice to say here that the dynamic performance is, in general, also improved by having a large value of $\frac{dT}{d\theta}$ at the stable torque-zero position. In the ideal characteristic proposed, it is of course infinite.

Practically, however, it is difficult to achieve a perfect rectangular torque/angle characteristic. The characteristic obtained for the simple induction stepper motor in chapter 2 (figure 2.8) above seems to be particularly poor in that the stiffness around the stable operating point is very low. It is possible that additional rotor coils might improve this characteristic. One extreme case is for two rotor coils in space quadrature. The configuration would however be expected to produce zero torque - like a single phase induction motor at standstill - if the coils were sinusoidally distributed in space. Nevertheless, having seen that the harmonic effects of the single rotor coil were found to be significant (figure 2.8 and 2.11) it is of interest to investigate the behavior of two non-ideal quadrature rotor windings. This is discussed by first

looking at the new physical model and then by extending the steady state analysis to this new configuration.

3.2 DESCRIPTION OF THE NEW MODEL

Figure 3.2 represents the new model for a 2-pole machine at two different rotor positions as indicated in reference 14. The additional β-axis rotor winding is identical to the α-axis winding and is placed in quadrature to it. Furthermore, this short circuited rotor winding is electrically separate from its counter part. Although both rotor windings are shown as concentrated coils, in general they each consist of a distributed set of coils. The actual rotor winding of the test machine is shown as a developed winding diagram in figure 3.3. The dotted lines are shown to distinguish between the top and the bottom conductor of the double layer winding. The external rotor winding connections just before the slip rings are also shown in the same figure.

3.3 STEADY STATE ANALYSIS

3.3.1 GENERAL TORQUE EQUATION

The static torque expression is derived below in terms of the mutual inductances. The essential features of the proceeding analysis are very similar to those given in chapter 2 for the case of only α-axis rotor windings. In the previous model the total number of windings associated with the coupled circuit were only two. Whereas, here, for the new rotor configuration in the test machine the additional winding also contributes to the torque. Hence, by retaining only appropriate parameters in the general torque equation 2.17 it can be written for the rotor model shown in figure 3.2 as

$$T_i = \frac{1}{2}[i_a \;\; i_\alpha \;\; i_\beta]\frac{d}{d\theta}\begin{bmatrix} 0 & M_{\alpha a} & M_{\beta a} \\ M_{\alpha a} & 0 & 0 \\ M_{\beta a} & 0 & 0 \end{bmatrix}\begin{bmatrix} i_a \\ i_\alpha \\ i_\beta \end{bmatrix} \qquad \ldots 3.1$$

The current phasors i_a, i_α and i_β are obtained from the voltage equations. For a three winding arrangement of the present sort the voltage equations are

$$\begin{bmatrix} v_a \\ 0 \\ 0 \end{bmatrix} = \begin{bmatrix} R_a + L_{aa}\frac{d}{dt} & M_{\alpha a}\frac{d}{dt} & M_{\beta a}\frac{d}{dt} \\ M_{\alpha a}\frac{d}{dt} & R_\alpha + L_{\alpha\alpha}\frac{d}{dt} & 0 \\ M_{\beta a}\frac{d}{dt} & 0 & R_\beta + L_{\beta\beta}\frac{d}{dt} \end{bmatrix} \begin{bmatrix} i_a \\ i_\alpha \\ i_\beta \end{bmatrix} \quad \ldots 3.2$$

For sinusoidal excitaion, the rms values of v_a, i_a and i_α are of the form as defined by equation 2.20 and that of i_β is equal to $\frac{1}{\sqrt{2}}\hat{I}_\beta e^{-j\beta}$. By substituting these quantities in equation 3.2 and simplifying the phasor expressions for the rotor currents I_α and I_β, they then become equal to

$$I_\alpha = -\frac{j\omega M_{\alpha a}}{R_\alpha + j\omega L_{\alpha\alpha}} I_a \quad \ldots 3.3$$

and

$$I_\beta = -\frac{j\omega M_{\beta a}}{R_\beta + j\omega L_{\beta\beta}} I_a \quad \ldots 3.4$$

The mutual inductance functions, $M_{\alpha a}(\theta)$ and $M_{\beta a}(\theta)$ appearing in the above equations have not yet been specified. However, for the test machine in chapter 2 having only the α-axis rotor winding it has been already shown that the mutual inductance function, $M_{\alpha a}(\theta)$, is not exactly a co-sinusoidal function and even though has a close approximation, the function was treated as an harmonic series, and was given in equation 2.24. In this case, the mutual inductance with respect to the β-axis rotor winding can also be expressed as a Fourier Series by phase shifting the expression for the α-axis winding by $\frac{\pi}{2}$. Thus $M_{\beta a}(\theta)$ is given by,

$$M_{\beta a} = \sum_{n=1}^{\infty} \hat{M}_n \cos n\left(p\theta - \frac{\pi}{2}\right) \quad \ldots 3.5$$

where $\hat{M}_n$ is the amplitude of the n th harmonic and is obtained from equation 2.25, since both α and β-axis rotor windings are assumed in this case to be identical to each other.

Equation 3.5 is plotted against rotor position for $p\theta$=0 to 180 electrical degrees in figure 3.4. In the same figure the measured values of the

corresponding mutual inductance are given along with the fundamental component for the predicted mutuals. Clearly, this figure shows that the position dependency of the mutual inductance, $M_{\beta a}$, does not depart greatly from the sinusoidal. The same results were found for M_{aa} in section 2.4.

Now, to obtain a general torque expression, equation 3.1 is expanded from its matrix form in conjunction with equations 2.24 and 3.5. After few algebraic simplifications the following result is obtained. That is

$$T_i = i_a \left[-p \sum_{n=1}^{\infty} n\hat{M}_n \sin np\,\theta\, i_\alpha + p \sum_{n=1}^{\infty} n\hat{M}_n \sin n\left(p\,\theta - \frac{\pi}{2}\right) i_\beta \right] \qquad \ldots 3.6$$

The average steady state torque is then of the form equal to

$$T_a = \mathrm{Re}\, I_a^{*} p \left[-\sum_{n=1}^{\infty} n\hat{M}_n \sin np\,\theta\, I_\alpha + \sum_{n=1}^{\infty} n\hat{M}_n \sin n\left(p\,\theta - \frac{\pi}{2}\right) I_\beta \right] \qquad \ldots 3.7$$

The simplification of equation 3.7 is continued by substituting the expressions for I_α and I_β from equations 3.3 and 3.4. This operation yields the static torque T_a, in terms of the stator current and is equal to

$$T_a = \mathrm{Re}\left| I_a \right|^2 p j\omega \left[\frac{\sum_{n=1}^{\infty}\sum_{m=1}^{\infty} n\hat{M}_n \hat{M}_m \sin np\,\theta \cos mp\,\theta}{R_\alpha + j\omega L_{\alpha\alpha}} - \frac{\sum_{n=1}^{\infty}\sum_{m=1}^{\infty} n\hat{M}_n \hat{M}_m \sin np\,\theta - \frac{\pi}{2} \cos mp\,\theta - \frac{\pi}{2}}{R_\beta + j\omega L_{\beta\beta}} \right] \qquad \ldots 3.8$$

For identical rotor windings such is the case with the present test machine, the rotor winding impedances $R_\alpha + j\omega L_{\alpha\alpha}$ and $R_\beta + j\omega L_{\beta\beta}$ are equal. Also, for sinusoidal excitation the expression for the stator current, I_a, can be obtained in phasor form by substituting $R_\beta + j\omega L_{\beta\beta} = R_\alpha + j\omega L_{\alpha\alpha}$ in equation 3.4, and then equations 3.3 and 3.4 in the first row of the determinant, equation 3.2. After simplification, I_a becomes

$$I_a = \frac{V_a (R_\alpha + j\omega L_{\alpha\alpha})}{A + jB} \qquad \ldots 3.9$$

where

$$A = R_a R_\alpha - \omega^2 [L_{aa} L_{\alpha\alpha} - (M_{\alpha a}^2 + M_{\beta a}^2)]$$
$$B = \omega (L_{aa} R_\alpha + R_a L_{\alpha\alpha}) \qquad \ldots 3.10$$

When, now the square of the magnitude of the stator current from equation 3.10 is substituted in equation 3.8 the following expression for the static torque is obtained. That is given as

$$T_a = \frac{pV_a^2 \omega^2 L_{\alpha\alpha}}{A^2 + B^2} \left[\sum_{n=1}^{\infty} \sum_{m=1}^{\infty} n \hat{M}_n \hat{M}_m (\sin np\,\theta \cos mp\,\theta + \sin np\,\overline{\theta - \frac{\pi}{2}} \cos mp\,\overline{\theta - \frac{\pi}{2}}) \right] \qquad \ldots 3.11$$

By expanding the series, which is present within the brackets, equation 3.11 can be rewritten as

$$T_a = T_{apk} \left[\frac{1}{2} \sum_{n=1}^{\infty} \sum_{m=1}^{\infty} n \hat{M}_n \hat{M}_m (\sin \overline{n-m}\,p\,\theta + \sin \overline{n-m}\,p\,\overline{\theta - \frac{\pi}{2}} + \sin \overline{n+m}\,p\,\theta + \sin \overline{n+m}\,p\,\overline{\theta - \frac{\pi}{2}}) \right]$$
$$\ldots 3.12$$

where

$$T_{apk} = \frac{pV_a^2 \omega^2 L_{\alpha\alpha}}{A^2 + B^2} \qquad \ldots 3.13$$

Equation 3.12 is a general torque expression and requires some interpretation. The factor T_{apk}, the first term, changes with change in rotor position and its magnitude at any given rotor position is proportional to the square of the magnitude of the stator voltage. However, this factor would never become zero for any finite value of stator excitation. Whereas the terms within the brackets, the second set of terms may be zero depending on the combinations of the values of n, m and the position of the rotor. Therefore the importance of these parameters is now discussed below.

For values of n=m=1, that is when the stator and rotor windings are sinusoidally distributed in space so that only a fundamental harmonic component of the space mutuals is considered, the static torque equation 3.12 reduces to zero value. The same conclusion applies for n=m=3, 5, 7, . . . etc. This means to say that there is no contribution to the torque when the machine has a perfect sinusoidal mutual inductance distribution, no matter what its peak value is. However, equation 3.12 predicts torque when the various harmonic components of the mutual inductances interact. This becomes more clear from the following equation which is written by expanding equation 3.12

for only odd harmonics as has been the case in the test model. That is,

$$
\begin{aligned}
T_a = T_{apk} \Big| & 4 \sin 4p\theta \,(\hat{M}_1\hat{M}_3+\hat{M}_1\hat{M}_5+\hat{M}_3\hat{M}_7+\hat{M}_5\hat{M}_9+\hat{M}_7\hat{M}_{11}+....) \\
& +8 \sin 8p\theta \,(\hat{M}_1\hat{M}_7+\hat{M}_1\hat{M}_9+\hat{M}_3\hat{M}_5+\hat{M}_3\hat{M}_{11}+\hat{M}_5\hat{M}_{13}+.....) \\
& +12 \sin 12p\theta \,(\hat{M}_1\hat{M}_{11}+\hat{M}_1\hat{M}_{13}+\hat{M}_3\hat{M}_9+\hat{M}_3\hat{M}_{15}+\hat{M}_5\hat{M}_7+...) \\
& +16 \sin 16p\theta \,(\hat{M}_1\hat{M}_{15}+\hat{M}_1\hat{M}_{17}+\hat{M}_3\hat{M}_{13}+\hat{M}_3\hat{M}_{19}+\hat{M}_5\hat{M}_{11}+...) \\
& +.. \quad .. \quad .. \quad .. \quad .. \\
& . \\
& +.. \quad .. \quad .. \quad .. \quad .. \Big|
\end{aligned}
\qquad \ldots 3.14
$$

where $\hat{M}_1$, $\hat{M}_3$, $\hat{M}_5$, . . . etc., are the amplitudes of the corresponding harmonics. Thus the above expression shows that the static torque at a given rotor position is produced not by the fundamental but, by the combined effects of all the pairs of harmonics.

To observe the peak stable and unstable torque-zero positions, equation 3.14 is plotted against rotor position for the test machine and the discussion of this is given below.

3.3.2 THE STATIC TORQUE/ANGLE CHARACTERISTIC

Figure 3.5 represents the variation of static torque with respect to rotor position. The measured values are also shown in the same figure for constant stator excitation voltage of 75 volts. Figures 3.6, 3.7 and 3.8 represent the variation of the stator current I_a, and rotor currents I_α and I_β as a function of rotor position respectively for both predicted and measured values. The torque and current variations for the fundamental component of the mutual inductance is also shown in the above figures.

The stable torque-zero positions can be seen to be at θ= 45, 135, . . . etc., electrical degrees. An interesting feature is the slope of the torque/angle characteristic at these positions. Here, it is higher than with only α-axis rotor windings. For example the $\frac{dT}{d\theta}$ around stable torque-zero position in figure 3.5

is approximately 2.5 Nm/electrical radians compared with 0.6 Nm/electrical radians for the α-axis rotor coil, in figure 2.8.

The unstable torque-zero position occur at θ= 0, 90, 180, . . . etc., electrical degrees from the reference axis. At these points the stator and rotor winding currents are at extreme values, that is, they are either at a maximum or minimum value. Further, the stator current varies cyclically and this pattern of variation arises because, the resultant rotor flux which is the sum of two perpendicular components does not remain constant in magnitude for varius rotor positions, due to the type of mutual inductance distribution. This would have been the case had the mutual inductance been sinusoidal and then there would have been no torque at all.

3.4 COMPARISON BETWEEN THE MODIFIED AND THE EXISTING STEPPER MOTOR MODELS

The discussions given so far have shown a method to predict the basic static performance characteristic of an existing as well as a modified rotor. The two important torque/angle characteristics (figures 2.8 and 3.5) have shown, in-general, the torque-zero positions both at stable and unstable points, and also varying torque gradient with respect to position between these two points. More importantly, there is a presence of equal and opposite restoring torque when the rotor is disturbed from its equilibrium position. These features indicate that the motor may be suitable for operation as a stepping motor, when stator phases are excited sequentially.

The ideal stepping motor, as has been introduced in section 3.1, should have a rectangular torque/angle characteristic so that the average torque between the adjacent stable and unstable torque-zero positions is equal to the peak static torque or holding torque. Also, there should ideally be an infinite $\frac{dT}{d\theta}$ at the stable torque-zero position. It would be however interesting to see how the present predicted torque/angle characteristics approximate to the ideal ones. This may be done by knowing the total average torque between the adjacent stable and unstable torque-zero positions, and also evaluating $\frac{dT}{d\theta}$ at the equilibrium position. These results give a basis for comparison between the two rotor models.

3.4.1 STATIC TORQUE/ANGLE CHARACTERISTIC WITH SINGLE STATOR PHASE EXCITED

Even though the total average torque over one half cycle due to one stator phase excitation is possible to obtain analytically,for the present purpose it has been found by using numerical summation techniques and they are in terms of peak static torque equal to

$$T_{av\,\alpha} = 0.31 T_{pk\,\alpha} \qquad \text{for } \alpha\text{-axis rotor}$$
$$T_{av\,\alpha\beta} = 0.51 T_{pk\,\alpha\beta} \qquad \text{for } \alpha \text{ and } \beta\text{-axes rotor} \qquad \ldots 3.15$$

where $T_{pk\,\alpha}$ and $T_{pk\,\alpha\beta}$ are the peak values of the static torques for α and $\alpha\beta$-axes rotor models. Since their predicted values are found to be

$$T_{pk\,\alpha} = 1.7\ Nm \quad \text{and} \quad T_{pk\,\alpha\beta} = 1.1\ Nm \qquad \ldots 3.16$$

the respective average torques become equal to

$$T_{av\,\alpha} = 0.53\ Nm \quad \text{and} \quad T_{av\,\alpha\beta} = 0.55\ Nm \qquad \ldots 3.17$$

The above results show that the average torque is not affected greatly by the presence of the β-axis rotor coil. However, the ratio between average torque to peak static torque is around 50% from equation 3.15 in the test machine for α and β-axis rotor model, which compare with unity for an ideal static torque/angle characteristic.

On the basis of the average torque capability between the two rotor configurations, in the test machine, there appears to be no great difference. Whereas, with respect to $\frac{dT}{d\theta}$ at the equilibrium positions, as shown in figure 3.9, the modified rotor shows about four times higher value. In this figure the predicted torque/angle characteristics of two rotor models are shown with the same scale on the torque axis, and with a different scale on the θ-axis. This has been done only to compare $\frac{dT}{d\theta}$ between the two characteristics.

It is also interesting to note that, there are two torque/angle cycles for a modified rotor model for every one such cycle with α-axis rotor arrangement. This becomes clear when the two θ-axes are drawn for the same angle, say 360 electrical degrees. In other words the entire torque/angle cycle over the rotor

periphery is doubled with the introduction of quadrature rotor coils. Thus, this is one of the important feature where the two rotor models have shown very distinct properties. To make this point clear, its importance is first considered with respect to the continuous stepping operation and then the influence of the governing parameters is discussed briefly, below.

3.4.2 STEP ANGLE

The halving effect of torque/angle cycle as identified in the previous discussion for an α and β-axis rotor model, changes what is known as 'step angle' of the machine. This term describes the angle covered by the machine, each time when it is stepping and is clearly described below after the discussion about continuous stepping operation.

The continuous, uni or bidirectional rotation of the present type of machine cannot be obtained by exciting only one stator phase winding such as the one considered so far, the 'A' phase winding. This is because of the stationary instantaneous flux set up due to the excitation of one stator phase winding. This flux only alternates in space, but does not rotate as in a conventional induction motor. Therefore, to set up this rotating field there must be at least another two such stator phase windings each displaced in stator slots by 120 electrical degrees to one another as shown in figure 3.10. In otherwords,the complete stator configuration is equivalent to a 3 phase induction motor stator.To obtain continuous rotation, the excitation is transferred from one phase to another in sequence. This effectively amounts to shifting the static torque/angle characteristic by 120 electrical degrees, each time when the corresponding stator phase winding is excited. This assumes that the speed of rotation is slow compared to the 50 Hz alternating of the applied voltage. To understand the stepping operation of both the rotor models, figures 3.11 and 3.12 are drawn, which represent all three torque/angle characteristics for such a type of 3 phases excited by considering one phase winding at a time. Since, the stator phase windings are identical to each other, the static torque/angle curves are also identical, but are displaced by 120 electrical degrees.

The total angular displacement from position 'b' to position 'd' in figures 3.11 and 3.12., when phase winding B is energised with the rotor previously at the stable torque-zero position of phase winding A is equal to one 'step angle'.

Similarly, when phase winding C is energised the rotor tries to move to a new position 'f' covering the same angle. In otherwords, this is the angle between the adjacent equilibrium positions. For the present test machine, with only α-axis rotor winding this angle is 60 electrical degrees and is halved with the α and β-axis rotor windings.

This step angle is in general, for the machine of the present type depends not only on the number of poles and the number of stator phase windings as in a conventional d.c. stepping motor but in addition seems to depend on the number of rotor windings also. By observation, the following general relationship for the step angle has been shown in reference 15 which is given by

$$\theta_s = \frac{180}{2pqr} \qquad \textit{Mechanical degrees} \qquad \ldots 3.18$$

with

θ_s = Step angle in degrees
p = Number of stator pole pairs
q = Number of stator phase windings
r = Number of pair of group of mutually perpendicular rotor windings per pole pair
= 1.0 for the modified rotor
= 0.5 for the α-axis rotor

Clearly, each of these parameter p, q and r influences the step angle but also they are very important with regard to the structure of the machine. A wide variety of values of these parameters seem to be possible in design strategy to obtain the required step angle. Some possible combinations of p, q and r are discussed in reference 15. Meanwhile, in the following subsection, some more comparisons can be made between the two rotor models with respect to figures 3.11 and 3.12, which follows next.

3.4.3 TORQUE/ANGLE CHARACTERISTIC WITH SEQUENTIAL EXCITATION OF STATOR PHASES

In this section, comparison between the two rotor models is made with respect to the maximum torque the test machine can show for the selected stator excitation voltage under continuous stepping operation. This can be

understood from figures 3.11 and 3.12 by considering the sequential stator winding excitations.

By observing the above torque/angle characteristic, three features can be identified. They are,

(1) The maximum average torque or pull-out torque, T_{po}, beyond which there is loss of synchronisation with the stepping rate.

(2) The maximum initial load torque, T_{max}, that can be applied so that the machine can drive it from standstill irrespective of the initial rotor position, and maintain the synchronism with the stepping rate.

(3) The ripple content in the torque/angle characteristics, during sequential excitation.

These torque characteristics are discussed in more detail below.

(1) Pull-out torque, T_{po}

By switching on the stator phase windings one at a time in a sequence such as A, B, C, A, . . . etc., with a steady switching frequency less than the supply frequency, the machine provides a continuous torque which consists of an average value, upto a maximum of T_{po}.

If the dynamics of the machine rotor are such that the torque pulsations do not cause any speed perturbations or any other instabilities then the average torque drives the motor at an average speed and the maximum average torque that can be produced without loss of synchronism is given by, T_{po}, or pull-out torque. The values of the pull-out torques for the present test models are given below which were derived numerically from the results in figures 3.11 and 3.12.

$$T_{po\alpha}=\frac{3}{\pi}\int_{0}^{\frac{\pi}{3}} T_{\alpha}\, d\theta \qquad =0.43T_{pk\alpha} \qquad =0.73N_m \qquad \text{... 3.19}$$

and

$$T_{po\,\alpha\beta}=\frac{6}{\pi}\int_0^{\frac{\pi}{6}} T_{\alpha\beta}\,d\theta \qquad =0.66T_{pk\,\alpha\beta} \quad =0.73Nm \qquad \text{... 3.20}$$

where, T_{α} and $T_{\alpha\beta}$ are the predicted static torques for α and β-axes rotor given by equations 2.30 and 3.11 respectively. These results show no difference between the two rotor models. These results show that the pull-out torques produced by the two alternative rotors is substantially the same. This appears to be a coincidental result as the peak torque values and the torque/angle characteristics with the two rotors are significantly different.

(2) Maximum initial load torque, $T_{\max}$

From figures 3.11 and 3.12 it is evident that the maximum load torque that a machine can drive from standstill is equal to a point on the T/θ curves where the adjacent characteristics intersect each other. The torque values for the two rotors obtained for figures 3.11 and 3.12 have been found to be

$$T_{\max\,\alpha}=0.16\ Nm \qquad \text{and} \qquad T_{\max\,\alpha\beta}=0.37\ Nm \qquad \text{... 3.21}$$

The above values show approximately two times higher torque in an $\alpha\beta$-axes rotor model. Thus, although there was around 50% more peak torque ($T_{pk\,\alpha}$=1.7Nm compared to $T_{pk\,\alpha\beta}$=1.1Nm) obtained with the α-axis rotor model, the actual torque available to drive the load from standstill, in the modified $\alpha\beta$-axes rotor shows an improvement of 130%. This therefore appears to be an important advantage with the $\alpha\beta$-axes rotor.

(3) Torque ripple

For smooth continuous slow stepping operation, it is normally desirable to have low static torque pulsations with respect to rotor position. In other words, the shaded areas in the figures 3.11 and 3.12 should be as small as possible. For an ideal, rectangular torque/angle characteristic, there would be no torque ripple.

Comparing the torque/angle characteristics in figures 3.11 and 3.12 there appear to be two advantages with the $\alpha\beta$-axes rotor. First the peak to peak

ripple torque about T_{po} is substantially reduced. i.e.,

$$T_{ripple-\alpha} = \begin{vmatrix} +133\% \\ -78\% \end{vmatrix}$$

$$T_{ripple-\alpha\beta} = \begin{vmatrix} +51\% \\ -49\% \end{vmatrix}$$

Secondly, because the step angle is halved the torque-angle integral is made smaller so that the changes in speed for a given mechanical system due to the ripple torque will be greatly reduced.

It appears therefore that the additional rotor winding on the β-axis produce considerable improvements to the performance of an induction stepping motor and the results discussed above are summerised in table 3.1.

The analytical and experimental results that have been presented in chapters 2 and 3 indicate that the production of torque in an induction stepping motor is a complex matter which depends on the harmonic content of the stator and rotor windings. These seem to affect both the peak torque amplitudes and the shape of the torque/angle characteristics. The insertion of the second rotor winding, the β winding has produced improvements in behaviour and it is likely that further design improvements are possible by careful choice of windings.

TABLE 3.1: Comparison between α-axis rotor and $\alpha\beta$-axes rotor

Sl No.	Items	Predicted values for α-axis rotor	Predicted values $\alpha\beta$-axes rotor
1	Peak static torque, T_{pk}	1.70 Nm	1.10 Nm
2	Average torque		
	(a) Actual values	0.53 Nm	0.55 Nm
	(b) Expression	0.31 $T_{pk\,\alpha}$	0.51 $T_{pk\,\alpha\beta}$
3	$\frac{dT}{d\theta}$ at equilibrium position	0.6 Nm/rad	2.5 Nm/rad
4	Step angle	60.0 elec. deg.	30.0 elec. deg.
5	Maximum Pull-out torque, T_{po}		-
	(a) Actual values	0.73 Nm	0.73 Nm
	(b) Expression	0.43 $T_{pk\,\alpha}$	0.66 $T_{pk\,\alpha\beta}$
6	T_{max}	0.16 Nm	0.37 Nm
7	Ripple torque around pull-out torque as a percentage of pull-out torque	+133.0 % -78.0 %	+51.0 % -49.0 %

CHAPTER 4

MULTIPHASE EXCITATION IN INDUCTION STEPPER MOTORS

4.1 INTRODUCTION

The previous chapter dealt with the sequential switching of stator phase windings, where they were switched in turn with only one stator phase winding carrying current at a time. In other words the machine was made to step with one-phase-on scheme of excitation. This type of excitation left the rest of the stator phases unexcited. The present chapter considers the excitation of more than one stator phase winding at a time and is referred to here as multiphase excitation.

An important feature of the a.c. stepping motor as well as for any stepping motor is the step angle which was defined in section 3.4.2 above. It is widely known that the step angle can be halved by changing the excitation mode from one-phase-on to alternately one and two-phase-on at a time (1). This results in smaller stepping angles which are useful when higher resolution is required.

In stepping motor terminology continuous stepping by exciting a fixed number of stator phases at a time (i.e., one at a time, or two at a time, say) is known as the full-stepping-mode of operation. The alternative, where say one stator phase is excited, followed by two excited together followed by one again and so on is known as the half stepping mode of operation. The full-stepping-mode of operation involving multiple stator phase excitation at a time is interesting because of the possible increase in the peak static torque compared to one-phase-on excitation. In addition, the torque/angle characteristic will be changed with the stable torque-zero position interposed between those of its constituent phases. The unstable torque-zero position will be displaced in a similar way. Ultimately therefore, the rotor can be held in any required position by suitably modulating the currents in two stator phases without altering the magnetic circuit of the machine and this is sometimes known as mini-stepping operation.

In the present chapter, this alternative energisation mode is discussed both

for the existing stepper motor model as well as the improved version of it with the α and β rotor coils. To understand their performance with two-phase-on excitation, the torque prediction techniques already described in chapters 2 and 3 have been extended for use under these new conditions. At first the static torque equations are developed for only α-axis rotor and then for both α and β-axis rotor when two stator phase windings such as A and B are excited. Some observations are made in relation to multiphase excitation with only α-axis rotor windings when there are harmonics present in the mutual inductance distribution.

The discussion is then extended to consider operation with all three stator phases excited at a time, or three-phase-on operation.

4.2 TWO-PHASE-ON EXCITATION IN α-AXIS ROTOR MODEL

4.2.1 THE PHYSICAL MODEL

The physical model used here to observe the steady state performance under two-phase-on scheme of full-stepping-mode of operation is shown schematically in figure 4.1. The stator has three identical phase windings each being displaced on the stator periphery by 120 electrical degrees (i.e., $p\lambda=120^o$) as indicated by the phase windings A, B and C. The rotor model has α-axis windings and the distribution of these windings were shown in chapter 2, figure 2.3.

It is of interest to identify corresponding reference axes for the stators in figure 4.1 and figure 2.2. In figure 2.2 Φ_a identifies the magnetic axis of the A winding which is the only stator phase winding on the machine. In figure 4.1, Φ_a again identifies the magnetic axis of the A phase winding but this summates with Φ_b for the B phase winding to give the resultant Φ_s. Hence, the Φ_s-axis in figure 4.1 corresponds to the Φ_s axis in figure 2.2. Also, the figure 4.1(a) represents the rotor at zero flux linkage position and figure 4.1(b) that at maximum flux linkage position.

4.2.2 DEVELOPMENT OF MACHINE EQUATIONS

In the coupled circuit model for two-phase-on excitation representing the

flux interaction between the stator and rotor windings, some additional terms come into the picture when the same is compared with the one-phase-on model. They are due to

* The mutual magnetic coupling between the two excited stator phase windings, since in the above physical model all the stator phase windings are housed on the same stator, and they are hence not magnetically separate to each other.

* The additional mutual magnetic coupling between the second stator phase windings such as B phase and the rotor windings on α-axis.

* The self flux linkage terms of the B phase winding.

By taking these terms into account, the voltage equations for the various windings are written below in terms of the usual matrix form. It should be remembered here that the two phase windings A and B are excited with the same sinusoidal a.c. supply so that these voltages are always the same in amplitude, phase and frequency, but they may draw different currents. Thus,

$$\begin{bmatrix} V_a \\ V_b \\ 0 \end{bmatrix} = \begin{bmatrix} R_a + j\omega L_{aa} & j\omega M_{ab} & j\omega M_{\alpha a} \\ j\omega M_{ab} & R_b + j\omega L_{bb} & j\omega M_{\alpha b} \\ j\omega M_{\alpha a} & j\omega M_{\alpha b} & R_\alpha + j\omega L_{\alpha\alpha} \end{bmatrix} \begin{bmatrix} I_a \\ I_b \\ I_\alpha \end{bmatrix} \qquad \text{... 4.1}$$

where for the present case,

$$V_a = V_b$$
$$R_a = R_b \qquad \text{and}$$
$$L_{aa} = L_{bb}$$

In the equation 4.1 above, M_{ab} represents the mutual inductance between the two stator phase windings A and B and is constant for a given phase displacement between them. I_a, I_b and I_α are the steady state rms phasors of A, B and α-axis winding currents respectively when the stator phase windings A and B are excited with the same excitation voltage of V_a volts which is the reference rms phasor as in chapter 2. The mutual inductances $M_{\alpha a}$ and $M_{\alpha b}$ are respectively those between α and A phase windings and α and B phase windings. They depend on the rotor position and the appropriate equations can be written in the following form by considering $p\lambda$ as the spatial phase

displacement between the two stator phase windings under consideration. They respectively are

$$M_{\alpha a} = \sum_{n=1}^{\infty} \hat{M}_n \cos np\,\theta$$

$$M_{\alpha b} = \sum_{n=1}^{\infty} \hat{M}_n \cos np\,(\theta - \lambda) \qquad \ldots 4.2$$

By solving for different winding currents I_a, I_b amd and I_α, from the matrix equation 4.1 these currents are expressed in terms of the machine parameters as below.

$$I_a = \frac{V_a (R_\alpha + j\omega L_{\alpha\alpha})(R' + jS')}{X + jY} \qquad \ldots 4.3$$

$$I_b = \frac{V_a (R_\alpha + j\omega L_{\alpha\alpha})(P' + jQ')}{X + jY} \qquad \ldots 4.4$$

$$I_\alpha = \frac{-V_a\, j\omega[(M_{\alpha a} R' + M_{\alpha b} P') + j(M_{\alpha a} S' + M_{\alpha b} Q')]}{X + jY} \qquad \ldots 4.5$$

with

$$\begin{aligned}
P' &= A_a + \omega^2 (M_{ab} L_{\alpha\alpha} - M_{\alpha a} M_{\alpha b}) \\
R' &= A_b + \omega^2 (M_{ab} L_{\alpha\alpha} - M_{\alpha a} M_{\alpha b}) \\
Q' &= \omega (L_{aa} R_\alpha + L_{\alpha\alpha} R_a - M_{ab} R_\alpha) \\
S' &= Q' \\
X &= A_a A_b - B^2 - \omega^4 (M_{ab} L_{\alpha\alpha} - M_{\alpha a} M_{\alpha b})^2 + \omega^2 M_{ab}^2 R_\alpha^2 \\
Y &= (A_a + A_b) B + 2\omega^3 M_{ab} R_\alpha (M_{ab} L_{\alpha\alpha} - M_{\alpha a} M_{\alpha b}) \\
A_a &= R_a R_\alpha - \omega^2 (L_{aa} L_{\alpha\alpha} - M_{\alpha a}^2) \\
A_b &= R_a R_\alpha - \omega^2 (L_{aa} L_{\alpha\alpha} - M_{\alpha b}^2) \\
B &= \omega (L_{aa} R_\alpha + R_a L_{\alpha\alpha})
\end{aligned} \qquad \ldots 4.6$$

Further, for the present winding configuration, the general equation for instantaneous torque is in the form equal to

$$T_i = \frac{1}{2} [i_a \;\; i_b \;\; i_\alpha] \frac{d}{d\theta} \begin{bmatrix} 0 & 0 & M_{\alpha a} \\ 0 & 0 & M_{\alpha b} \\ M_{\alpha a} & M_{\alpha b} & 0 \end{bmatrix} \begin{bmatrix} i_a \\ i_b \\ i_\alpha \end{bmatrix} \qquad \ldots 4.7$$

with the usual conventions.

By substituting equation 4.2 in equation 4.7 and taking the time average of the instantaneous torque, the resulting static torque may be written in the following form.

$$T_{ab} = \frac{p\omega^2 L_{\alpha\alpha}}{R_\alpha^2+\omega^2 L_{\alpha\alpha}^2} \left|I_a\right|^2 \left| \sum_{n=1}^{\infty}\sum_{m=1}^{\infty} n\hat{M}_n \hat{M}_m \sin np\,\theta \cos mp\,\theta \right|$$

$$+\frac{p\omega^2 L_{\alpha\alpha}}{R_\alpha^2+\omega^2 L_{\alpha\alpha}^2} \left|I_b\right|^2 \left| \sum_{n=1}^{\infty}\sum_{m=1}^{\infty} n\hat{M}_n \hat{M}_m \sin np\,\overline{\theta-\lambda} \cos mp\,\overline{\theta-\lambda} \right|$$

$$+\mathrm{Re}\left[\frac{j\omega p I_a^* I_b}{R_\alpha+j\omega L_{\alpha\alpha}}\right] \left| \sum_{n=1}^{\infty}\sum_{m=1}^{\infty} n\hat{M}_n \hat{M}_m \sin np\,\theta \cos mp\,\overline{\theta-\lambda} \right|$$

$$+\mathrm{Re}\left[\frac{j\omega p I_a^* I_b}{R_\alpha+j\omega L_{\alpha\alpha}}\right] \left| \sum_{n=1}^{\infty}\sum_{m=1}^{\infty} n\hat{M}_n \hat{M}_m \cos np\,\theta \sin mp\,\overline{\theta-\lambda} \right| \qquad \ldots 4.8$$

where 'Re' is used to represent the 'Real Part of ...' and '*' indicates the conjugate of the current phasors. It can be seen from these equations that although analytical results can be achieved they are of such a complexity that it is difficult to make deductions from them. They can however be computed very easily in the usual way.

The various machine winding parameters used in the above expressions were predicted by extending the techniques already discussed in chapter 2. In the following section the actual measured and computed parameters are shown. After this the comparison between the computed and the measured static torques are discussed.

4.2.3 COMPARISON BETWEEN THE COMPUTED AND MEASURED PARAMETERS

The stator and rotor self inductances of the test model as well as the mutual inductances between them were calculated during one-phase-on studies in chapter 2 at 75 volts excitation. They therefore apply for the present work and are included in table 4.1 for completeness. In addition, the mutual inductance between the two stator phase windings, M_{ab}, is also shown. This was calculated from the following relationship and the expression is written below by referring to figure 2.4 in chapter 2.

$$M_{ab} = \left[\sum_{101}^{300} B_A(N) + \sum_{121}^{320} B_A(N) + \sum_{141}^{280} B_A(N) \right] \frac{N_s l_s r_s \frac{\pi}{2} p}{180} \qquad \ldots 4.9$$

The functions $B_A(N)$, represent the resultant flux density wave due to A stator phase winding and is given by the equation 2.7 in chapter 2. The summation limits correspond to the positions of the individual coils in B phase stator winding, since the prototype machine has three coils in each stator phase (figure 2.3).

The predicted values are in close agreement with measurements - typically within 5% - as shown in table 4.1. (Although the method of measuring M_{ab} gave its amplitude but not its sign, the computed value showed it to be negative. This is the expected result because it is well known that the mutual inductance between two phases of a three phase winding is negative.)

TABLE 4.1

	V_a	R_a	R_α	L_{aa}	$L_{\alpha\alpha}$	M_{ab}
Measured values	75 V	4.3 Ω	8.0 Ω	0.23 H	0.32 H	0.087 H
Predicted values	.	.	.	0.237H	0.326H	-0.091H

Further the measured and predicted values of the mutual inductances between the A phase stator winding and the α-axis rotor winding, $M_{\alpha a}$, at a given supply voltage equal to 75 volts has already been shown in figure 2.7. Also, the harmonic contents of this mutual inductance for the predicted values were given in table 2.3. Those values are being used here. Furthermore, the mutual inductance, $M_{\alpha b}$, between the B phase stator winding and the α-axis rotor is measured with respect to the rotor position at the same excitation voltage and is shown in figure 4.2. $M_{\alpha b}$ is the same as $M_{\alpha a}$ in amplitude but shifted in phase as defined by equation 4.2. It can be seen that they agree with the predicted values. The predicted values were obtained from the following

expression which is written by referring to figures 2.4 and 2.5. That is,

$$M_{ab} = \left\{ \sum_{\theta+15+1}^{165} B_B(N) + \sum_{\theta-15+1}^{195} B_B(N) + \sum_{\theta+15+2}^{165} B_B(N) + \sum_{\theta-15+2}^{195} B_B(N) + \ldots\ldots + \ldots\ldots + \ldots\ldots + \ldots\ldots + \sum_{\theta+15+15}^{165} B_B(N) + \sum_{\theta-15+15}^{195} B_B(N) \right\} \frac{2l_r N_r r_r \frac{\pi}{2} p}{15 \times 180} \quad \ldots 4.10$$

where $B_B(N)$ is the resultant stator flux density wave linking with the α-axis rotor winding and is given by equation 2.7 in chapter 2.

4.2.4 COMPARISON OF THE PREDICTED AND MEASURED TORQUE/ANGLE CHARACTERISTIC

In figure 4.3 the predicted values of the static torque, T_{ab}, given by equation 4.8 are plotted against the rotor position for 42 harmonic components of the mutual inductances. There are three different curves shown in this figure. These are the time average values of the pulsating torque produced at any given rotor position. Curves 1 and 2 illustrate the measured results and the results predicted when the harmonic spectrum up to the 42nd harmonic of the mutual inductances is taken into account. It can be seen that there is very close agreement, the prediction follows the complex torque angle characteristic almost precisely.

Curve 3 is a set of predicted results where the fundamental component only of the mutual inductance is taken into account. That is, it is assumed that all windings are sinusoidally distributed in space. It was found in chapter 2 and 3 that this was a inadequate description of the machine behaviour and here again the characteristic is shown to depart radically from measured results.

In addition to the above characteristic, the winding currents are plotted against rotor position in figures 4.4, 4.5 and 4.6 using the current equations 4.3, 4.4 and 4.5, respectively. The predicted values were again for 42 harmonic

components of the space mutuals. These values show good agreement with the respective measured current variations. The current variations calculated from the fundamental components of inductance do not depart greatly from the measured values and yet the predicted stator torque values for the same conditions were quite different as seen in figure 4.3 above.

4.2.5 DISCUSSIONS

In figure 4.3, by applying the usaul sign convention for the static torque,i.e., positive torque producing the rotor movement in the clockwise direction and the negative torque in the anticlockwise direction, it can be seen that for curves (1) and (2) there are two stable torque-zero positions, points 'b' and 'd', and two unstable torque-zero positions, points 'a' and 'c'. These points are for the torque/angle curve spread of 180 electrical degrees starting from $p\theta = 0$ degree, which is in fact the plane of A phase stator winding as in figure 4.1(a).

Now by considering the rotor positions as depicted in figures 4.1(a) and 4.1(b) in conjunction with the curves (1) and (2) in figure 4.3, it can be seen that both the minimum and the maximum flux linkage positions of the rotor correspond to stable torque-zero points. Also, clearly the unstable torque-zero positions 'a' and 'c' are in the region between the planes of A and B phase stator windings. In addition to this the complete torque/angle curve for $p\theta$ between 0 and 180 electrical degrees shows an asymmetrical torque/angle distribution. This is generally not suitable for continuous stepping operation as seen in the later part of this section. Therefore, by comparing the torque/angle characteristic and the extreme flux linkage positions of the rotor for gp excitations it can be concluded that, here in the test machine there are some observations which are contrary to each other. They are:

(1) The presence of the stable torque-zero position apparently at both the maximum and the minimum flux linkage points in case of two-phase-on excitation. Whereas in one-phase-on excitation, the maximum flux linkage position was identified as an unstable position and the minimum one as a stable torque-zero point.

(2) The asymmetry in torque/angle distribution.

Now, by focussing the attention towards curve (3) in figure 4.3, which is the

predicted static torque/angle curve for fundamental mutual inductance distribution above, it is clear that point 'b' has been transformed to an unstable torqe-zero position, and incidentally point 'd' remains as a stable position and points 'a' and 'c' are totally absent. This curve has equal restoring torque and is symmetrical throughout the rotor position. Also, it coincides with the observations made earlier in chapter 2 with the one-phase-on situation. This is because, in figure 4.1(a), the rotor being at stable torque-zero position, any current in the rotor coil, would produce an mmf in space quadrature with the stator mmf which hence becomes the best 'torque angle' position. Unfortunately, there is no flux linkage in this position and hence no induced voltage and no current flow. If the rotor is disturbed slightly from this symmetrical position, then restoring torque is produced and this is therefore the stable torque-zero position. In figure 4.1(b) the rotor is shown in the position of maximum flux linkage and hence maximum induced voltage and current. However here the 'torque angle' is zero so no torque is again produced. By comparison between these two and the one-phase-on excitations, this maximum flux linkage position, hence becomes the unstable torque-zero position. Then the complete transfer from the unstable to stable torque-zero position, point 'b', in the actual static torque/angle characteristic may have been produced due to the combined effect of some of the predominant harmonic contents of the mutual inductance distribution.

To consolidate this viewpoint, in figure 4.7 the static torque/angle curve is drawn using the predicted static torque equation 4.8 by considering both the fundamental and the third harmonic components (i.e., for n=1 and n=3) of the mutual inductance distribution. Since the third harmonic component is more dominant one after the fundamental, as quoted in table 2.3 only these two components were considered while plotting the torque values. Comparing the shape of this torque/angle curve with that obtained for 42 harmonic components, it is clear that it is the combined effect of the first and the third harmonic which has been giving this rather peculiar shape.

Further, in order to see the inadequecy of the general shape of the torque/angle characteristic, figure 4.3, for continuous stepping operation figure 4.8 has been drawn for AB, BC and CA windings excited at a time. A close examination of this figure shows that for the excitation sequence AB, BC, CA, AB, ... so on alternate higher and lower peak torque regions are involved. This

produces a reduction in the maximum pull-out torque capabilities of the machine.

4.3 TWO PHASE EXCITATION IN THE MODIFIED INDUCTION STEPPER MOTOR

4.3.1 INTRODUCTION

In this section, at first steady state analysis of the two-phase-on model of the $\alpha\beta$-axis rotor is presented. The physical model used here has been sketched in figure 4.9 with the rotor at a given arbitrary position, $p\theta$. The analysis is centered on predicting the static torque/angle characteristic, so that the two-phase-on, full-mode and also half-mode-stepping operation can be understood.

4.3.2 STEADY STATE ANALYSIS

By using the same analytical process as presented in the previous section the equation for the steady state static torque is derived from the instantaneous electromagnetic torque of the model shown in figure 4.4. The instantaneous electromagnetic torque, T_i, for this type of model is however of the general form equal to

$$T_i = \frac{1}{2}[i_a \;\; i_b \;\; i_\alpha \;\; i_\beta] \frac{d}{d\theta} \begin{bmatrix} 0 & 0 & M_{\alpha a} & M_{\beta a} \\ 0 & 0 & M_{\alpha b} & M_{\beta b} \\ M_{\alpha a} & M_{\alpha b} & 0 & 0 \\ M_{\beta a} & M_{\beta b} & 0 & 0 \end{bmatrix} \begin{bmatrix} i_a \\ i_b \\ i_\alpha \\ i_\beta \end{bmatrix} \qquad \ldots 4.11$$

By expanding the associated products in the above equation and taking the time average the resultant equation becomes

$$T_{ab} = \mathrm{Re}\, \overset{*}{I}_a \left| I_\alpha \frac{dM_{\alpha a}}{d\theta} + I_\beta \frac{dM_{\beta a}}{d\theta} \right| + \mathrm{Re}\, \overset{*}{I}_b \left| I_\alpha \frac{dM_{\alpha b}}{d\theta} + I_\beta \frac{dM_{\beta b}}{d\theta} \right| \qquad \ldots 4.12$$

The steady state values of the stator and rotor winding currents are obtained by solving the voltage equations from the following matrix equations.

$$\begin{bmatrix} V_a \\ V_b \\ 0 \\ 0 \end{bmatrix} = \begin{bmatrix} R_a + j\omega L_{aa} & j\omega M_{ab} & j\omega M_{\alpha a} & j\omega M_{\beta a} \\ j\omega M_{ab} & R_b + j\omega L_{bb} & j\omega M_{\alpha b} & j\omega M_{\beta b} \\ j\omega M_{\alpha a} & j\omega M_{\alpha b} & R_\alpha + j\omega L_{\alpha\alpha} & 0 \\ j\omega M_{\beta a} & j\omega M_{\beta b} & 0 & R_\alpha + j\omega L_{\alpha\alpha} \end{bmatrix} \begin{bmatrix} I_a \\ I_b \\ I_\alpha \\ I_\beta \end{bmatrix} \quad \text{... 4.13}$$

For the present case,

$$V_a = V_b \ , \quad R_a = R_b \quad \text{and} \quad L_{bb} = L_{aa}$$

The stator and rotor winding currents are

$$I_a = \frac{V_a (R_\alpha + j\omega L_{\alpha\alpha})(R' + jS')}{X + jY} \quad \text{... 4.14}$$

$$I_b = \frac{V_a (R_\alpha + j\omega L_{\alpha\alpha})(P' + jQ')}{X + jY} \quad \text{... 4.15}$$

$$I_\alpha = \frac{-V_a \, j\omega[(M_{\alpha a} R' + M_{\alpha b} P') + j(M_{\alpha a} S' + M_{\alpha b} Q')]}{X + jY} \quad \text{... 4.16}$$

$$I_\beta = \frac{-V_a \, j\omega[(M_{\beta a} R' + M_{\beta b} P') + j(M_{\beta a} S' + M_{\beta b} Q')]}{X + jY} \quad \text{... 4.17}$$

with

$$\begin{aligned}
P' &= A_a - (C - \omega^2 M_{ab} L_{\alpha\alpha}) \\
R' &= A_b - (C - \omega^2 M_{ab} L_{\alpha\alpha}) \\
Q' &= B - \omega M_{ab} R_\alpha \\
S' &= Q' \\
X &= A_a A_b - B^2 - C(C - 2\omega^2 M_{ab} L_{\alpha\alpha}) + (R_\alpha^2 - \omega^2 L_{\alpha\alpha}^2)\omega^2 M_{ab}^2 \\
Y &= (A_a + A_b)B - 2\omega M_{ab} R_\alpha (C - \omega^2 M_{ab} L_{\alpha\alpha}) \\
A_a &= R_a R_\alpha - \omega^2 (L_{aa} L_{\alpha\alpha} - \overline{M_{\alpha a}^2 + M_{\beta a}^2}) \\
A_b &= R_a R_\alpha - \omega^2 (L_{aa} L_{\alpha\alpha} - \overline{M_{\alpha b}^2 + M_{\beta b}^2}) \\
B &= \omega (L_{aa} R_\alpha + L_{\alpha\alpha} R_a) \\
C &= \omega^2 (M_{\alpha a} M_{\alpha b} + M_{\beta a} M_{\beta b})
\end{aligned} \quad \text{... 4.18}$$

and the mutual inductances, $M_{\alpha a}$, $M_{\beta a}$ and $M_{\alpha b}$ are given by equations 2.24, 3.5 and 4.2 respectively. On similar grounds the expression for $M_{\beta b}$ can be written down as follows.

$$M_{\beta b} = \sum_{n=1}^{\infty} \hat{M}_n \cos np\,(\theta - \lambda - \frac{\pi}{2}) \qquad \text{... 4.19}$$

After substituting the appropriate current and mutual inductance equations in equation 4.11, the general torque equation becomes,

$$T_{ab} = \frac{p\,\omega^2 L_{\alpha\alpha} V_a^2 (R'^2 + S'^2)}{X^2 + Y^2} \left\{ \sum_{n=1}^{\infty}\sum_{m=1}^{\infty} n\hat{M}_n \hat{M}_m \sin np\,\theta \cos mp\,\theta \right.$$

$$\left. + \sum_{n=1}^{\infty}\sum_{m=1}^{\infty} n\hat{M}_n \hat{M}_m \sin np\,\overline{\theta - \frac{\pi}{2}} \cos mp\,\overline{\theta - \frac{\pi}{2}} \right\}$$

$$+ \frac{p\,\omega^2 L_{\alpha\alpha} V_a^2 (P'^2 + Q'^2)}{X^2 + Y^2} \left\{ \sum_{n=1}^{\infty}\sum_{m=1}^{\infty} n\hat{M}_n \hat{M}_m \sin np\,\overline{\theta - \lambda} \cos mp\,\overline{\theta - \lambda} \right.$$

$$\left. + \sum_{n=1}^{\infty}\sum_{m=1}^{\infty} n\hat{M}_n \hat{M}_m \sin np\,\overline{\theta - \lambda - \frac{\pi}{2}} \cos mp\,\overline{\theta - \lambda - \frac{\pi}{2}} \right\}$$

$$+ \frac{p\,\omega V_a^2 [\omega L_{\alpha\alpha}(R'P' + Q'^2) + R_\alpha (P' - R')Q']}{X^2 + Y^2}$$

$$\left\{ \sum_{n=1}^{\infty}\sum_{m=1}^{\infty} n\hat{M}_n \hat{M}_m \sin np\,\theta \cos mp\,\overline{\theta - \lambda} \right.$$

$$\left. + \sum_{n=1}^{\infty}\sum_{m=1}^{\infty} n\hat{M}_n \hat{M}_m \sin np\,\overline{\theta - \frac{\pi}{2}} \cos mp\,\overline{\theta - \lambda - \frac{\pi}{2}} \right\}$$

$$+ \frac{p\,\omega V_a^2 [\omega L_{\alpha\alpha}(R'P' + Q'^2) + R_\alpha (P' - R')Q']}{X^2 + Y^2}$$

$$\left\{ \sum_{n=1}^{\infty}\sum_{m=1}^{\infty} n\hat{M}_n \hat{M}_m \sin np\,\overline{\theta - \lambda} \cos mp\,\theta \right.$$

$$\left. + \sum_{n=1}^{\infty}\sum_{m=1}^{\infty} n\hat{M}_n \hat{M}_m \sin np\,\overline{\theta - \lambda - \frac{\pi}{2}} \cos mp\,\overline{\theta - \frac{\pi}{2}} \right\} \qquad \text{... 4.20}$$

The above equation is again a complex function of rotor position and hence from this it is difficult to make general conclusions. However, for given values of the machine parameters the plot of steady state static torque with respect to

rotor position, say between 0 and 180 electrical degrees gives useful information. This is done after comparing the predicted values of the mutual inductance $M_{\beta b}$ with the experimental values since all other mutual inductances such as $M_{\alpha a}$, $M_{\alpha b}$ and $M_{\beta a}$ were already done in the previous section

4.3.3 COMPARISON BETWEEN THE PREDICTED AND MEASURED MUTUAL INDUCTANCE DISTRIBUTION, $M_{\beta b}$

The mutual inductance values between B phase stator winding and the β-axis rotor winding is predicted based on similar predictions discussed in chapter 2. By referring to figures 2.4 and 2.5, $M_{\beta b}$ is expressed as follows in terms of the known machine dimensions and the resultant flux density wave $B_B(N)$.

$$M_{\beta b} = \left\{ \sum_{\theta+15+90+1}^{165+90} B_B(N) + \sum_{\theta-15+90+1}^{195+90} B_B(N) + \sum_{\theta+15+90+2}^{165+90} B_B(N) + \sum_{\theta-15+90+2}^{195+90} B_B(N) + \ldots\ldots + \ldots\ldots - \ldots\ldots + \ldots\ldots + \sum_{\theta+15+90+15}^{165+90} B_B(N) + \sum_{\theta-15+90+15}^{195+90} B_B(N) \right\} \frac{2l_r N_r r_r \frac{\pi}{2} p}{15\times 180} \qquad \ldots 4.21$$

As before, equation 4.21 is plotted against rotor position in figure 4.10. The experimental points are also shown in the same figure. These results show that, as expected, at 120 electrical degrees there is zero mutual inductance and at 30 electrical degrees it is maximum. Thus $M_{\beta b}$ is displaced by 120+90 electrical degrees away from the plane of A phase stator winding.

The fundamental component of space variation of this mutual inductance is also shown in figure 4.10. Although it is very close to the actual values, the full harmonic series has been used, because as found previously in sections 2.4, 3.3 and 4.2 the harmonic components contributed to the production of torque.

4.3.4 STATIC TORQUE/ANGLE CHARACTERISTIC

In figure 4.11 torque equation 4.20 is plotted against rotor position between 15 and 105 electrical degrees, curve (2), where suitable torque measurement were obtained. As the torque/angle cycle is symmetrical throughout the rotor/stator periphery, it was found sufficient to observe the shape of any given torque/angle cycle. Therefore it was decided to plot one such cycle between the two unstable torque-zero positions as in the above figure. The experimental points are also shown in the same figure, curve(1), for over the same torque/angle cycle as the predicted one. It can be seen that the two curves (1) and (2) show considerable agreement in general shape although the peak measured torque is around 15% less than predicted.

The predicted values in the above figure were obtained by using 42 harmonic components of the space mutuals. As before, if the fundamental component only of the mutual inductance values, were used then there is no torque as shown by curve (3). Also, it has been found using a computer programme for equation 4.20 that the torque is zero for all other odd harmonic components when considered one at a time. Thus by implication, as was with one phase-on excitation, here also there appears no torque for a sinusoidal mutual inductance distribution. Furthermore, the marked difference that exist between curve (3) of figure 4.3 and that of figure 4.11 may be again predominantly due to the combined effect of first and the third harmonic components. This is evident from figure 4.12 in which curve 2 represents the predicted torque/angle characteristic under the present of first and the third harmonic components. Whereas curves (1) and (3) are similar to those of figure 4.11.

In addition to this figures 4.13 to 4.16 are plotted to represent winding current variations with respect to rotor position for 42 harmonic components as well as for fundamental component only. Measured values are also plotted in the same figures. It can be seen that the modulation of the two stator currents with rotor position in figures 4.13 and 4.14 is quite pronounced although the depth of modulation of the measured current is less than the predicted. If fundamental components of mutual inductance only were used, then the stator current modulation would be expected to be zero, and the predicted result using this assumption confirms this. The rotor currents characteristics shown in figures 4.15 and 4.16 are quite complex although measured and predicted

results agree very well in both magnitude and shape. The results if all non-fundamental harmonics are excluded are also shown.

4.3.5 SEQUENTIAL STEPPING OPERATION

4.3.5.1 Full-mode-stepping operation

In this section the features of torque/angle characteristics which are relevant to two-phase-on excitation are examined further for continuous stepping operation.

To observe the appropriate switching of stator phase windings for continuous stepping operation torque/angle characteristics in figure 4.17 has been shown with pairs of windings excited sequentially in the order AB, BC, CA . . . etc.

With reference to figure 4.9 it can be seen that this sequence produces clockwise rotation while the sequences AB, CA, BC, AB, ... etc., produces anticlockwise movement. The principal features of this torque characteristic are summarised in table 4.2. It can be seen that the torque characteristic with continuous stepping now appears to be quite good, with the pull-in torque being some 70% of the average pull-out torque. This compared with the same ratio being 20% for one-phase-on excited with the $\alpha\beta$ rotor. Ideally this ratio would be 100%.

TABLE 4.2: Principal features of T/θ characteristics for two-phase-on excitation of an $\alpha\beta$-axes rotor

Sl. No.	Items	Predicted values
1	Peak static torque, $T_{pk\,\alpha\beta}$	2.1 Nm
2	Average torque	
	(a) Actual values	1.22 Nm
	(b) Expression	0.57 $T_{pk\,\alpha\beta}$
3	$\frac{dT}{d\theta}$ at equilibrium position	6.4 Nm/rad
4	Step angle	30.0 elec. deg.
5	Maximum pull-out torque, T_{po}	
	(a) Actual values	1.44 Nm
	(b) Expression	0.67 $T_{pk\,\alpha\beta}$
6	T_{max}	1.0 Nm
7	Ripple torque around pull-out torque as a percentage of pull-out torque	+46.0 % -31.0 %

4.4 THREE-PHASE-ON EXCITATION USING $\alpha\beta$-WINDING ROTOR

4.4.1 INTRODUCTION

The principle associated with the three-phase-on stepping operation. in broad terms, is not very different in comparison with the previous two types of one and two-phase-on excitations. In those scheme of excitations each time, some phase windings were left unexcited. This means, that not all the built in machine hardware is being used while stepping each time. Taking this into account the steady state analysis to predict the static torque/angle characteristic with three-phase-on excitation has been described below on similar grounds as in the previous chapters.

A conventional polyphase machine uses m phases (where m usually equals three), which are distributed in space by $\frac{2\pi}{m}$ radians. This ideally produces a rotating field of constant amplitude. In the present case we have a conventional three phase winding from which the maximum pulsating field is required, and for which the in-phase voltages are applied to each stator winding. The stator windings need to cooperate as shown in figure 4.18 and this is obtained by reversing the direction of excitation of one of the windings, as denoted by $A^{+}B^{+}\bar{C}$ say.

4.4.2 STEADY STATE STATIC PERFORMANCE

The distribution of the steady state static torque against rotor position for any particular type of excitation, for example, $A^{+}B^{+}\bar{C}$ is obtained from the following analysis which is the extension of the previous work to the present model.

Referring to the schematic arrangement of the machine shown in figure 4.18, the modelling equations are written in matrix form as below.

$$\begin{bmatrix} V_a \\ V_b \\ V_c \\ 0 \\ 0 \end{bmatrix} = \begin{bmatrix} R_a + j\omega L_{aa} & j\omega M_{ab} & j\omega M_{ac} & j\omega M_{\alpha a} & j\omega M_{\beta a} \\ j\omega M_{ab} & R_b + j\omega L_{bb} & j\omega M_{bc} & j\omega M_{\alpha b} & j\omega M_{\beta b} \\ j\omega M_{ac} & j\omega M_{bc} & R_c + j\omega L_{cc} & j\omega M_{\alpha c} & j\omega M_{\beta c} \\ j\omega M_{\alpha a} & j\omega M_{\alpha b} & j\omega M_{\alpha c} & R_\alpha + j\omega L_{\alpha\alpha} & 0 \\ j\omega M_{\beta a} & j\omega M_{\beta b} & j\omega M_{\beta c} & 0 & R_\alpha + j\omega L_{\alpha\alpha} \end{bmatrix} \begin{bmatrix} I_a \\ I_b \\ I_c \\ I_\alpha \\ I_\beta \end{bmatrix} \quad \text{... 4.22}$$

In the case of present studies,

$$V_a = V_b = V_c$$
$$R_a = R_b = R_c$$
$$L_{aa} = L_{bb} = L_{cc}$$

From equations 4.22 the rotor winding currents, I_α and I_β are expressed in terms of the stator phase currents as

$$I_\alpha = \frac{-j\omega(M_{\alpha a} I_a + M_{\alpha b} I_b + M_{\alpha c} I_c)}{R_\alpha + j\omega L_{\alpha\alpha}} \quad \text{... 4.23}$$

$$I_\beta = \frac{-j\omega(M_{\beta a} I_a + M_{\beta b} I_b + M_{\beta c} I_c)}{R_\beta + j\omega L_{\beta\beta}} \quad \text{... 4.24}$$

In order to determine the stator winding currents, the voltage equations of the stator phase windings alone are extracted from equation 4.22 and are then rearranged in conjunction with equations 4.23 and 4.24 such that the resulting equations appear in a simple matrix form as shown below.

$$\begin{bmatrix} P_a & Q_b & R_a \\ Q_a & P_b & Q_c \\ R_a & Q_c & P_c \end{bmatrix} \begin{bmatrix} I_a \\ I_b \\ I_c \end{bmatrix} = \begin{bmatrix} S_a \\ S_a \\ S_a \end{bmatrix} \quad \text{... 4.25}$$

where

$$P_a = A_a + jB$$
$$P_b = A_b + jB$$
$$P_c = A_c + jB$$
$$Q_a = C_{ab} + jD_a$$
$$Q_b = C_{ab} + jD_a$$
$$Q_c = C_{bc} + jD_b$$

$$
\begin{aligned}
R_a &= C_{ac} + jD_c \\
S_a &= V_a (R_\alpha + j\omega L_{\alpha\alpha}) \\
A_a &= R_a R_\alpha - \omega^2 (L_{aa} L_{\alpha\alpha} - \overline{M_{\alpha a}^2 + M_{\beta a}^2}) \\
A_b &= R_a R_\alpha - \omega^2 (L_{aa} L_{\alpha\alpha} - \overline{M_{\alpha b}^2 + M_{\beta b}^2}) \\
A_c &= R_a R_\alpha - \omega^2 (L_{aa} L_{\alpha\alpha} - \overline{M_{\alpha c}^2 + M_{\beta c}^2}) \\
B &= \omega (L_{aa} R_\alpha + L_{\alpha\alpha} R_a) \\
C_{ab} &= \omega^2 [M_{\alpha a} M_{\alpha b} + M_{\beta a} M_{\beta b} - M_{ab} L_{\alpha\alpha}] \\
C_{bc} &= \omega^2 [M_{\alpha b} M_{\alpha c} + M_{\beta b} M_{\beta c} - M_{bc} L_{\alpha\alpha}] \\
C_{ac} &= \omega^2 [M_{\alpha a} M_{\alpha c} + M_{\beta a} M_{\beta c} - M_{ac} L_{\alpha\alpha}] \\
D_a &= \omega M_{ab} R_\alpha \\
D_b &= \omega M_{bc} R_\alpha \\
D_c &= \omega M_{ac} R_\alpha \\
M_{ac} &= -M_{ab} \\
M_{bc} &= -M_{ab}
\end{aligned}
\qquad \text{... 4.26}
$$

After simplification the stator winding currents are obtained from equations 4.25 and 4.26 and they are written as

$$
I_a = \frac{S_a}{\Delta} [P_b P_c - Q_c^2 + Q_c (R_a + Q_b) - (Q_b P_c + R_a P_b)] \qquad \text{... 4.27}
$$

$$
I_b = \frac{S_a}{\Delta} [P_a (P_c - Q_c) - (Q_a P_c - R_a Q_c) + R_a (Q_a - R_a)] \qquad \text{... 4.28}
$$

$$
I_c = \frac{S_a}{\Delta} [P_a (P_b - Q_c) - Q_b (Q_a - R_a) + (Q_a Q_c - R_a P_b)] \qquad \text{... 4.29}
$$

with

$$
\Delta = \begin{vmatrix} P_a & Q_b & R_a \\ Q_a & P_b & Q_c \\ R_a & Q_c & P_c \end{vmatrix} \qquad \text{... 4.30}
$$

Also, based on similar techniques described earlier, in chapter 2 the instantaneous electro-magnetic torque developed is given by the following equation.

$$T_i = \frac{1}{2}[i_a \;\; i_a \;\; i_c \;\; i_\alpha \;\; i_\beta] \; \frac{d}{d\theta} \begin{vmatrix} 0 & 0 & 0 & M_{\alpha a} & M_{\beta a} \\ 0 & 0 & 0 & M_{\alpha b} & M_{\beta b} \\ 0 & 0 & 0 & M_{\alpha c} & M_{\beta a} \\ M_{\alpha a} & M_{\alpha b} & M_{\alpha c} & 0 & 0 \\ M_{\beta a} & M_{\beta b} & M_{\beta c} & 0 & 0 \end{vmatrix} \begin{bmatrix} i_a \\ i_b \\ i_c \\ i_\alpha \\ i_\beta \end{bmatrix} \qquad \ldots 4.31$$

Then expressing equations 4.27, 4.28 and 4.29 in terms of real and imaginary parts, they are written in simple form as,

$$\begin{aligned} I_a &= I_{ar} + jI_{ai} \\ I_b &= I_{br} + jI_{bi} \\ I_c &= I_{cr} + jI_{ci} \end{aligned} \qquad \ldots 4.32$$

For the stator phase winding displacement shown in figure 4.18, the various mutual inductance corresponding to any position, θ, of the rotor are

$$\begin{aligned} M_{\alpha a} &= \sum_{n=1}^{\infty} \hat{M}_n \cos np\,\theta \\ M_{\alpha b} &= \sum_{n=1}^{\infty} \hat{M}_n \cos np\,\overline{\theta - \lambda} \\ M_{\alpha c} &= \sum_{n=1}^{\infty} \hat{M}_n \cos np\,\overline{\theta - \frac{\lambda}{2}} \\ M_{\beta a} &= \sum_{n=1}^{\infty} \hat{M}_n \cos np\,\overline{\theta - \frac{\pi}{2}} \\ M_{\beta b} &= \sum_{n=1}^{\infty} \hat{M}_n \cos np\,\overline{\theta - \lambda - \frac{\pi}{2}} \\ M_{\beta c} &= \sum_{n=1}^{\infty} \hat{M}_n \cos np\,\overline{\theta - \frac{\lambda}{2} - \frac{\pi}{2}} \end{aligned} \qquad \ldots 4.33$$

Finally, by substituting equations 4.32 and 4.33 in the rotor winding current equations, 4.23 and 4.24 and then substituting the resulting equations in the steady state value of the torque obtained from equation 4.31, a general expression for the torque follows which is equal to

$$T_{abc} = \frac{p\,\omega^2 L_{\alpha\alpha}}{R_\alpha^2 + \omega^2 L_{\alpha\alpha}^2} \left| I_a \right|^2 \left[\sum_{n=1}^{\infty} \sum_{m=1}^{\infty} n \hat{M}_n \hat{M}_m \left\{ \sin np\,\theta \cos mp\,\theta + \sin np\,\overline{\theta - \frac{\pi}{2}} \cos mp\,\overline{\theta - \frac{\pi}{2}} \right\} \right]$$

$$+\frac{p\,\omega^2 L_{\alpha\alpha}}{R_\alpha^2+\omega^2 L_{\alpha\alpha}^2}\left|I_b\right|^2\left|\sum_{n=1}^{\infty}\sum_{m=1}^{\infty} n\hat{M}_n\,\hat{M}_m\left\{\begin{array}{l}\sin np\,\overline{\theta-\lambda}\,\cos mp\,\overline{\theta-\lambda}\\ +\sin np\,\overline{\theta-\lambda-\frac{\pi}{2}}\,\cos mp\,\overline{\theta-\lambda-\frac{\pi}{2}}\end{array}\right\}\right|$$

$$+\frac{p\,\omega^2 L_{\alpha\alpha}}{R_\alpha^2+\omega^2 L_{\alpha\alpha}^2}\left|I_c\right|^2\left|\sum_{n=1}^{\infty}\sum_{m=1}^{\infty} n\hat{M}_n\,\hat{M}_m\left\{\begin{array}{l}\sin np\,\overline{\theta-\frac{\lambda}{2}}\,\cos mp\,\overline{\theta-\frac{\lambda}{2}}\\ +\sin np\,\overline{\theta-\frac{\lambda}{2}-\frac{\pi}{2}}\,\cos mp\,\overline{\theta-\frac{\lambda}{2}-\frac{\pi}{2}}\end{array}\right\}\right|$$

$$+p\frac{\omega^2 L_{\alpha\alpha}I_{abr}-\omega R_\alpha I_{abi}}{R_\alpha^2+\omega^2 L_{\alpha\alpha}^2}\left|\sum_{n=1}^{\infty}\sum_{m=1}^{\infty} n\hat{M}_n\,\hat{M}_m\left\{\begin{array}{l}\sin np\,\theta\,\cos mp\,\overline{\theta-\lambda}\\ +\sin np\,\theta-\frac{\pi}{2}\,\cos mp\,\overline{\theta-\lambda-\frac{\pi}{2}}\end{array}\right\}\right|$$

$$+p\frac{\omega^2 L_{\alpha\alpha}I_{abr}+\omega R_\alpha I_{abi}}{R_\alpha^2+\omega^2 L_{\alpha\alpha}^2}\left|\sum_{n=1}^{\infty}\sum_{m=1}^{\infty} n\hat{M}_n\,\hat{M}_m\left\{\begin{array}{l}\sin np\,\overline{\theta-\lambda}\,\cos mp\,\theta\\ +\sin np\,\overline{\theta-\lambda-\frac{\pi}{2}}\,\cos mp\,\overline{\theta-\frac{\pi}{2}}\end{array}\right\}\right|$$

$$+p\frac{\omega^2 L_{\alpha\alpha}I_{acr}-\omega R_\alpha I_{aci}}{R_\alpha^2+\omega^2 L_{\alpha\alpha}^2}\left|\sum_{n=1}^{\infty}\sum_{m=1}^{\infty} n\hat{M}_n\,\hat{M}_m\left\{\begin{array}{l}\sin np\,\theta\,\cos mp\,\overline{\theta-\frac{\lambda}{2}}\\ +\sin np\,\overline{\theta-\frac{\pi}{2}}\,\cos mp\,\overline{\theta-\frac{\lambda}{2}-\frac{\pi}{2}}\end{array}\right\}\right|$$

$$+p\frac{\omega^2 L_{\alpha\alpha}I_{acr}+\omega R_\alpha I_{aci}}{R_\alpha^2+\omega^2 L_{\alpha\alpha}^2}\left|\sum_{n=1}^{\infty}\sum_{m=1}^{\infty} n\hat{M}_n\,\hat{M}_m\left\{\begin{array}{l}\sin np\,\overline{\theta-\frac{\lambda}{2}}\,\cos mp\,\theta\\ +\sin np\,\overline{\theta-\frac{\lambda}{2}-\frac{\pi}{2}}\,\cos mp\,\overline{\theta-\frac{\pi}{2}}\end{array}\right\}\right|$$

$$+p\frac{\omega^2 L_{\alpha\alpha}I_{bcr}-\omega R_\alpha I_{bci}}{R_\alpha^2+\omega^2 L_{\alpha\alpha}^2}\left|\sum_{n=1}^{\infty}\sum_{m=1}^{\infty} n\hat{M}_n\,\hat{M}_m\right.$$

$$\left.\left\{\sin np\,\overline{\theta-\lambda}\,\cos\overline{\theta-\frac{\lambda}{2}}\;+\sin np\,\overline{\theta-\lambda-\frac{\pi}{2}}\,\cos mp\,\overline{\theta-\frac{\lambda}{2}-\frac{\pi}{2}}\right\}\right|$$

$$+p\frac{\omega^2 L_{\alpha\alpha} I_{bcr} + \omega R_\alpha I_{bci}}{R_\alpha^2 + \omega^2 L_{\alpha\alpha}^2} \left[\sum_{n=1}^{\infty} \sum_{m=1}^{\infty} n \hat{M}_n \hat{M}_m \right.$$

$$\left. \left\{ \sin np\overline{\theta - \frac{\lambda}{2}} \cos\overline{\theta - \lambda} + \sin np\overline{\theta - \frac{\lambda}{2} - \frac{\pi}{2}} \cos mp\overline{\theta - \lambda - \frac{\pi}{2}} \right\} \right] \quad \text{... 4.34}$$

with

$$I_{abr} = I_{ar} I_{br} + I_{ai} I_{bi}$$
$$I_{abi} = I_{ar} I_{bi} - I_{ai} I_{br}$$
$$I_{acr} = I_{ar} I_{cr} + I_{ai} I_{ci}$$
$$I_{aci} = I_{ar} I_{ci} - I_{ai} I_{cr}$$
$$I_{bcr} = I_{br} I_{cr} + I_{bi} I_{ci}$$
$$I_{bci} = I_{br} I_{ci} - I_{bi} I_{cr}$$

Equation 4.34 appears to be far more complex than any other torque equations shown earlier. This equation has been programmed to observe the torque variation with respect to rotor position in the next section following this.

4.4.3 COMPARISON BETWEEN THE MEASURED AND THE PREDICTED PARAMETERS

Since the predicted parameters connected with the A, B and α, β windings have already been compared with the measured values, in this subsection only those which have appeared in the voltage equations due to the C-phase stator windings have been considered below. Their predicted values are obtained from the following equations.

$$M_{ac} = \left[\sum_{41}^{240} B_A(N) + \sum_{61}^{260} B_A(N) + \sum_{81}^{220} B_A(N) \right] \frac{N_s l_s r_s \frac{\pi}{2} p}{180} \quad \text{... 4.35}$$

$$M_{bc} = \left[\sum_{41}^{240} B_B(N) + \sum_{61}^{260} B_B(N) + \sum_{81}^{220} B_B(N) \right] \frac{N_s l_s r_s \frac{\pi}{2} p}{180} \quad \text{... 4.36}$$

$$M_{\alpha c} = \left\{ \sum_{\theta+15+1}^{165} B_C(N) + \sum_{\theta-15+1}^{195} B_C(N) \right.$$
$$+ \sum_{\theta+15+2}^{165} B_C(N) + \sum_{\theta-15+2}^{195} B_C(N)$$
$$+ \ldots\ldots + \ldots\ldots$$
$$+ \ldots\ldots + \ldots\ldots$$
$$\left. + \sum_{\theta+15+15}^{165} B_C(N) + \sum_{\theta-15+15}^{195} B_C(N) \right\} \frac{2l_r N_r r_r \frac{\pi}{2} p}{15 \times 180} \qquad \ldots 4.37$$

and

$$M_{\beta c} = \left\{ \sum_{\theta+15+90+1}^{165+90} B_C(N) + \sum_{\theta-15+90+1}^{195+90} B_C(N) \right.$$
$$+ \sum_{\theta+15+90+2}^{165+90} B_C(N) + \sum_{\theta-15+90+2}^{195+90} B_C(N)$$
$$+ \ldots\ldots + \ldots\ldots$$
$$+ \ldots\ldots + \ldots\ldots$$
$$\left. + \sum_{\theta+15+90+15}^{165+90} B_C(N) + \sum_{\theta-15+90+15}^{195+90} B_C(N) \right\} \frac{2l_r N_r r_r \frac{\pi}{2} p}{15 \times 180} \qquad \ldots 4.38$$

where $B_A(N)$, $B_B(N)$ and $B_C(N)$ were flux density waves which were defined already in chapter 2.

By solving equations 4.45 to 4.48 with the help of the computer the following results were obtained.

$M_{ac} = +0.0913H$
$M_{bc} = +0.0913H$
$M_{\alpha c}$ – *as shown in figure* 4.19
$M_{\beta c}$ – *as shown in figure* 4.20

The results shown above for M_{ac} and M_{bc} are same in magnitude but positive in sign when compared to M_{ab} because of the well known reasons. Also, the predicted values of $M_{\alpha c}$ and $M_{\beta c}$ show better agreement with the measured as was the case before with the other mutual inductance values. In

addition to this the fundamental components for both the mutual inductances are shown so as to compare the developed torque

* when all the harmonics are present

* when the higher order harmonics other than the fundamental are absent.

4.4.4 COMPARISON BETWEEN THE PREDICTED AND THE MEASURED STATIC PERFORMANCE CURVES

In figure 4.21, curve (2) represents the steady state static torque values as obtained from equation 4.44 against rotor position between two unstable torque-zero positions. As was the case with two-phase-on excitation of $\alpha\beta$ rotor, here also the remaining torque/angle cycles are identical to that shown in figure 4.21.

Curve (1) represents the measured values and is seen to have the general agreement with the predicted shape of the curve. However, the predicted peak static torque is about 15% higher then the measured value. The stable torque-zero position is in agreement with those of the predicted curve.

When only fundamental components of the mutual inductances are considered, the predicted torque values {curve (3)} become zero as expected. Thus, the present excitation pattern has shown the same type of results as those shown earlier for one and two-phase-on excitations.

In figure 4.22, the curves (1) and (3) are reproduced and curve (2) is the predicted torque when only fundamental and the third harmonic component of the mutual inductance distributions are considered. From this figure, it is possible to conclude that, with the three-phase-on excitation torque is again produced mainly by the interaction of the first and third harmonic component of the mutual inductance distribution.

Figures 4.23 to 4.27 illustrate measured and predicted currents in the three stator phases and the two rotor windings. These are for the case illustrated in figure 4.18 where the C coil is reversed, as described in section 4 above. As the rotor position is moved the currents are modulated as shown. There is general agreement in shape and amplitude for all these currents, although the predicted

amplitudes tend to be lower than measured values by upto 20%. Results calculated assuming sinusoidal variations of mutual inductance are also included and demonstrate that the stator currents are not modulated, thus reinforcing the prediction of zero torque for their conditions.

It is interesting to note that the C coil current is different in shape and amplitude from the A and B coil currents. The reason for this can be deduced from the physical picture in figure 4.18 which shows that C is the middle coil. Coil A has mutual flux contributions for coil C, at 60° to it and coil B at 120° to it. Currents in coils A and B are expected to have similar maximum and minimum values and these were found to be the case. Coil C however has mutual flux contribution from coil A at 60° to it at coil B at 60°. Hence it has greater resultant mutual flux contribution from the other two coils, and the current in C is therefore less than in the other two.

4.4.5 SEQUENTIAL STEPPING

Continuous stepping can be obtained with three phases by changing the direction of current in appropriate phases in turn. The straightforward way of doing this is illustrated in figure 4.28(a) where the sequence is

$$A^+B^+\bar{C} \rightarrow \bar{A}B^+\bar{C} \rightarrow \bar{A}B^+C^+ \rightarrow \bar{A}\bar{B}C^+$$

This requires all three phases to have to be switched by semiconductors so that relative phase reversals are possible. This arrangement requires 4 devices per phase, giving a total of twelve devices.

It should be recognised however that as the field produced for any one pattern is pulsating then it is only the relative sense between phases and not the absolute sense that matters. Hence, as shown in figure 4.28(b) rotation of the pulsating field can also be produced by the sequence.

$$A^+B^+C^- \rightarrow A^-B^+C^- \rightarrow A^+\bar{B}\bar{C} \rightarrow A^+B^+\bar{C}$$

in which case C phase may be permanently connected to the supply so that only two phases need to be switched, requiring eight semiconductor devices. These aspects are considered in more detail in chapter 6 below.

The resulting torque pattern that is suitable for continuous rotation is shown in the usual way in figure 4.29 where the relevant torque parameters, T_{po} , T_{max} and $T_{pk\,\alpha\beta}$ are indicated.

A summary of the conditions obtainable with three-phase-on excitation is given in table 4.3.

TABLE 4.3: Principal features of T/θ characteristics for three-phase-on excitation of an $\alpha\beta$-axes rotor

Sl. No.	Items	Predicted values
1	Peak static torque, $T_{pk\,\alpha\beta}$	2.0 Nm
2	Average torque	
	(a) Actual values	1.04 Nm
	(b) Expression	0.52 $T_{pk\,\alpha\beta}$
3	$\frac{dT}{d\theta}$ at equilibrium position	4.7 Nm/rad
4	Step angle	30.0 elec. deg.
5	Maximum pull-out torque, T_{po}	
	(a) Actual values	1.11 Nm
	(b) Expression	0.56 $T_{pk\,\alpha\beta}$
6	T_{max}	0.6 Nm
7	Ripple torque around pull-out torque as a percentage of pull-out torque	+80.0 % -46.0 %

4.5 CONCLUSIONS

The main results from tables 3.1, 4.2 and 4.3 are summarised in table 4.4. Here, the main torque parameters may be compared for the different machine arrangements, namely one-phase-on, with α-axis rotor and $\alpha\beta$-axes rotor, two-phase-on with $\alpha\beta$-axes rotor and three-phase-on, with $\alpha\beta$-axes rotor. Also shown in Table 4.4 is the total I^2R loss in the stator plus rotor windings when the machines are producing the maximum average torque, known as the pull-out torque, T_{po}. This loss figure allows the torque parameters to be compared for equivalent conditions as the maximum output from a machine is ultimately limited by its temperature rise. The parameter T_{po}/watt has been used for this comparison.

The one-phase-on excitation of the α-axis rotor appears to give the best result, with 0.0251 Nm/watt. However, the stiffness about the equilibrium position, $dT/d\theta$ is very low and T_{max}, the maximum torque that it can start against is very low, at 0.16 Nm. These factors, combined with a high torque ripple were found in chapter 3 to make this arrangement unsuitable for most practical applications. Comparing the $\alpha\beta$-axes rotor for the one and two-phase-on methods of excitations, two-phase-on gives a slightly higher T_{po}/watt, namely 0.0113 Nm/watt compared to 0.0092 Nm/watt but in addition T_{max} per watt is about 60% greater at 0.0078 Nm/watt compared with 0.0047 Nm/watt and this improvement is reflected in the other parameters such as peak static torque and stiffness $dT/d\theta$.

When three-phase-on excitation is employed it appears that the torque parameters per watt all deteriorate compared with the two-phase-on excitation. Three-phase-on excitation does not therefore seem to show any benefits at this stage.

Of the four excitations considered therefore, two-phase-on excitation with an $\alpha\beta$-axes rotor gives the best overall results.

TABLE 4.4: Comparison between one, two and three-phases-on excitations

Sl. No.	Items	One-phase-on		Two-phase-on	Three-phase-on
		α-axis rotor	$\alpha\beta$-axes rotor	$\alpha\beta$-axes rotor	$\alpha\beta$-axes rotor
1	Maximum pull-out torque, T_{po} in Nm	0.73	0.73	1.44	1.11
2	T_{max} in Nm	0.16	0.37	1.0	0.6
3	Peak static torque in Nm	1.7	1.1	2.1	2.0
4	$\frac{dT}{d\theta}$ in Nm/rad	0.6	2.5	6.4	4.7
5	Torque ripple in %	+133.0 -78.0	+51.0 -49.0	+46.0 -31.0	+80.0 -46.0
6	Total copper loss at T_{po} in watts	29.0	79.0	128.0	207.0
7	T_{po} /watt	0.0251	0.0092	0.0113	0.0054

CHAPTER 5

TRANSIENT STUDIES

5.1 INTRODUCTION

It has been shown in the previous chapters that there is an equilibrium position for the rotor. This is where the torque acts to restore the rotor to this position if the rotor is disturbed in either direction. Typical conditions are sketched in figure 5.1.

Clearly an equilibrium position exist for any static load torques within the capability of the machine. If the rotor is disturbed from its equilibrium position and released it will normally return to the equilibrium position after a series of oscillations which depend upon the mechanical characteristics of the load system, especially its inertia.

The present chapter investigates the behaviour of the induction stepping motor under these present conditions. This type of positon response in stepping motor terminology, is often known as 'single step response'.

Many authors (16,17) have adopted different techniques to predict the single step response of d.c. stepper motors. For example, in references 16 and 17 Lawrenson and Hughes and Robinson and Taft have analysed the position response of V.R. and P.M. stepping motors by linearising the machine modelling equations. These linearised modelling equations were converted from time domain to frequency domain and then the position response was obtained. Subsequent results were then used to represent the step response in terms of the known machine parameters. Similar analytical techniques to formulate and solve linearised small perturbation equations was also used by Rogers (18) to study the transient behaviour of conventional induction motors. The techniques used by above authors assumed small perturbations in the rotor and for d.c. stepper motors the oscillations were set up near the equilibrium position. However the approach on the basis of this assumption gives inaccurate position response for large rotor disturbances.

The alternative approach by the direct solution of complete set of non linear voltage and rotor dynamic equations is an ideal solution, but is very complex to solve. For the present machine, therefore, it was decided to predict the position response by means of numerical techniques. This is thought to be more reliable eventhough it does not give directly the significance of the various machine parameters. A technique based on numerical predictions has been used by Nishumira (19) for d.c stepper motors. Arockiasany (20) and Evans (10) used a numerical "step-by-step" method of solution of set of non-linear machine equations successfully to induction motors, single phase variable airgap reluctance motors and disc-geometry reluctance motors. Since there is, in principle, no difference between the equations of a conventional inductance machine and the present type of special induction machine the same general methods of solutions have therefore been used here in predicting the position response. The techniques involved in this method are now discused below in greater detail.

5.2 THE PHYSICAL MODEL

The machine model used for predicting the single-step response is the same as the one which was shown in figure 4.18. However, in figure 5.2 the rotor is shown at two different positions - the rotor windings sketched by thick lines at rotor position, $p\theta_0=45^o$, correspond to the rotor at the equilibrium position when only stator phase winding A is excited. Whereas, the rotor windings sketched by dotted lines at rotor position $p\theta_i$ represents the rotor at this position such that when it is released with only A stator phase winding excited, it undergoes few oscillations over the equilibrium position, $p\theta_0$ and finally comes to rest at $p\theta_0$. Thus $p\theta_i$ becomes the initial rotor position from where the rotor oscillations are set up and $p\theta_0$ the final steady position.

There is in essence no difference with two-phase-on excitation in setting up oscillations to observe the single step response. For this the equilibrium position, $p\theta_0$, is 60 electrical degrees and $p\theta_i$ is appropriately chosen while predicting the step response.

5.3 MODELLING EQUATIONS

At first a complete mathematical model of figure 5.2 for a 3-phase machine

is considered. From this it is in general, possible to obtain rotor position response for one and two-phase-on models, separately.

A complete mathematical model comprises of the following two parts

(i) The voltage equations representing the coupled circuit model of the machine.

(ii) The rotor dynamic equation, since there is a rotating mass, rotor to which the interchange of energy takes place from the electrical system.

The voltage equations are written by considering the voltage and currents as time dependent quantities. Thus, these equations in matrix form are given by

$$\begin{bmatrix} v_a \\ v_b \\ v_c \\ 0 \\ 0 \end{bmatrix} = \begin{bmatrix} R_a & 0 & 0 & 0 & 0 \\ 0 & R_b & 0 & 0 & 0 \\ 0 & 0 & R_c & 0 & 0 \\ 0 & 0 & 0 & R_\alpha & 0 \\ 0 & 0 & 0 & 0 & R_\beta \end{bmatrix} \begin{bmatrix} i_a \\ i_b \\ i_c \\ i_\alpha \\ i_\beta \end{bmatrix}$$

$$+ \frac{d}{dt} \begin{bmatrix} L_{aa} & M_{ab} & M_{ac} & M_{\alpha a} & M_{\beta a} \\ M_{ab} & L_{bb} & M_{bc} & M_{\alpha b} & M_{\beta b} \\ M_{ac} & M_{bc} & L_{cc} & M_{\alpha c} & M_{\beta c} \\ M_{\alpha a} & M_{\alpha b} & M_{\alpha c} & L_{\alpha\alpha} & 0 \\ M_{\beta a} & M_{\beta b} & M_{\beta c} & 0 & L_{\beta\beta} \end{bmatrix} \begin{bmatrix} i_a \\ i_b \\ i_c \\ i_\alpha \\ i_\beta \end{bmatrix} \quad \text{... 5.1}$$

The parameters used in the above matrix equations have been predicted and the techniques involved in the calculation are already shown in chapters 2, 3 and 4. The differential operator d/dt is used to operate on the product of inductance and current matrices.

The rotor dynamic equation is written by assuming zero viscous friction and zero load torque which is equal to

$$J\frac{d^2\theta(t)}{dt^2} + T_f = T_i \quad \text{... 5.2}$$

where

J = Rotor inertia in Kgs.

T_f = Frictional torque in Nm.

and T_i represents the instantaneous electromagnetic torque developed in the machine. Since the stator and rotor self inductances do not change with respect to the rotor position this developed torque is already shown in equation 4.31, chapter 4.

5.4 SOLUTION OF THE MODELLING EQUATIONS

The voltage equations given by equation 5.1 above may also be expressed in a single matrix form as follows.

$$[v]=[R][i]+\left\{\frac{d}{dt}[L][i]\right\} \qquad \ldots 5.3$$

where

$[v]$ = voltage matrix
$[R]$ = Resistance matrix
$[i]$ = Current matrix
$[L]$ = Inductance matrix

These matrices contain the appropriate circuit parameters of the machine and the individual elements of these matrices are however shown in equation 5.1 above.

To predict the motor performance it is now required to solve equation 5.3 for various winding currents for a given type of stator excitation voltage. From these winding currents the instantaneous torque developed by the machine can be predicted which when used in conjunction with equation 5.2 gives an estimate of the rotor positon response, $\theta(t)$. However, the solution of equation 5.3 is difficult and can be seen by expanding the product of inductance and current matrices as shown below.

$$[v]=[R][i]+\left\{[L]\frac{d[i]}{dt}+[i]\frac{d[L]}{dt}\right\} \qquad \ldots 5.4$$

$$=[R][i]+[L]\frac{d[i]}{dt}+[i]\frac{d[L]}{d\theta}.\frac{d\theta}{dt} \qquad \ldots 5.5$$

In the above equation there are three terms on the right hand side, each one representing the following components

(i) Resistive voltage drop

(ii) Voltages induced due to 'transformer action'

(iii) Voltages induced due to the rotor motion namely 'motional voltages'. This term is responsible for power conversion.

The third term, indicating the motional voltages contain the product of two differentials and therefore it introduces non-linearity in the above equation. Hence it is difficult to solve these equations by direct analytical methods.

In the numerical step-by-step method, solution of equation 5.5 considers initial and final position during each finite small time-step-interval. The method can be represented in mathematical form by rewriting equation 5.3 as below

$$\frac{[v]'+[v]''}{2}=[R]\left\{\frac{[i]'+[i]''}{2}\right\}+\frac{[L]''[i]''-[L]'[i]'}{\delta t} \qquad \ldots 5.6$$

or

$$[i]''=\frac{\frac{[v]'+[v]''}{2}-\frac{[R][i]'}{2}+\frac{[L]'[i]'}{\delta t}}{\frac{[R]}{2}+\frac{[L]''}{\delta t}} \qquad \ldots 5.7$$

where the superscripts ' and " indicate the electrical quantities at the beginning and end of the time-step-interval, δt. Also, the time derivative of the function $[L][i]$ has been expressed in finite difference form and other functions such as $[v]$ and $[i]$ are averaged over the same time-step-interval. The inductance matrix $[L]$ has been considered to change at the end of the interval. This is clearly to incorporate the position dependency of the mutual inductance since the position in turn is a function of time when rotor movement takes place.

The principle of numerical step-by-step method as seen from equation 5.6 involves initially the collection of the required parameters for the first time-step-interval. After this, the current matrix, $[i]''$, is evaluated from equation

5.7 at the end of the interval by using the known parameters which were prevailing at the beginning of the same interval. For the next immediate time interval the values which were calculated at the end of the previous interval were considered as the initial values. This operation is carried out to the remaining successive time intervals for the duration of the total period under consideration.

A close examination of equation 5.7 shows that the inductance matrix $[L]''$ is required when the winding currents have to be predicted at the end of each time interval. The mutual inductances which are present in the inductance matrix depend on the rotor position which in turn depends on the instantaneous torque developed by the machine. This torque is again a function of motor winding currents. Thus each one of them is inter-related and therefore the numerical prediction needs further careful examination.

In reference 10 the solution of the above equation was undertaken on two basis - (1) Steady state solution and (2) Transient solution. The problem connected with the present study is, on the whole again categorised as above. This is because, the steady state solution is useful mainly to know the first initial conditions when the rotor was held at position θ_i.

5.4.1 STEADY STATE SOLUTION

In this method of solution, the machine performance can be predicted at a fixed position, θ_i, by making $\frac{d\theta}{dt}$ in equation 5.5 equal to zero. The fixed rotor position introduces no time dependency on the inductance matrices, thus making the denominator of equation 5.7 determinable from the mutual inductance values at position, θ_i. By using the predicted results of equation 5.7 at the end of the interval into the torque equation 4.31, instantaneous values of the developed torque can be obtained. The average value of this over a definite time period then gives the average static torque.

The above technique, at first was used to predict the static torque in order to compare with the analytical techniques discussed in chapters 2.4. Figure 5.3 shows the flowchart of the programme which was written in Fortran 77 for Multics operating system. The same programme structure was however extended later for the transient studies also. In figure 5.4 the predicted results

of the steady state torque from the above two techniques are compared for one-phase-on, excitation of an $\alpha\beta$-axes rotor. The analytical prediction involved 42 harmonics and in the numerical approach the time-step-interval, δt, was chosen to be equal to 0.5 ms.

The comparison between the two curves show very good agreement with each other which therefore gives some confidence in both methods of solving the machine equations. This method also extends for constant rotational speed of the rotor, when the rotor position, and hence the inductance values are known at the end of each step interval.

5.4.2 TRANSIENT SOLUTION

In the transient solution since the rotor is released from rest at position θ_i, to oscillate over the equilibrium position, the voltage equation, 5.7 must be solved in conjunction with equation 5.2 which defines the dynamics of the mechanical system. Hence, to develop the solution, equation 5.2 is rewritten in the following form by considering v' and v'' as the speed of the rotor at the beginning and end of the time-step-interval, δt

$$J\frac{v''-v'}{\delta t}=T_i-T_f \qquad \text{... 5.8}$$

By retaining v'' on the left hand side and transferring the remaining values to the right side of the above equation, v'' can be written as

$$v''=v'+\frac{\left\{T_i-T_f\right\}}{J}\delta t \qquad \text{... 5.9}$$

From this equation the rotor speed at the end of the interval can be obtained provided T_i is known. Then, the rotor position at the end of the interval, θ'', can be predicted from the following equation which is written from the equation $v=\frac{d\theta}{dt}$ for θ'' when θ' is the rotor position at the beginning of δt. Thus,

$$\frac{\theta''-\theta'}{\delta t}=\frac{v''+v'}{2}$$

or

$$\theta''=\theta'+\left\{\frac{v''+v'}{2}\right\}\delta t \qquad \text{... 5.10}$$

The method of transient solution is, in general based on iterative process. The value of T_i in equation 5.9 is not possible to calculate unless the winding currents at the end of the interval $[i]''$ are known. This in itself is difficult because of the intrinsic physical non-linearity present in the predictive equation 5.7 due to $[L]''$. Therefore an approximate estimate of the value of T_i must be made by extrapolating from the results of previous time-step-intervals. However, the procedure involved in the complete transient solution is discussed below.

(i) For the first time-step-interval the first estimate is made from the instantaneous torque calculated during the steady state solution. The estimation from the steady state condition is useful because when the rotor is about to be released from position θ_i it is held at rest and the torque is pulsating. The instant at which it is going to be released is the instant from where the transient solution should begin. Hence for the rotor to start moving away from θ_i (i.e., at t=0) the instantaneous torque could be anywhere between the maximum (positive) and minimum (negative) values of the steady state pulsating torque characterstic.

(ii) Using the estimated torque values at the end of the time-step-interval along with the remaining known parameters namely T_f , J , δt and v' the rotor speed v'' is calculated from equation 5.9. Here v' at t=0 is zero.

(iii) The rotor angle at the end of the interval is then obtained from equation 5.10. Here θ' at t=0 is θ_i .

(iv) The matrix $[L]''$ is therefore known.

(v) Using $[L]''$ thus calculated above into equation 5.7, $[i]''$ is determined. Consequently the instantaneous torque is calculated and then compared with the estimated value as in (i) above. When this value is the same as the estimated value to within 1%, the next time-step-interval is selected. Otherwise, the new value is inserted into step (i) above, and the iteration is repeated until the test is found to be satisfacory. After selecting the

new time-step-interval the values calculated at the end of the previous interval are used as the new initial values and the computation is repeated from step (ii) to (v) until the rotor oscillations have ceased.

A flow chart describing all these steps is shown in figure 5.4. Also table 5.1 show the measured values of rotor inertia and frictional torque.

TABLE 5.1

Parameters	Measured values
Rotor inertia	3.82×10^{-3} Nm sec^2/rad^2
Frictional torque	0.0334 Nm

5.5 COMPARISON BETWEEN PREDICTED AND EXPERIMENTAL RESULTS

The experimental work was carried out on the test machine for one- and two-phase-on excitations using $\alpha\beta$-axes rotor. A servo potentiometer was used to record the rotor oscillations. These oscillations were set up in the manner described in section 5.2 above.

Figure 5.6 shows the predicted and experimental values of the rotor position against time for one-phase-on excitation. Here, θ_i=31 electrical degrees. The predicted response show the rotor settling time of 1.1 secs as against the measured value of 1.0 secs and are indicated in the figure. This implies that the predicted rotor oscillations have ceased in as much at the same time as the actual measured oscillations.

In addition to the agreement with the settling times, it can also be seen however, that the predicted and measured envelopes of the decaying rotor oscillations compare with good accuracy. This means therefore that the amplitudes of the rotor oscillations appear to have been predicted within 5% accuracy with the present numerical solution. The frequency of the damped rotor oscillations agree within about 25%, the theoretical value is 278 mS and measured is 211 mS. This difference leads to an accumulated error between the

measured and predicted rotor oscillations, but it is clear that there is good overall agreement between the two curves.

In figures 5.7, 5.8 and 5.9 the predicted oscillograms of the stator and rotor winding currents are shown. Figure 5.10 show the measured oscillograms of the various winding currents mentioned above along with the measured position response. All these curves were recorded using a digital storage oscilloscope-Nicolet. By comparing the predicted oscillograms from figures 5.7, 5.8 and 5.9 with the corresponding measured current oscillograms, it can be concluded that the overall trend is correctly predicted by the theory eventhough the actual period of oscillations are not quite the same. In figures 5.11, 5.12 and 5.13 the positive and negative peak amplitudes of the above current oscillograms are plotted with respect to time. In the same figures the corresponding peak to peak amplitudes of the measured current oscillograms are also plotted against time, to compare them. As expected the predicted and measured envelopes are not in phase, and also as found in the steady state performance curves in figures 3.6, 3.7 and 3.8, the peak amplitudes of the predicted currents are about 15% less than those measured.

In figure 5.14 the predicted values of the rotor speed is shown against time. The predicted values of the pulsating torques are also shown in figure 5.15 against time. Here, from these two figures it can be clearly seen that when the average value of the pulsating torque is maximum the speed is zero. That is, always at these points the rotor would have reached to its one end of the peak position in its oscillating period, and thereafter is attemptingto change the course of direction from its previous one.

The measurements were also done for two-phase-on excitations by exciting usual A and B stator phase windings together and releasing the rotor from rest at 14 electrical degrees away from the equilibrium position. The recorded rotor oscillations are shown in figure 5.16 in which the predicted values are also shown against time. The comparison between these two curves are given in table 5.2.

	Predicted	Measured
Settling time in seconds	3.8	3.7
Period of first oscillating cycle in mS	152	116

Here also the agreement is good as far as the settling time and envelope of the oscillating rotor amplitudes are concerned, but again the period of the oscillating cycle appear to show around 25% difference.

5.6 CONCLUSIONS

An accurate computer model which was described in sections 5.3 and 5.4 has been shown to be capable of predicting the transient motor position response when released from a given rotor position. This method does not give design criteria for the motor performance, but is particularly useful, though not essential for simulating the transient behaviour of the motor. A digital computing facility is an essential tool to perform the full numerical computations involved. In addition to the present method it supplements further work with regard to the prediction of motor behaviour such as multiphase sequential excitation under various stepping rates, predicting the damping performance etc. Since in these cases, the basic numerical computation is on similar grounds as explained in this chapter, and say for multiphase sequential excitation, the introduction of the excitation of the other two phases with proper considerations in switching times, can predict the rotor speed and torque. Similarly, to proceed with damping studies, the work needs to be modified to include appropriate input parameters depending on viscous or frictional damping.

CHAPTER 6

A SIMPLE DRIVE SYSTEM FOR ONE, TWO, AND ALL THREE-PHASE-ON EXCITATIONS

6.1 INTRODUCTION

Following early work on d.c. stepper motors, detailed studies have emerged at various levels with regard to their drive circuits as well as their control techniques (1,5,21). The fundamental switching strategy used for the new induction stepping motor proposed here is, in principle, similar to that used for d.c. stepping motors. In that windings are excited in turn in order to step the rotor around.

As described earlier, in order to step the machine it is required that the stator phase windings A, B and C are energised by connecting each phase windings in sequence to an a.c. voltage source. Bidirectional power switches are needed for this and a pair of naturally commutated back to back thyristors are suitable. For the present work a triac was used as this combines the function of two thyristors. This type of controller is low cost and reliable and is thought to be one of the potential advantages of the a.c. stepper motor system. The system for one static winding is shown in figure 6.1.

To provide the various drive configurations that have been described in chapter 2 to 3 which require one, two and three phase sequential switching stages of different sorts, a Z-80 based microprocessor system was used to generate the trains of unidirectional gate pulses to the triacs. This arrangement is most suitable for the research work as it produces a flexible system and minimises the proliferation of control electronics.

The description of the power electronics equipment and its associated control and auxiliary circuits is given below.

6.2 DESCRIPTION OF THE INTERFACING CIRCUIT

The logic circuit discussed in this section is one of the many ways of developing an appropriate interfacing circuit between the microprocessor and the power switching device. This circuit, as shown in figure 6.2, incorporates zero-level detection of the supply voltage and frequency multiplication. Although the former feature has no useful application for one and two-phase-on excitations, its presence is required to ensure that all the control timing signals are always in synchronism with the supply voltage for three-phase-on operation.

6.2.1 ZERO LEVEL DETECTION CIRCUIT

The purpose of this circuit is to detect the zero-cross over points of the sinusoidal supply voltage. A 240/12 volts centre-tapped transformer is used, as shown in figure 6.2, to sense the supply voltage, provide isolation from the mains and lower its level to a convenient value. The output of the transformer is firstly rectified and then its peak is regulated to 5 volts using a zener diode, BZX79C. figure 6.3(a) to (e) show the actual voltage signals at various points in this circuit and hence clearly illustrate its operation also.

The positive going edge of an output pulse from the transistor BC108, as illustrated in figure 6.3(c), occurs slightly earlier than the zero-cross over point of the supply voltage. However, the combination of two Schmitt trigger gates, 74LS14, in figure 6.2, with a resistor and a capacitor provide the necessary delay for these pulses. Thus, the final output of the zero-level detector is shown in figure 6.3(a), which is clearly in phase with the zero-cross over points of the supply voltage and is also of 100 Hz frequency.

These 100 Hz unidirectional pulses are used to trigger a triac of high frequency firing pulses to ensure reliable operation of the triacs. These high frequency pulses were generated at 10 KHz using a phase-locked loop, as described below.

6.2.2. FREQUENCY MULTIPLIER CIRCUIT

A self contained CMOS phase-locked loop, CD4046B, is used here in this

part of the circuit in conjuction with two other CMOS divide-by-N counters, HEF4018B, as shown in figure 6.2. A 555 timer operating on monostable mode provides an adjustable duty cycle and also, required 'fan out' for the input signals to the phase-locked loop. Before this, the input signals to the trigger point, pin 2, of the timer have to be inverted since the state of the timer output reaches high only at the falling edge of the trigger signal. This is done by using another transistor, BC108, at the input side of the timer, which also makes the signal compatible to the timer for a common 10 volts supply rail. The output of the timer available at pin 3 is of variable duty cycle and is coupled directly to the phase-locked loop at pin 14. Furthermore, the high state of the timer output is adjusted to around 50 percent duty cycle by merely varying a 22 kilo ohms resistor connected between pin 7 and the +10 volts supply point, since this is rquired to maximise the frquency 'lock range' of the phase-locked loop. Now, the operation of the phase-locked loop can be understood from the following block diagram approach.

Figure 6.4 is a block diagram of the frequency multiplier circuit mentioned above. Two divide-by-10 counters are connected between the phase detector and the voltage controlled oscillator, VCO, circuits, thus completing the loop. The input signal frequency to the phase-locked loop is compared to the output frequency of the second divide-by-ten counter in a built in phase detector circuit. The output of the phase detector is now a voltage signal which is a measure of the phase difference between the two inputs. Furthermore, this voltage signal is filtered, amplified and finally used to control the frequency of the VCO so that the VCO will remain locked to the input frequency. The VCO output is a locally generated frequency and in this particular case is fixed at its centre frequency equal to 100 times the input frequency.

The VCO centre frequency is arranged to be 100 times the input frequency by fixing the values of R_1 and C_1 in figure 6.2 such that, $R_1=100K\,\Omega$ and $C_1=0.001\mu f$, since these external components directly determine the centre frequency of the VCO. The component values of the loop-filter, $R_3=4.7K\,\Omega$, $R_4=150k\,\Omega$ and $C_2=10\mu f$ in figure 6.2, are set empirically. The two potentiometers shown in this multiplier circuit are adjusted until the VCO frequency always remains locked to the input frequency. The VCO output available at pin 4 of CD4046B is now at the desired 10 KHz frequency locked to the supply voltage and hence is routed to the next stage. In the next immediate

stage a transistor, BC108, with its collector connected to the +5 volts point is used to interface the VCO signal with the subsequenct TTL gates.

Thus, having generated pulses of 10 KHz frequency in synchronism with the excitation voltage, it is appropriate now to describe the algorithms. This is done in the following section for various types of excitations.

6.3 DESCRIPTION OF THE ALGORITHMS

A block diagram of the complete system representing the interfacing circuit discussed so far is shown in figure 6.5. In this, the parallel input/output chip (PIO) of the Z-80 microprocessor is represented by a block and only the selected output lines are shown. Understanding of this block diagram is helpful while discussing the algorithms. The pins representing 'A_0 to A_7' correspond to 8 bits in port A and is preset to operate only on mode 0 (output mode) basis. In port B, only two bits namely B_0 and B_7 are used. This latter port is also preset but in this case to operate on control mode.

To synchronise the PIO output with the supply voltage, which is required for three-phase-on operation, the pulses from the zero-level deterctor are routed to bit 'B_0' of the PIO. Further, bit 'B_7' is used to deactivate the output from port A whenever required merely by pulling bit B_7 to ground.

Now, programming the microprocessor requires programming this PIO chip itself, so as to control the switching operation. For one-phase-on operation, the generated timing signals are to be such that the turn-on of one stator phase coincides with the turn-off of the previous stator phase. figure 6.6 shows the required timing signals for one-phase-on operation. Similarly, figures 6.7 and 6.8 show the timing signals for two-phase-on and half stepping operation. The excitation frequency for each of these operations is shown below the timing diagrams.

Figure 6.9 illustrates briefly the algorithms specially prepared to execute the above switching profiles. In this figure the program flow described for one-phase-on excitation is used also for two-phase-on and half-stepping operations by merely changing the specific values of the data. Here it is the value of the constant DAT.

For one and two-phase-on operations as well as the half-stepping operation a total of only three triacs are used - one for each stator phase winding. For this reason it is sufficient to activate only three bits of the PIO, say A_0, A_1 and A_2 with only 1's and 0's depending upon which triac or triacs are required to be switched on or off.

These 1's and 0's are represented in hexadecimal codes beneath each set of timing diagrams in figure 6.6 to 6.8. For one and two-phase-on excitations, it can be clearly seen that the repetition of a given number occurs after every three steps, whereas for half-stepping operation, it is after every six steps.

These numbers are continuously transmitted by the microprocessor to the external circuits through the PIO and the delay between the successive transitions are monitored by the 'key board scan' routine. Each time a key is pressed the step interval is reduced by 10 mS, thus increasing the stepping rate.

The algorithms shown in full in figure 6.9 are for the one-phase-on and three-phase-on cases as these are different. The half-stepping and two-phase-on algorithms are very similar to the one-phase-on case.

6.4 SWITCHING TECHNIQUE INVOLVED IN THREE-PHASE-ON EXCITATION

In chapter 4 it was shown that three-phases-on excitation could be performed by following the excitation patterns in the sequence, $\bar{A}B^{+}\bar{C}, A^{+}B^{+}\bar{C}, A^{+}\bar{B}\bar{C}, \bar{A}B^{+}\bar{C}, \cdots$ etc., which does not require phase reversal of winding C and this reduces the number of solid state devices required. In the present case the A and B phase windings were given this phase reversal.

To cater for this, the A and B phase windings are each fed from the output of a four triac bridge as shown in figure 6.10. In this figure the triacs are numbered T_0 to T_7 and their corresponding gate drive circuits derive the firing signals from the PIO terminals A_0 to A_7 respectively. In this arrangement there are no switches for the C phase winding. The phase commutation is performed by firing the commutating triacs in accordance with the switching signals generated by the microprocessor.

Such typical timing signals with 1's and 0's are shown in figure 6.11. In this figure the supply voltage waveform as well as the resultant supply current waveform for continuous stepping at a particular stepping rate are also shown. Clearly, the lines such as A_0 and A_1, A_2 and A_3, $\overline{A}_4$ and A_5 and A_6 and A_7, corresponding to the triacs T_0 and T_1, T_3, T_4 and T_5, T_6 and T_7, must always have level '0' output for over half the period of the supply frequency, 10 mS, in this case, so that no two triacs conduct together at the same time and short the supply. This occurs always at the phase reversal points. Therefore, to protect the present circuit against the possibility of short circuit failure, the zero voltage points are sensed at these critical points and a preset delay of 25 mS was added for safety.

A much more sophisticated drive could be designed to sense the current zero points and then initiate the phase reversal process instantaneously. This would reduce the likelihood of short circuit failures and avoid the delay at the phase reversal points. A shorter delay is helpful in order to run the machine at higher stepping rates. This technique was not however pursued further in the present work.

Furthermore, the algorithm of figure 6.9 mentioned in section 6.3 can now be discussed in conjuction with the timing diagrams. Here the output from the PIO during one step interval is divided into two groups. One of them is for the whole step interval in which the actual data propagated from the PIO on to the gate circuits is DAT - its values for different step intervals are shown beneath the timing diagrams in figure 6.11. The second group of data deposited on this bus, is DATO, which is output to prevent any short circuit failures at the phase reversal points.

The required delay at these phase reversal points is done in a special way. First, a delay count of say, 3, is initialised. Then the processor is alerted to track the contents in bit B_0. Soon after '1' is encountered, meaning that the supply voltage has just crossed its zero point, the computer is further instructed to wait for 5 more milliseconds after this, and then the message in the form of data, DATO, is transmitted to the gate bus until the delay count becomes 3. On the other hand, the first group of data, DAT, is output in a way similar to that adopted for the previous types of excitations. Here also the motor speed is varied by using a similar 'key board scan' routine as mentioned

earlier.

The triac triggering circuits now receive the output of both the PIO and the frequency multiplier circuit. Using a 3-input AND gate, 74 LS11, these signals are combined to give a train of short pulses with 10 KHz frequency over a duration specified by the switching signals from the PIO. This train of pulses arriving regularly one after another at the triac gate ensures that the device switches on and is the method commonly adopted rather than using a constant d.c. signal. Here the buffer, 74 LS07, is used to supply the required amount of gate current to switch the triac.

The drive circuits and software techniques described above could also be extended quite simply to provide drive signals for particular operating sequences, such as the intermittent forward and backward rotation through an arc which is typical of valve or switch operation. This behaviour was demonstrated successfully for a range of speeds and arc lengths.

CHAPTER 7

CONCLUSIONS

The work presented in this thesis has been concerned with an unusual form of machine, which is known as an induction stepping motor. This is a machine which may have advantages for some actuator applications but about which very little has been written. The Introduction, Chapter 1, therefore presented a preliminary discussion and description of the mahine.

Chapter 2 considered an existing form of the a.c. stepping motor which contains one stator winding and one rotor winding. A method of calculating the inductances of the machine was described which took account of individual coil positions. The mutual inductances were presented in terms of harmonic series so that mmf harmonics were taken into account. Slot permeance effects on the otherwise uniform airgap were excluded from consideration. The currents and torques of the motor were calculated for steady state conditions with sinusoidal voltage excitation by solving the voltage and torque equations. A steady state Torque-position characteristic was produced for the machine and it was shown to agree very closely with measurements. The shape of the torque-position curve for this configuration was found not to be ideal for a stepping motor because of a low stiffness ($\frac{dT}{d\theta}$) about the equilibrium position, and a low average torque.

An improved version of the machine was considered in Chapter 3 in which two windings in space quadrature were inserted in the rotor, and which in this thesis was called $\alpha\beta$-axes rotor. The analysis of Chapter 2 was extended to take the second rotor winding into account, and analysis of steady state conditions was also produced in the same way. This analysis demonstrated that zero torque would be produced if all windings - both stator and rotor were sinusoidaly distributed in space, because the machine then corresponds to a single phase induction motor which has zero starting torque. However the analysis also showed that torque was produced by interaction of the different harmonic components which described the variation of mutual inductance with rotor position. Production of steady state characteristics of this machine with

one stator winding excited were found to agree well with measurements, for both current and torque. The shape of this torque-position characteristic was better than for the α-axis rotor in that average torque was increased and the stiffness about the equilibrium position was also better. This was partly due to the fact that the step angle was halved with the $\alpha\beta$-axes rotor.

The behaviour of the motor with sequential excitation of the three stator coils, to give continuous stepping action, was also treated in Chapter 3 for both the α-axis and $\alpha\beta$-axes rotor windings. It was found that the $\alpha\beta$-axes rotor was to be preferred for its maximum starting torque and reduced torque ripple.

Chapter 4 investigated the performance of the machine when two stator phases were excited with α-axis rotor and $\alpha\beta$-axes rotors separately. It was found that the torque/angle distribution obtained for an α-axis rotor alone was asymmetrical over one complete cycle. The cause of this asymmetry was attributed to the non-sinusoidal mutual inductance distribution and was mainly due to the interaction of the first and third harmonics. The theory shows that an α-axis rotor can be used for continuous two-phase-on stepping operation when the stator and rotor windings are designed to have sinusoidal space distributions.

On the otherhand the steady state analysis of an $\alpha\beta$-axes rotor for two-phase-on excitation showed no asymmetry in torque/angle distribution. Also, from the analysis it was observed that this configuration developed torque due to the combined effect of first and the higher order harmonic components of the mutual inductance. Had there been sinusoidal winding distributions the torque developed would have been zero, as was observed with one-phase-on excitation of the same rotor.

In the test machine, it was also seen that a three-phase-on excitation of the $\alpha\beta$-axes rotor produced torque. The measurements were in agreement with predictions and also the torque/angle distribution was found to be favourable to step the rotor. However at this stage the merits of three-phase-on excitation were not found to be superior to one and two-phase-on excitation due to increased total copper loss.

A general comparision between all types of excitations studied in this thesis

was summarised in table 4.4. In that it was seen that the total power loss at the pull-out point with the two-phase-on scheme for $\alpha\beta$-axes rotor was found to be around 60% more than that of the one-phase-on excitation of the same rotor even though the pull torque was doubled. Also several other figures of merits such as maximum pull-out torque, maximum starting torque, stiffness of static torque/angle curve, ripple content of the torque during continuous stepping operatio and torque/watt ration have comparatively higher values for two-phase-on excitation. Thus, two-phase-on excitation has so far been identified as the best scheme for the experimental machine.

In Chapter 5 a numerical technique has been shown with which both steady state and transient behaviour of the machine was studied. The steady state results obtained from this numerical approach were compared with steady state results from the analytical methods in chapters 2, 3 and 4 and were found to be identical. Further, the numerical method was used to produce transient solutions for the single step response of the rotor. It was found that measured and predicted values of settling times and rotor oscillations agreed within 5%, the envelope of the oscillations of currents agreed within 15% and the frequencies of oscillations agreed within 25%. This technique is useful for simulating the steady state and transient behaviour of the machine.

In Chapter 6, a microprocessor controlled power electronics drive system was described. It was developed to produce the sequential stepping operation for the various types of excitations studied in this thesis. Triacs were used as the power switches. This solid state drive system was used successfully to demonstrate and measure the behaviour of the stepping motor.

This thesis has therefore presented an investigation of a.c. stepping motor and a method of analysis has been described which enables their behaviour to be predicted with some confidence. This provides a good basis for the next stage in the development of these machines which must concern optimum design techniques for them. Work is already in hand in this area. It is necessary for example to determine how to maximise the rotor torque by optimum winding design so that space harmonics contribute to the wanted torque characteristics in a positive way. In conjuction with this the power loss per unit torque must be assessed so that the maximum performance from a given frame size can be achieved. The possible use of rotor saliency to enhance the torque characteristic.

is also under consideration and the methods of analysis already described can be extended to include this effect. The use of capacitance in the rotor circuits is also being studied with a view to improving the rotor power factor and hence output torque.

Improved drive strategies are also being investigated with a view to improving the controllability of the machine without loosing the essential simplicity of the drive electronics.

APPENDIX A

MEASUREMENT OF SELF AND MUTUAL INDUCTANCES

A.1 OPEN CIRCUIT TEST ON STATOR SIDE

In this test the rotor windings were open circuits and the measurements were carried out on the phase A winding of the stator side using the circuit diagram shown in figure A.1 (a). Figure A.1 (b) is the equivalent circuit of figure A.1(a) which incorporates the no-load components (no load in this context means when the rotor windings are open). From figure A.1(b) the following equations can be written down.

$$R_a + R'_o = Z_{oa} \cos\phi_{oa} \quad \text{... A.1}$$

$$X_{la} + X'_m = Z_{oa} \sin\phi_{oa} \quad \text{... A.2}$$

with

$$Z_{oa} = \frac{V_{oa}}{I_{oa}} \quad \text{and} \quad \phi_{oa} = \cos^{-1}\frac{W_{oa}}{V_{oa} I_{oa}}$$

It is more convenient to use parallel equivalent of $R'_0 + jX'_m$ which is

$$X_m = \frac{R'^2_0 + X'^2_m}{X'_m} \quad \text{and} \quad R_0 = \frac{R'^2_0 + X'^2_m}{R'_0} \quad \text{... A.3}$$

A.2 SHORT CIRCUIT TEST ON STATOR SIDE

In this test the α-axis rotor windings are shorted. It was held at the maximum flux linkage position during the measurements and the meters were connected in the stator circuit. Figure A.2(a) and (b) show the connection diagram and its equivalent circuit respectively with all the rotor parameters being referred to the stator side. In mathematical terms the following relations are useful in separating the parameters.

$$R_a + R'_r = Z_{sa} \sin\phi_{sa} \quad \text{... A.4}$$

$$X_{la} + X'_{lr} = Z_{sa} \sin\phi_{sa} \quad \text{... A.5}$$

with

$$Z_{sa} = \frac{V_{sa}}{I_{sa}} \quad \text{and} \quad \phi_{sa} = \cos^{-1} \frac{W_{sa}}{V_{sa} I_{sa}}$$

The different winding resistances are measured by exciting the windings individually with direct current, equivalent to the rated alternating value. By assuming the stator leakage reactance to be equal to the referred rotor leakage reactance (i.e., $X_{la} = X'_{lr}$) and using the above relationships for both open circuit and short circuit test, X_m and X_{la} are calculated.

Asssuming the turns ratio as $K_r = \frac{N_r}{N_s}$, X_{lr} and X_{mr} in the rotor circuit are given by

$$X_{lr} = X'_{lr} K_r^2$$

$$X_{mr} = X_m K_r^2 \quad \text{... A.6}$$

Thus the measured values of the total stator and rotor self inductances are obtained from the following relationship.

$$L_{aa} = \frac{X_{ls} + X_m}{2\pi f} \quad \text{... A.7}$$

$$L_{\alpha\alpha} = \frac{X_{lr} + X_{mr}}{2\pi f} \quad \text{... A.8}$$

The mutual inductance $M_{\alpha a}$ between the stator and rotor windings is measured by measuring the open circuit induced voltage in the rotor winding at a particular rotor position. If $E_r(\theta)$ is this induced voltage and I_m is the true magnetising component of the stator winding current which develops a mutually linking flux between the stator and the rotor, then,

$$M_{\alpha a}(\theta) = \frac{E_r(\theta)}{\omega I_m} \quad \text{... A.9}$$

The separated parameters from the measured data at 75 volts excitation are shown in the main text.

REFERENCES

(1) Hughes, A.: 'Using stepping motors', Proc. of the first European conf. on electrical drives and motor controls, University of Leeds, July 1982, pp 109-23.

(2) Hassan, S.A., Mohammadein, A.L., El-Shanawany, M.M., and Diab, H.M.M.: 'Operation of modified induction motors as stepping motors. Comparison between different rotor types', J.Eng. Sci., University of Riyadh, Vol. 7, No. 2, pp 161-167 (1981).

(3) Dawson, C., and Bolton, H.R.: 'Performance prediction of a wide-angle limited motion rotory actuator', Proc. IEE, Vol. 125, No. 9, Sept 1978.

(4) Dawson, C., and Bolton, H.R.: 'Limited motion rotory actuators of the toroidal-stator, permanent-magnet rotor type', Proc. IEE, Vol. 129, Pt. B, No. 4, July 1982.

(5) Acarnley, P.P.: 'Stepping motors: a guide to modern theory and practice', IEE Control Engineering Series, No. 19.

(6) Winston Fenton.: 'Some aspects of the design and operation of a high-torque step motor', IEEE Trans., Vol. IA-10, No. 1, Jan/Feb 1974.

(7) Ferraris, P., Vagati, A., and Villata, F.: 'Inverter driven power step motors', Proc. of Int. Conf. on stepping motors and systems, University of Leeds, July 1976.

(8) Michio Nakano, Tadashi Inoue, and Kensuke Hasegawa.: 'The Alternating-magnetic-field-type step motor', Proc. of annual symposium on motion control systems and devices, University of Illinois, May 1977.

(9) Hore, D.L.: 'An A.C. Induction stepping motor', IEE Conf. publication; small and Special Electric Machines, Sept. 1981, No. 202.

(10) Evans, P.D.: 'Disc-Geometry Reluctance Motors', Ph.D Thesis 1977, Imperial College, London.

(11) Say, M.G.: 'Alternating Current Machines', Fourth Edition 1976, Pitman Publishing Ltd.

(12) Seely, S.: 'Electromechanical Energy Conversion', McGraw-Hill Book Company, Inc. 1962. London.

(13) Fitzerald, A.E., Kingsley, C., and Kusko.: 'Electric Machinery', Third Edition, 1971, Mc Graw-Hill Book Company, Inc. 1971.

(14) Fryett, M.L.: 'An Induction Stepping Motor', British Patent Application No. 8404213.

(15) Mestha, L.K.: 'An Induction Stepping Motor with Salient Poles', British Patent Application No. 8411779.

(16) Hughes, A., and Lawrenson, P.J.: 'Electromagnetic damping in stepping motors', Proc. IEE, Vol. 122, No. 8, Aug. 1975.

(17) Robinson, D.J., and Taft, C.K.: 'A dynamic analysis of magnetic stepping motors', IEEE Trans., IECI - 16, pp 111-125, Sept. 1969.

(18) Rogers, G.J., and Graduate, I.E.E.: 'Linearised analysis of induction motor transients', Proc. IEE, Vol. 122, No. 10, Oct. 1965.

(19) Nishimura, M., Murakami, Y., and Togashi, N.: 'Analysis of transient behaviour of step motor', ibid., 18, pp. 119-129, 1968.

(20) Arockiasamy, R.: 'Development and Analysis of Thyristor Controlled Induction Motors', Ph.D. Thesis 1969, Imperial College, University of London.

(21) Takashi Kenjo.: 'Stepping motors and their microprocessor controls', Monographs in electrical and electronic engineering, Clarendon Press, Oxford 1984.

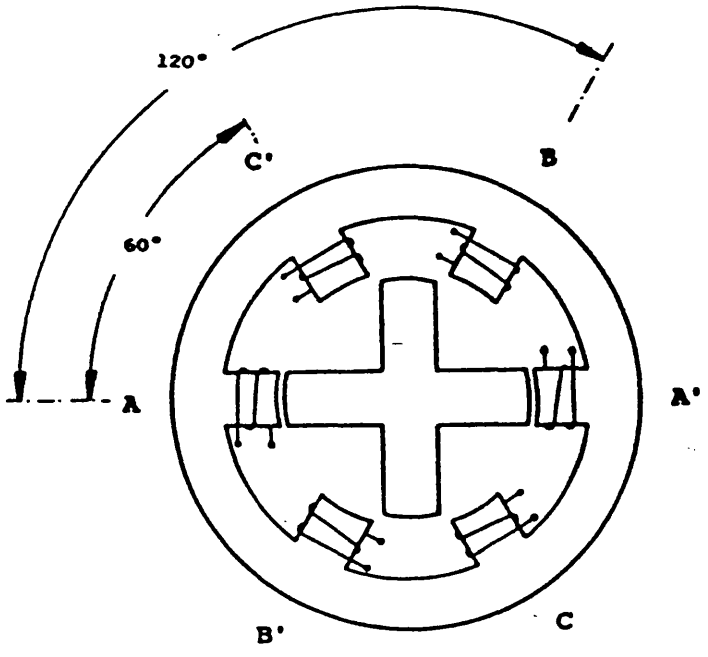

Fig. 1.1 Variable-Reluctance stepping motor

A-A' B-B' C-C' Stator windings

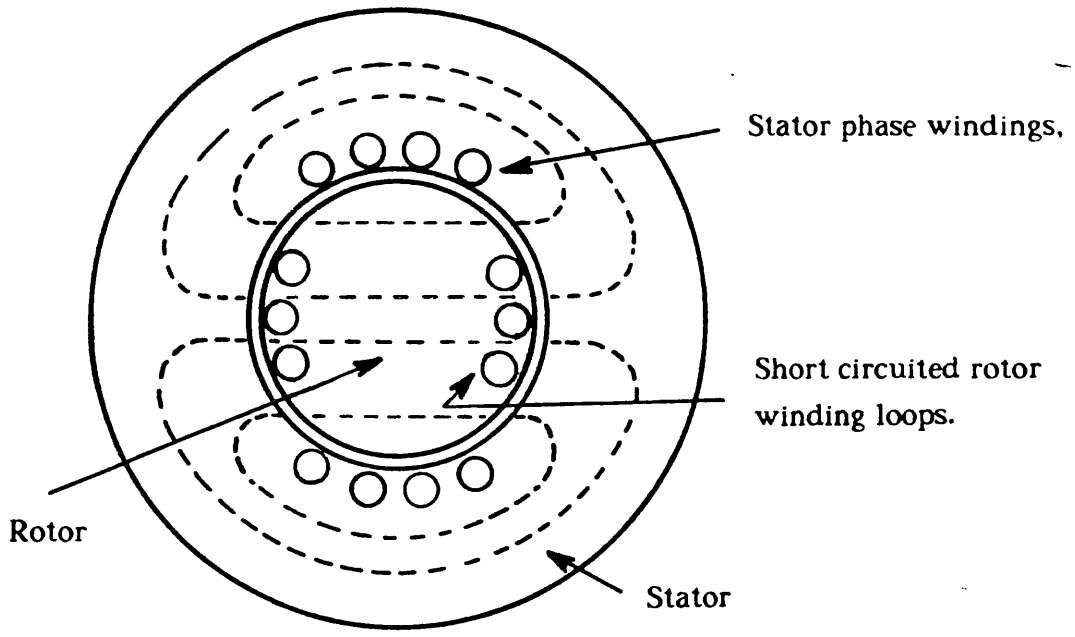

Fig. 1.2 Hore's Model: Existing a.c. stepper motor
at stable torque-zero position

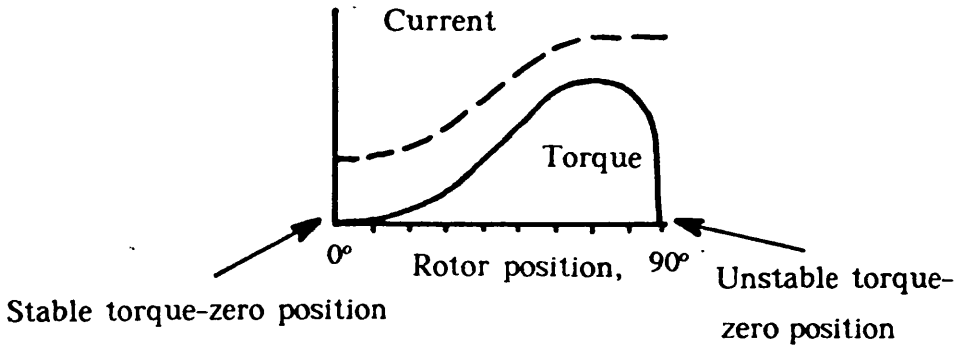

Fig. 1.3 Average static torque/rotor position characteristic
of an existing a.c. stepper motor.

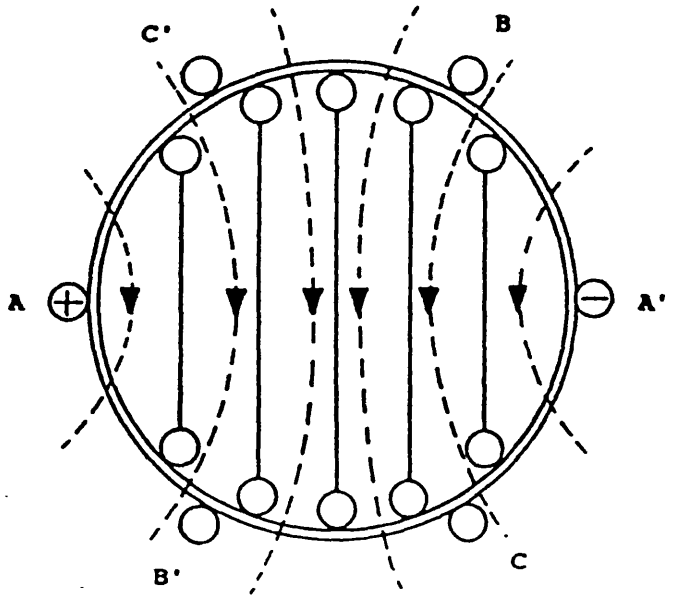

Fig. 2.1 Existing a.c. stepper motor model with three stator phase windings.

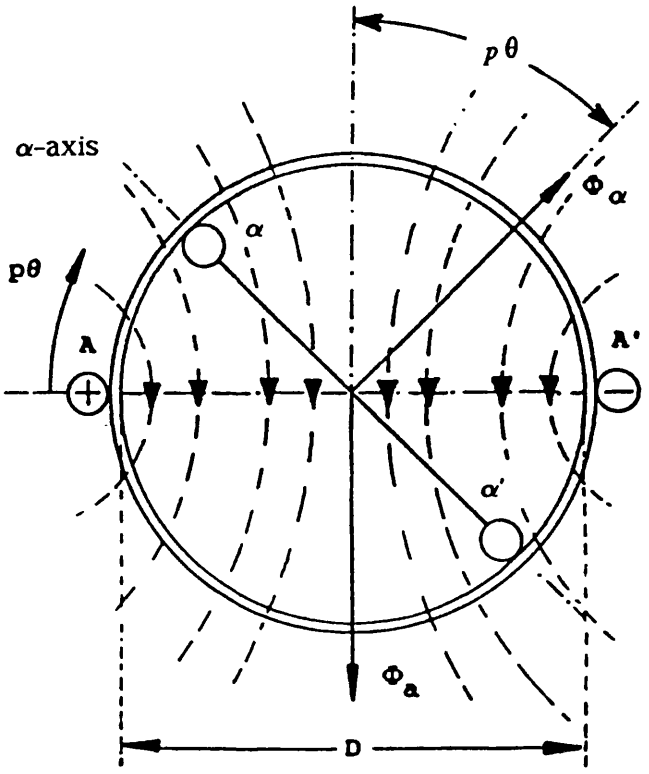

Fig. 2.2 A.C. stepping motor with concentrated rotor winding

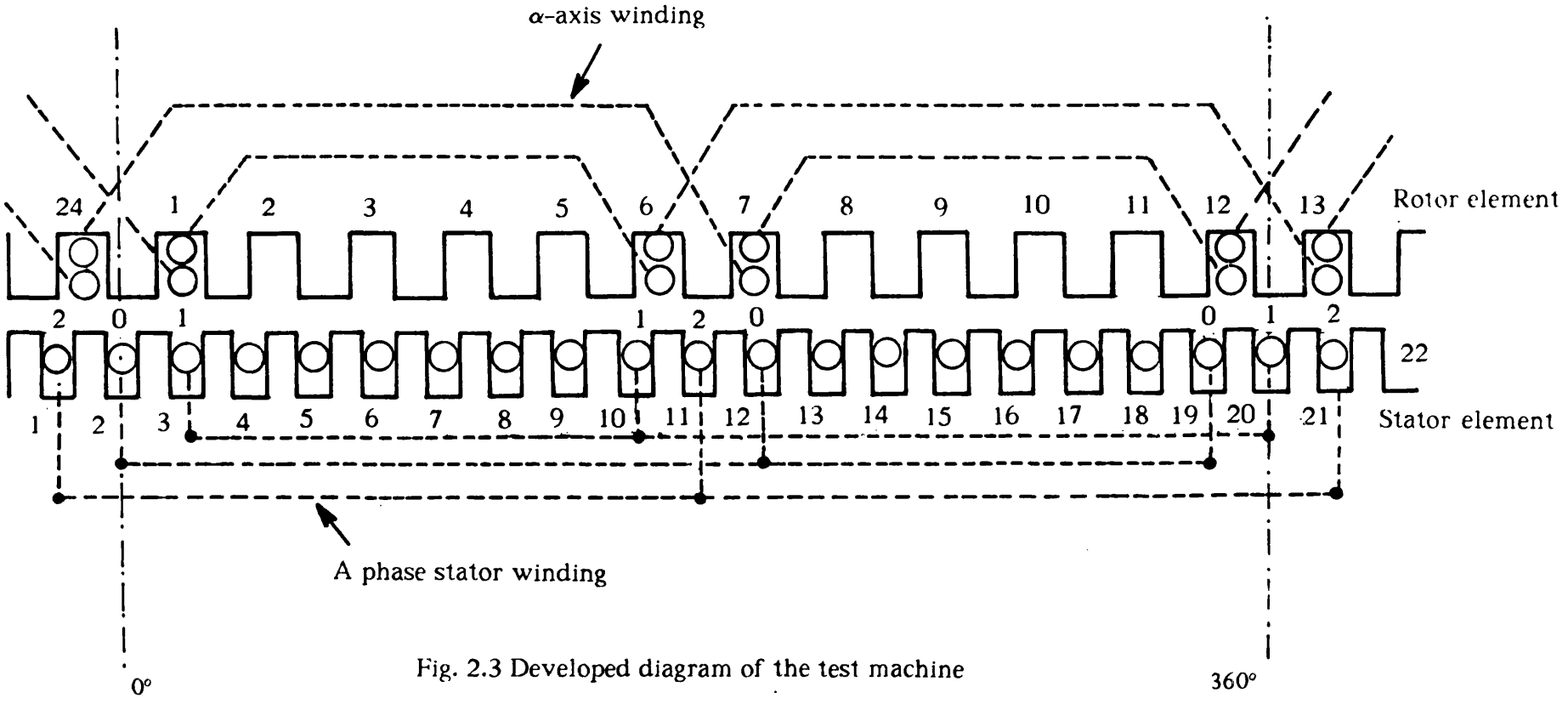

Fig. 2.3 Developed diagram of the test machine

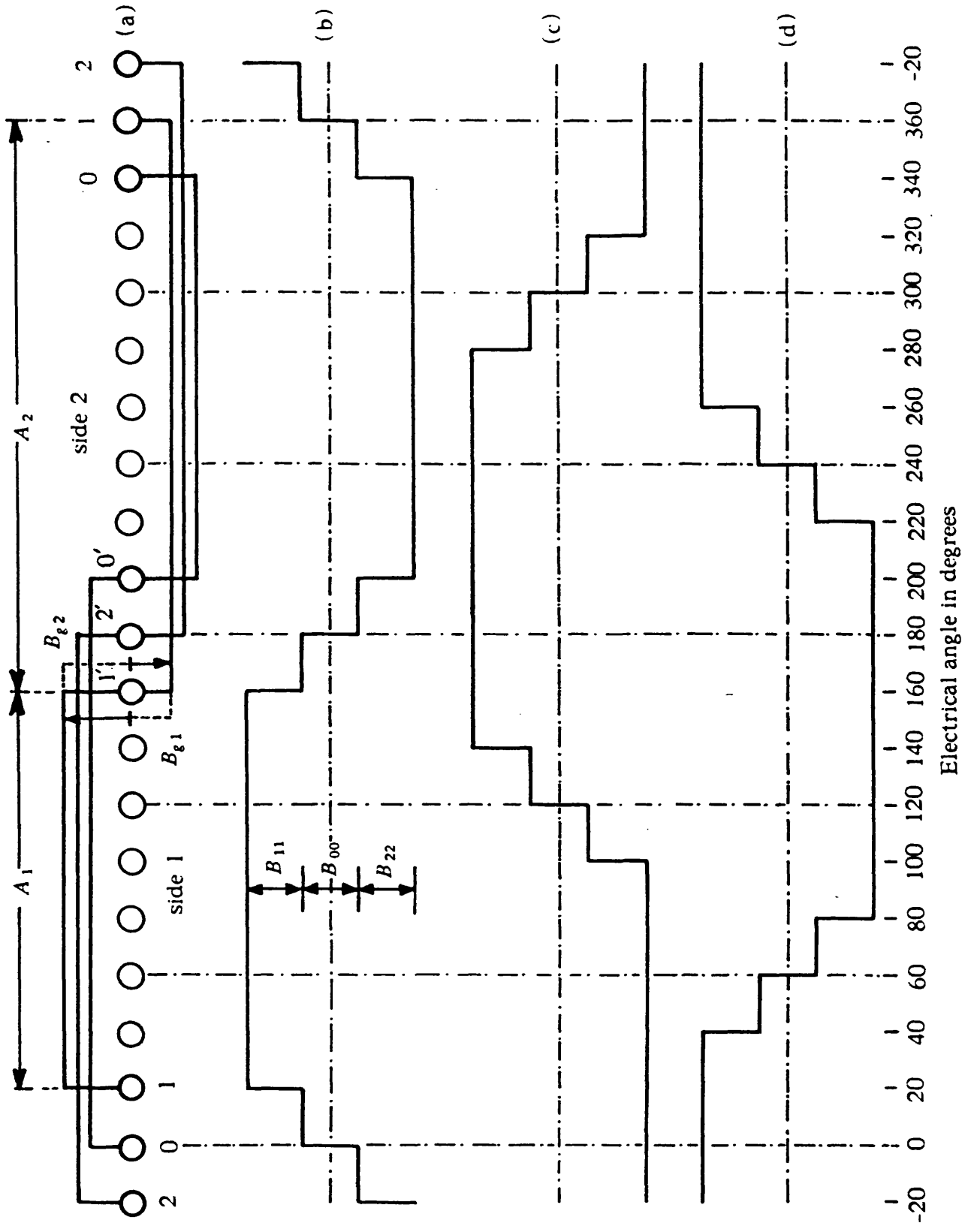

Fig. 2.4(a) Stator flux density waves due to individual coils in A phase

Fig. 2.4(b) Resultant flux density wave for A phase

Fig. 2.4(c) Resultant flux density wave for B phase

Fig. 2.4(d) Resultant flux density wave for C phase

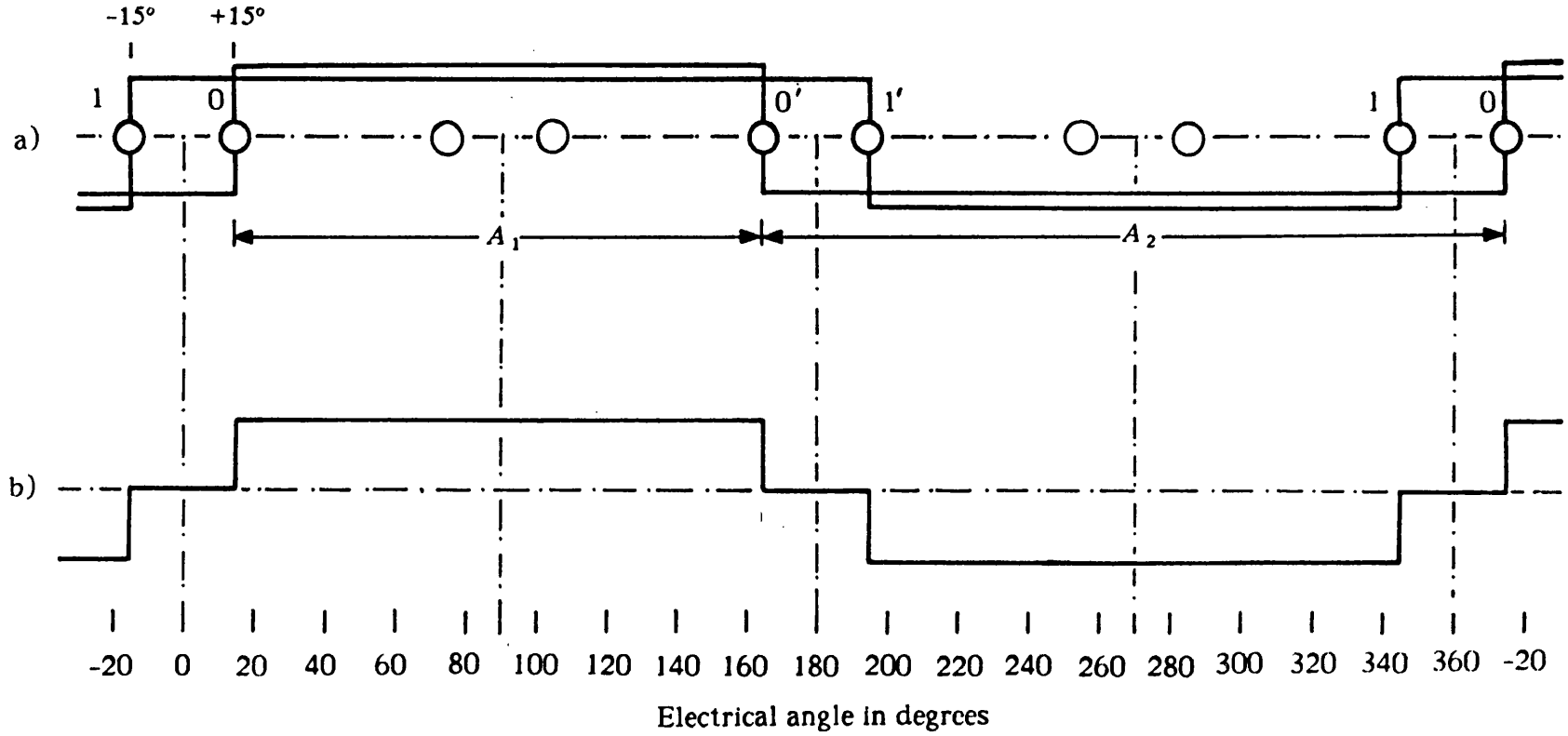

Fig. 2.5(a) Rotor flux density wave for individual coils in α-axis windings

Fig. 2.5(b) Resultant flux density wave

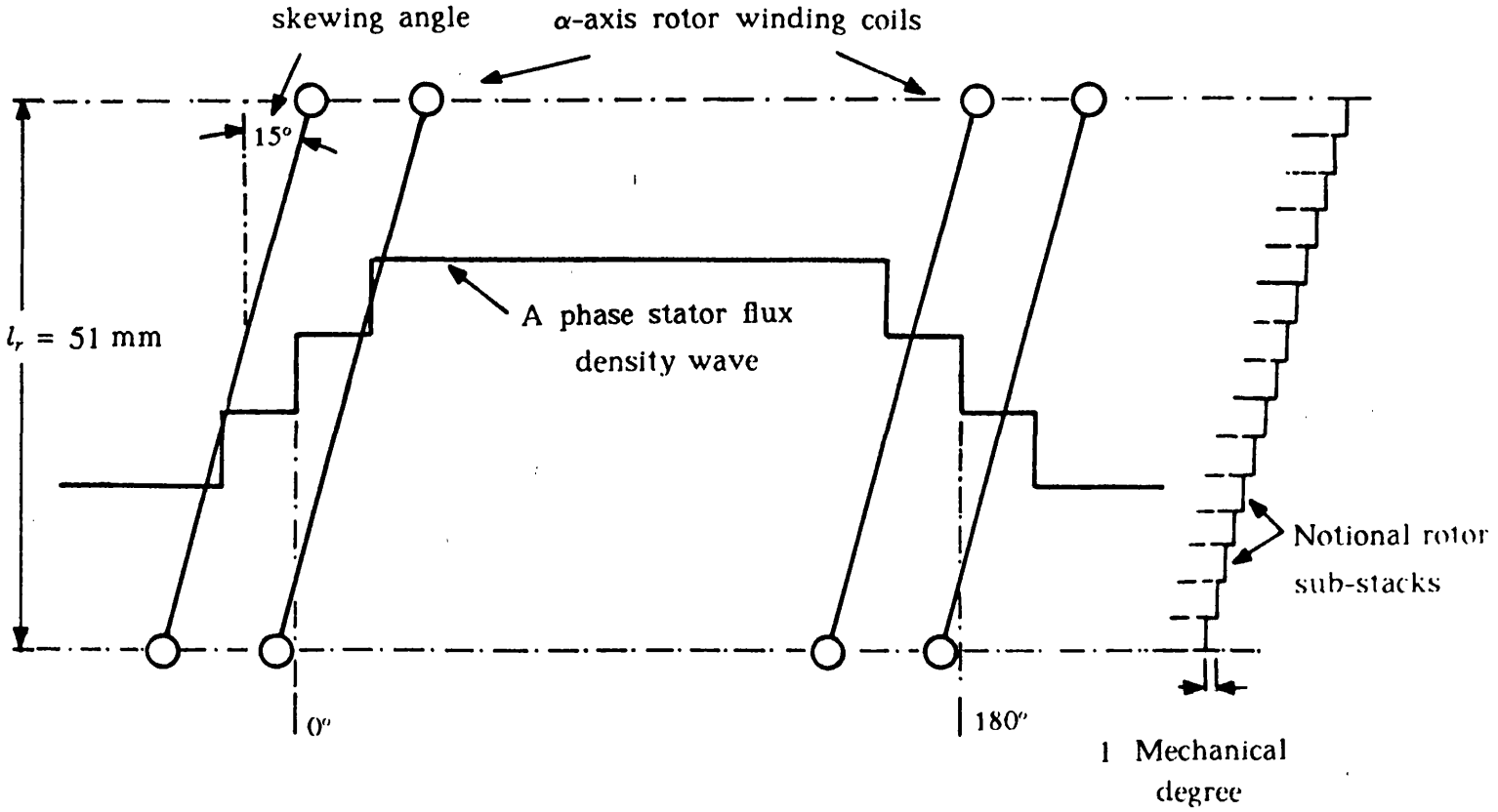

Fig. 2.6 Schematic diagram representing the rotor skewing

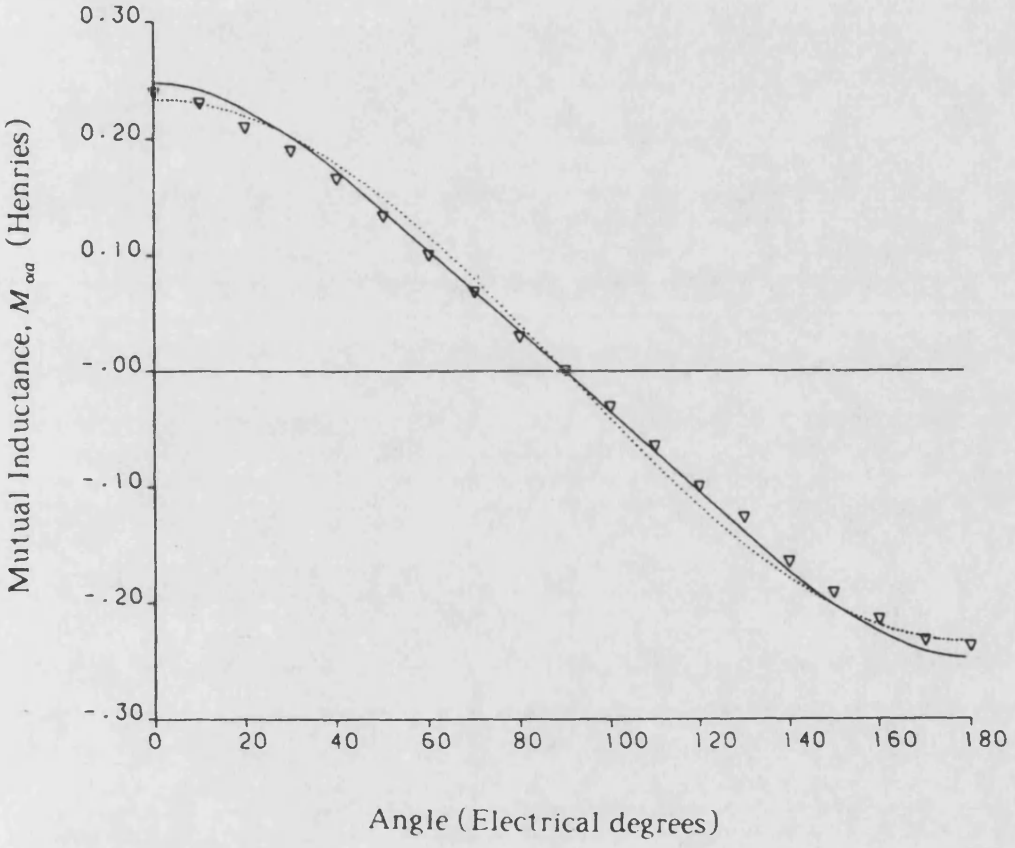

Fig. 2.7 Mutual inductance variation, M_{aa}, with respect to rotor position

——— Predicted values

▽ ▽ ▽ Measured values

····· Fundamental component of predicted values

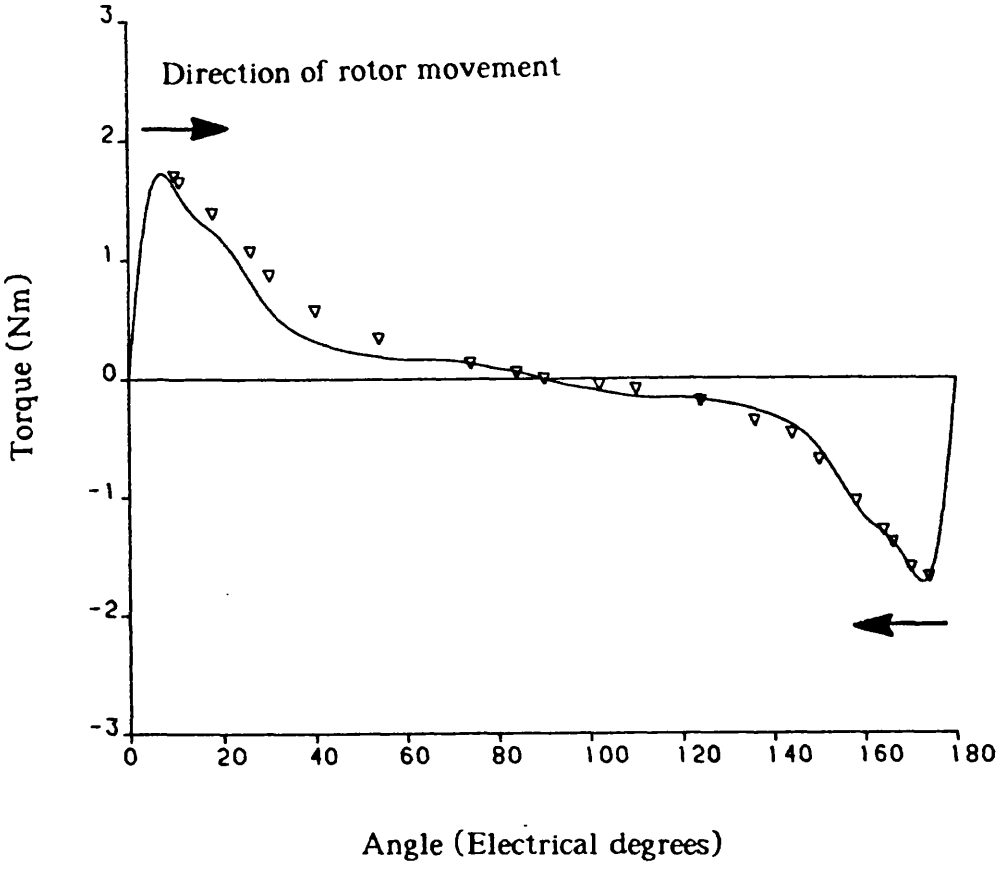

Fig. 2.8 Average static torque variation with respect to rotor position

——— Predicted values

▽ ▽ ▽ Measured values

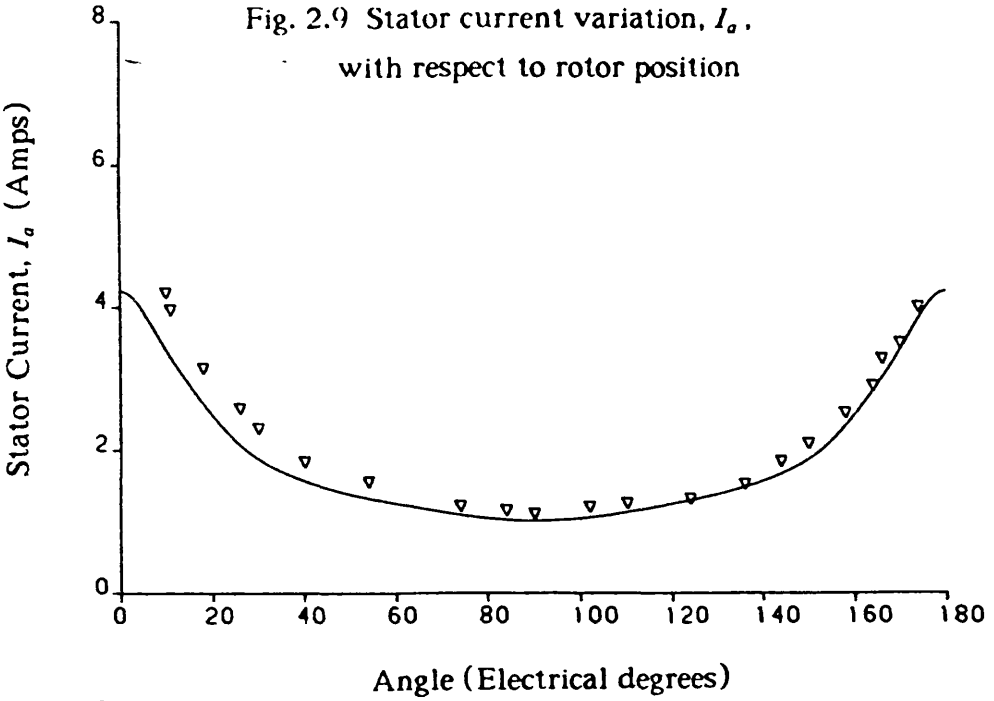

Fig. 2.9 Stator current variation, I_a, with respect to rotor position

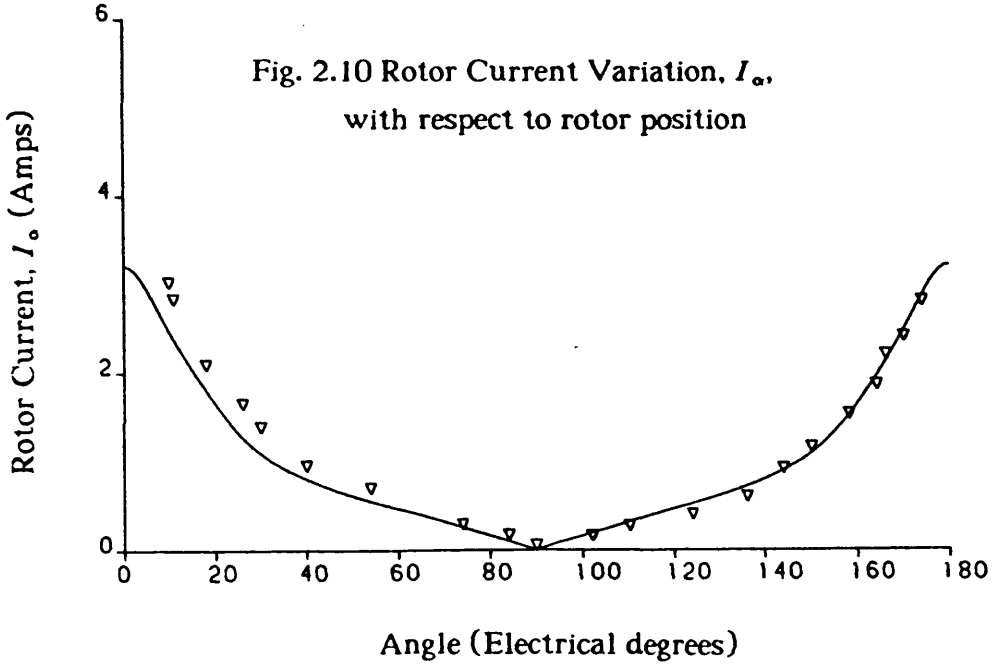

Fig. 2.10 Rotor Current Variation, I_a, with respect to rotor position

——— Predicted values

▽ ▽ ▽ Measured values

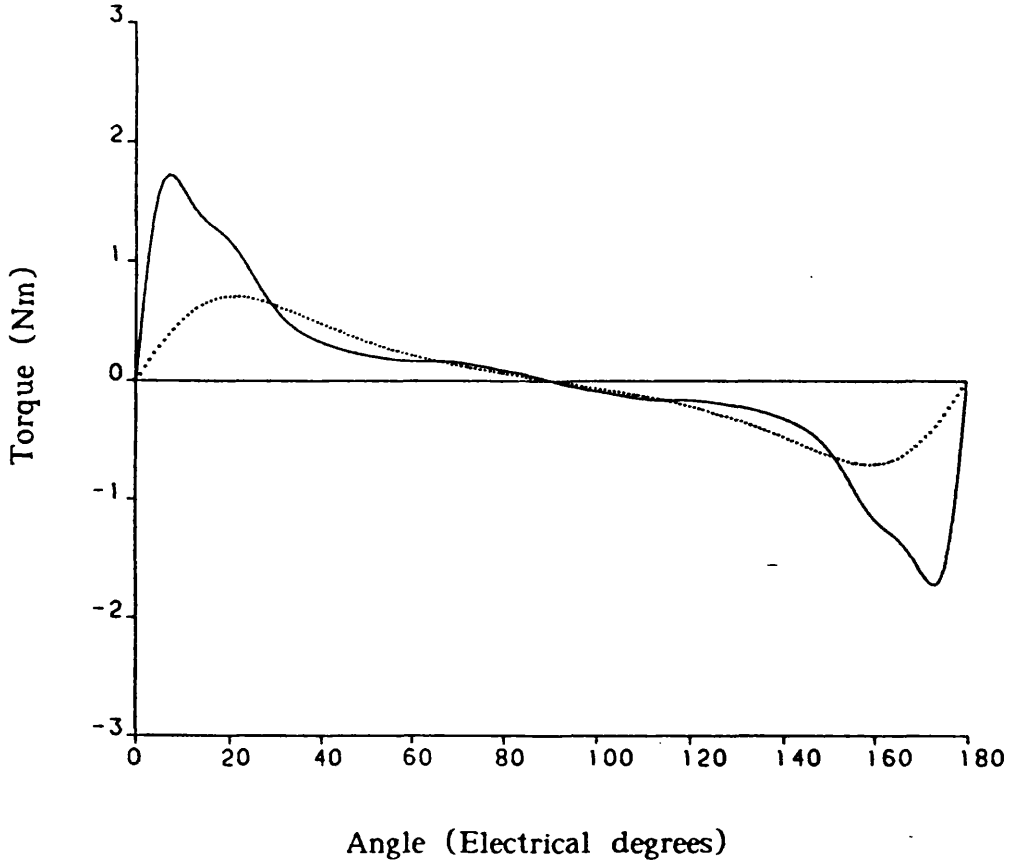

Fig. 2.11 Comparison between the predicted static torque variation for actual and the fundamental component of the mutual inductance distribution

——— Predicted values for actual mutual inductance distribution

····· Predicted values for fundamental component of the mutual inductance distribution

Fig. 2.12 Variation of stator current, I_a, with respect to rotor position for actual and fundamental component of the mutual inductance distribution

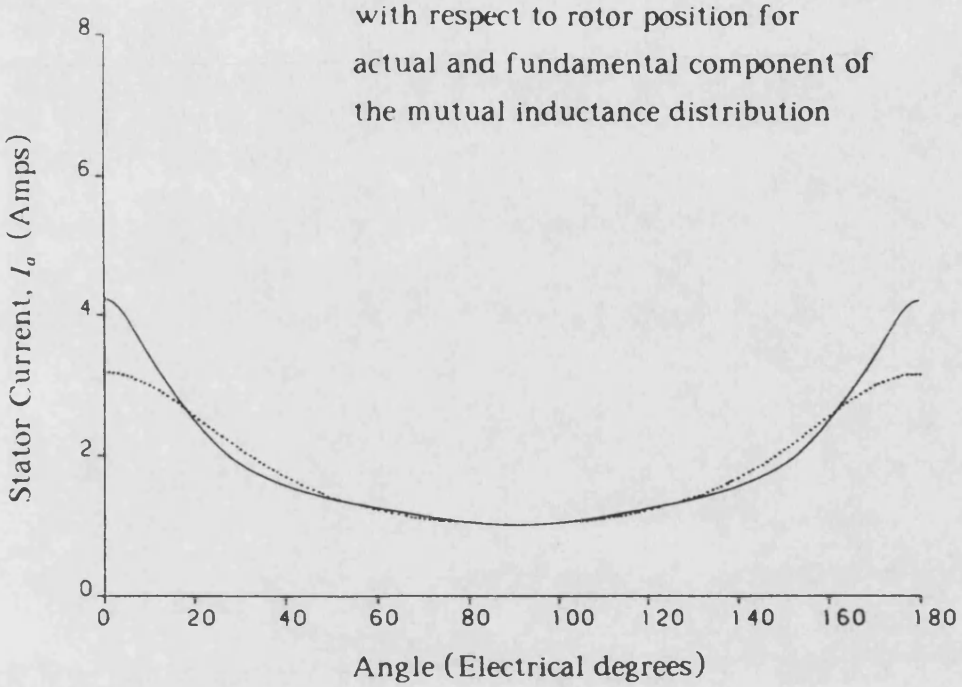

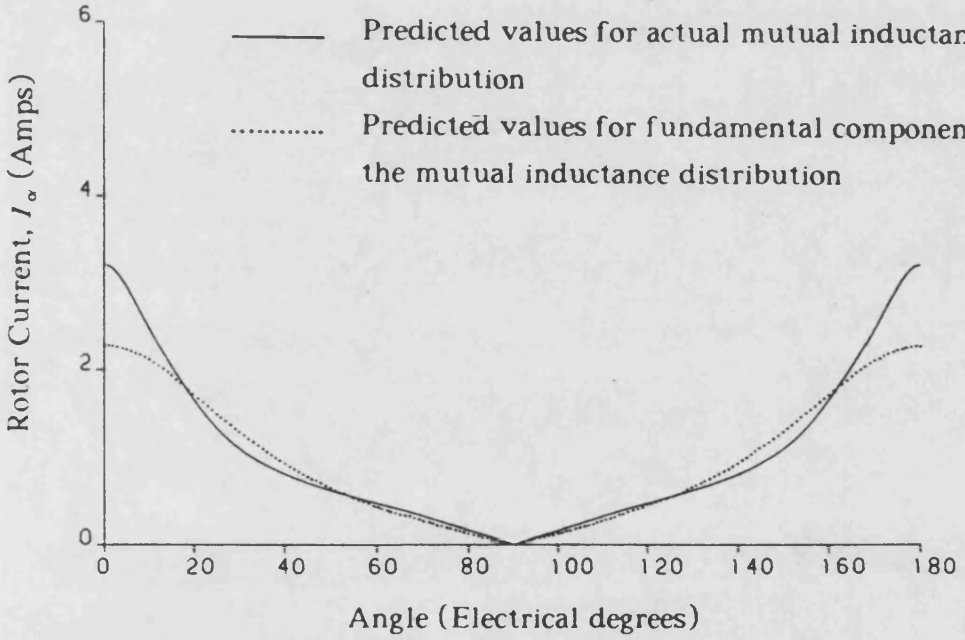

——— Predicted values for actual mutual inductance distribution

..... Predicted values for fundamental component of the mutual inductance distribution

Fig. 2.13 Variation of rotor current, I_α, with respect to rotor position for actual and fundamental component of the mutual inductance distribution

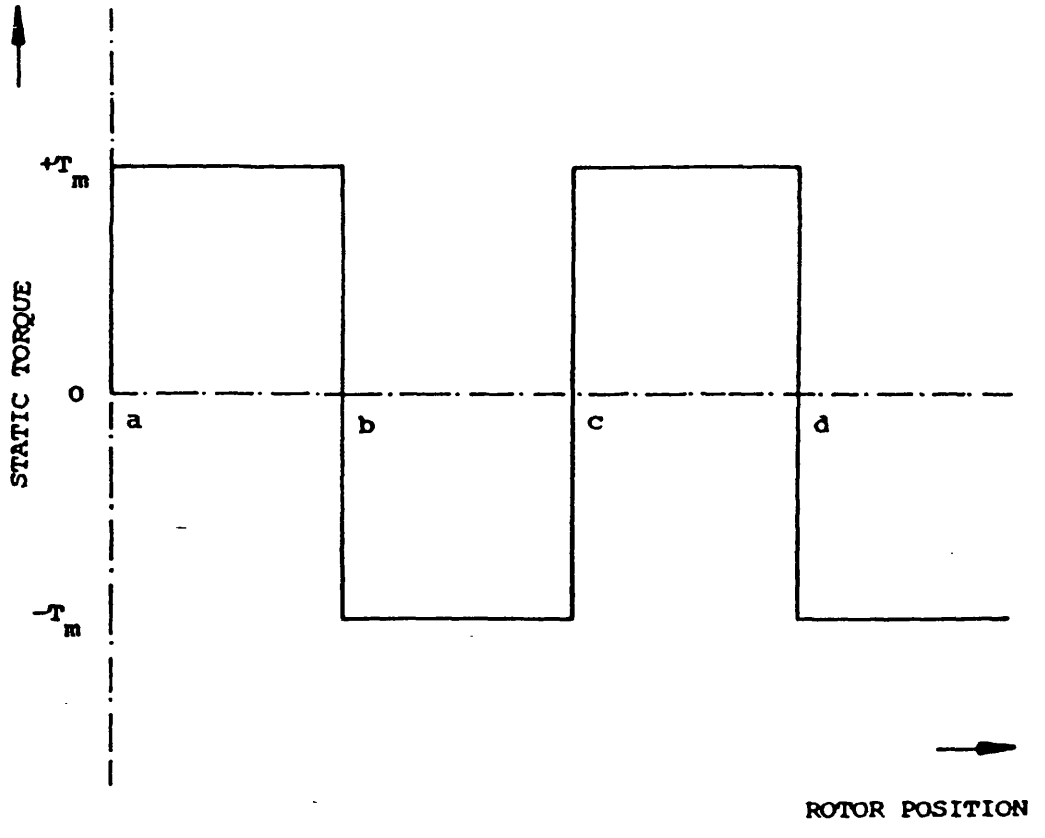

Fig. 3.1 Ideal static torque/angle curve

a, c, Unstable torque-zero positions
b, d, Stable torque-zero positions
T_m Peak static torque

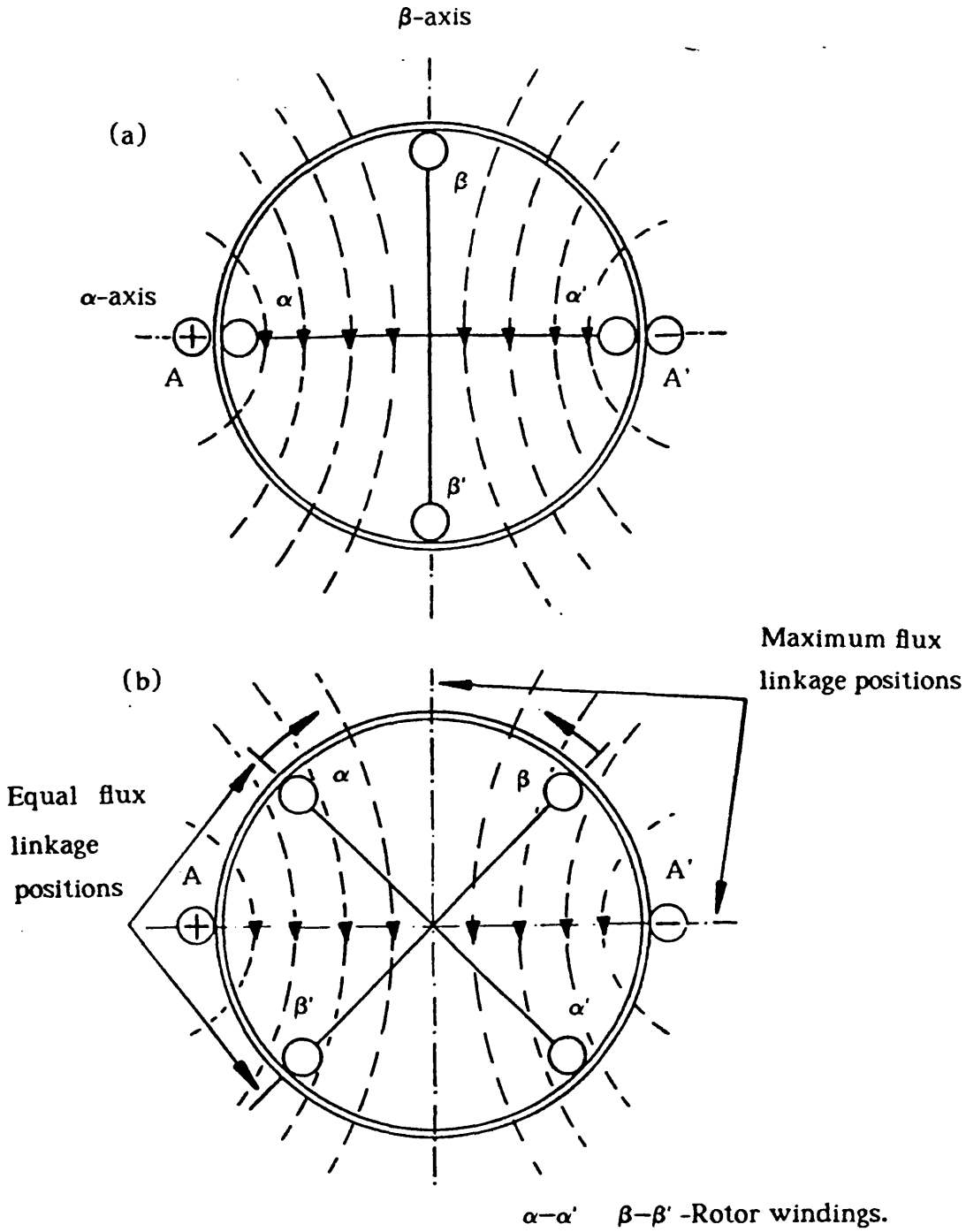

Fig. 3.2 An a.c. stepper motor with both $\alpha\beta$-axes winding rotor

(a) α-axis rotor winding at the maximum flux linkage position and the β-axis rotor winding at the zero flux linkage position

(b) α and β-axes rotor windings at the equal flux linkage position

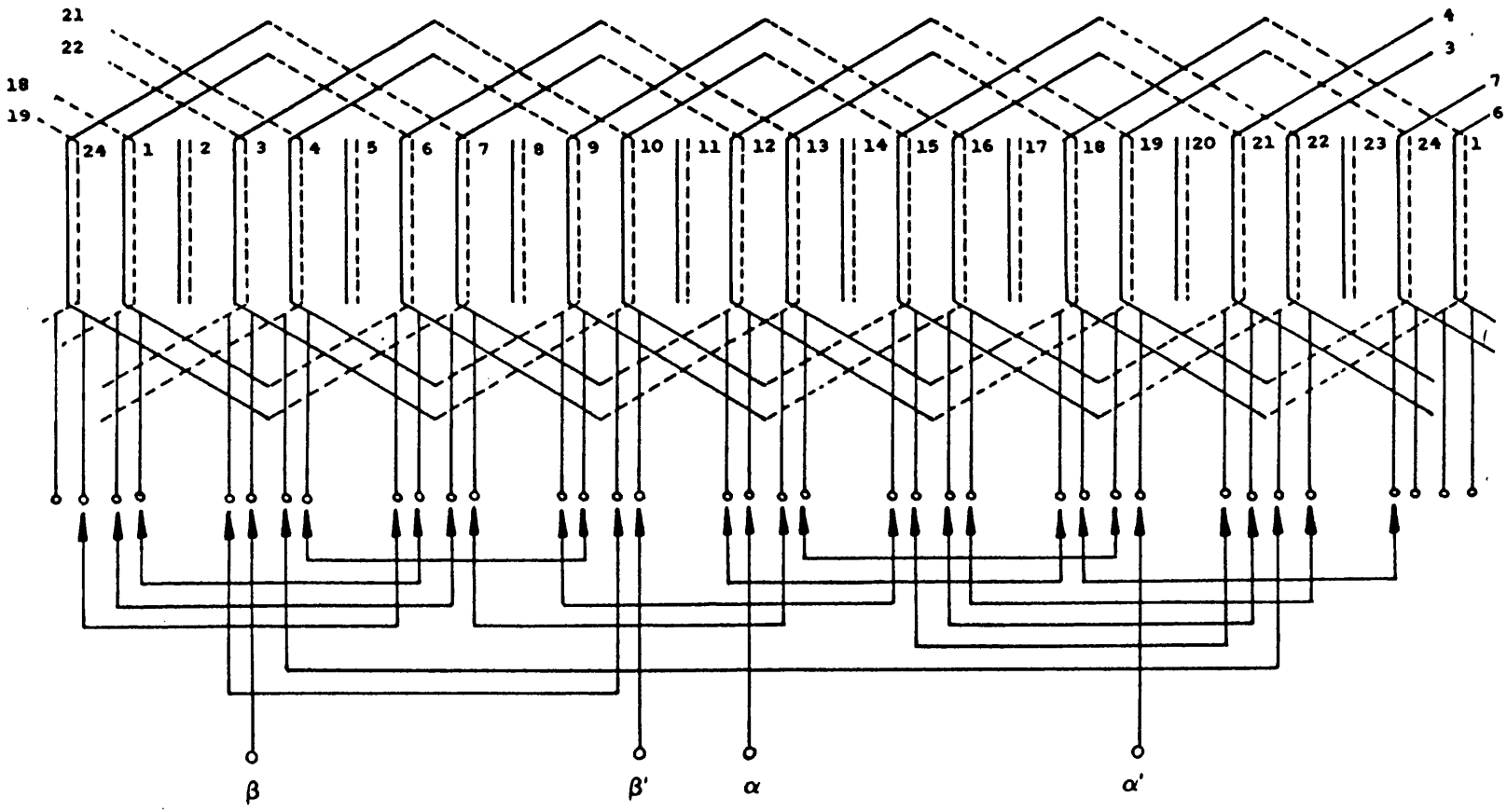

Fig. 3.3 Rotor winding diagram of the test machine

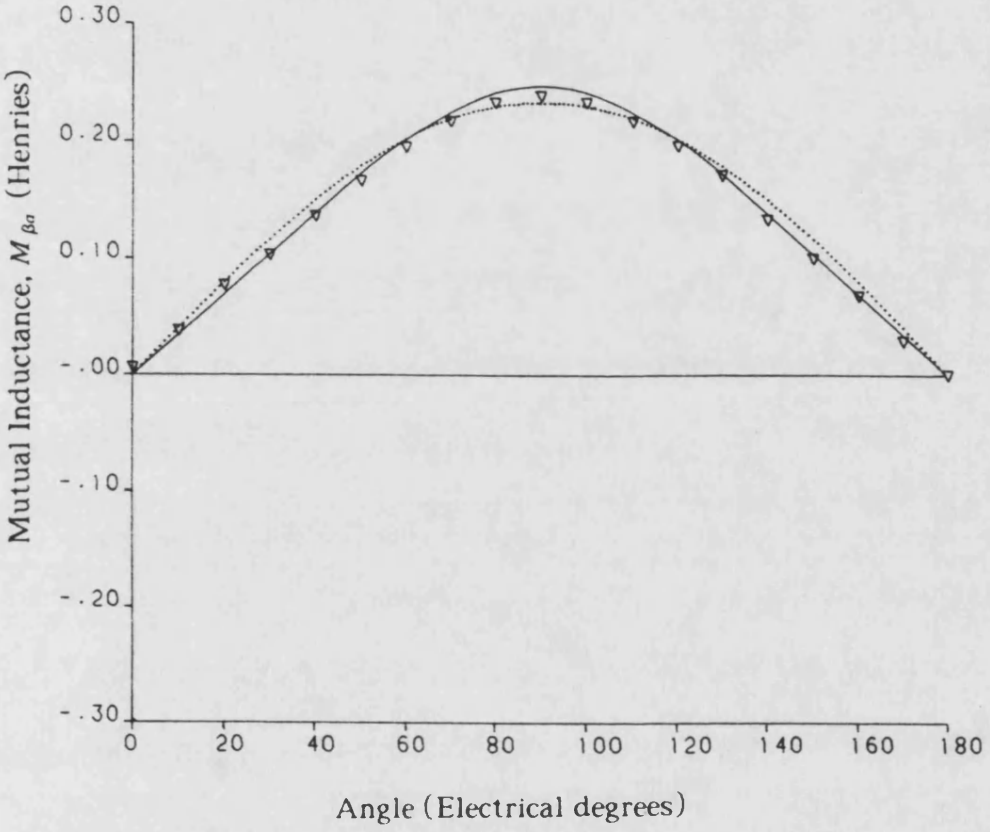

Fig. 3.4 Mutual inductance variation, $M_{\beta a}$, with respect to rotor position

——— Predicted values

▽ ▽ ▽ Measured values

..... Fundamental component of predicted values

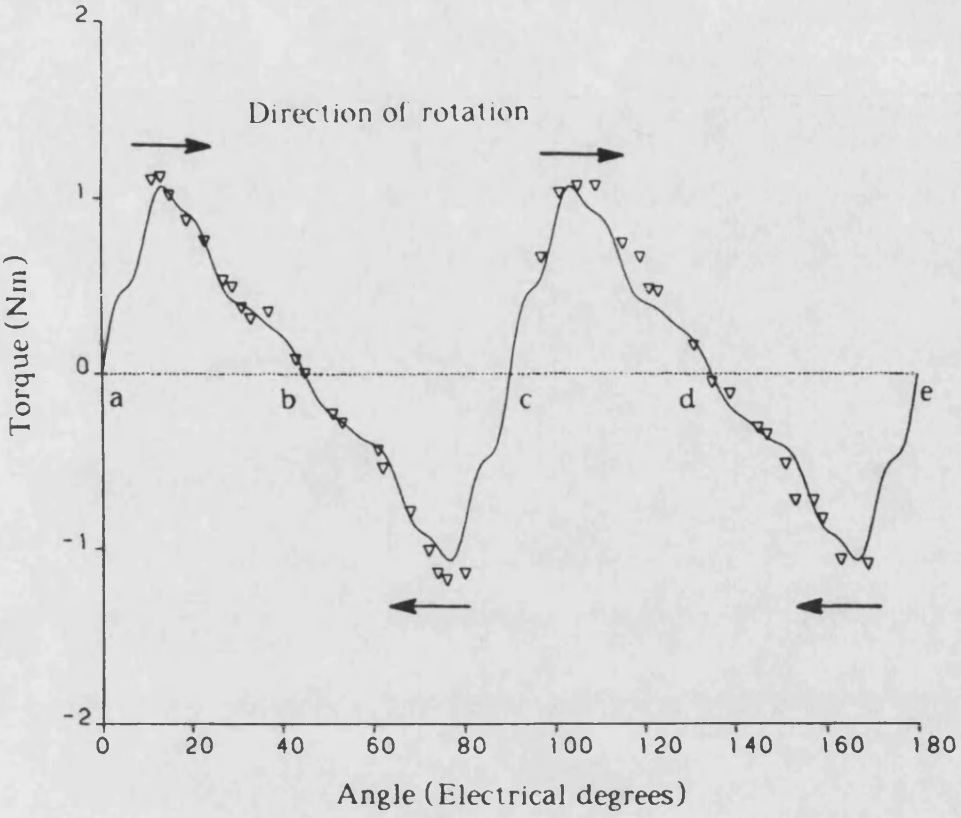

Fig. 3.5 Torque/angle characteristic

b,d Stable torque-zero positions

a,c,e Unstable torque-zero positions

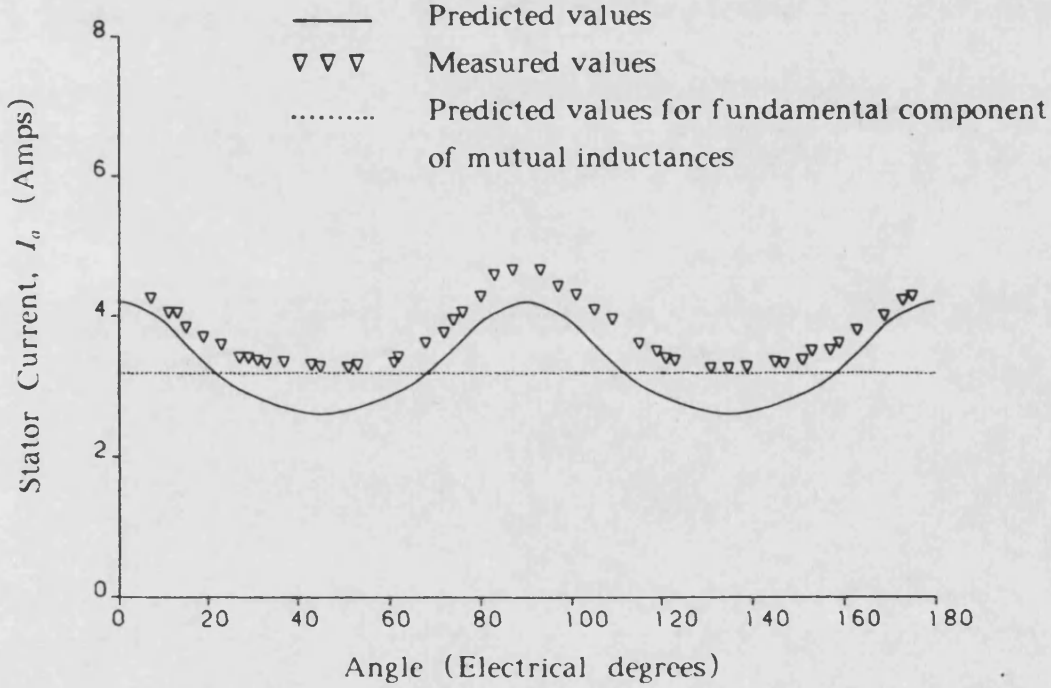

Fig. 3.6 Stator current variation, I_a, with respect to rotor position

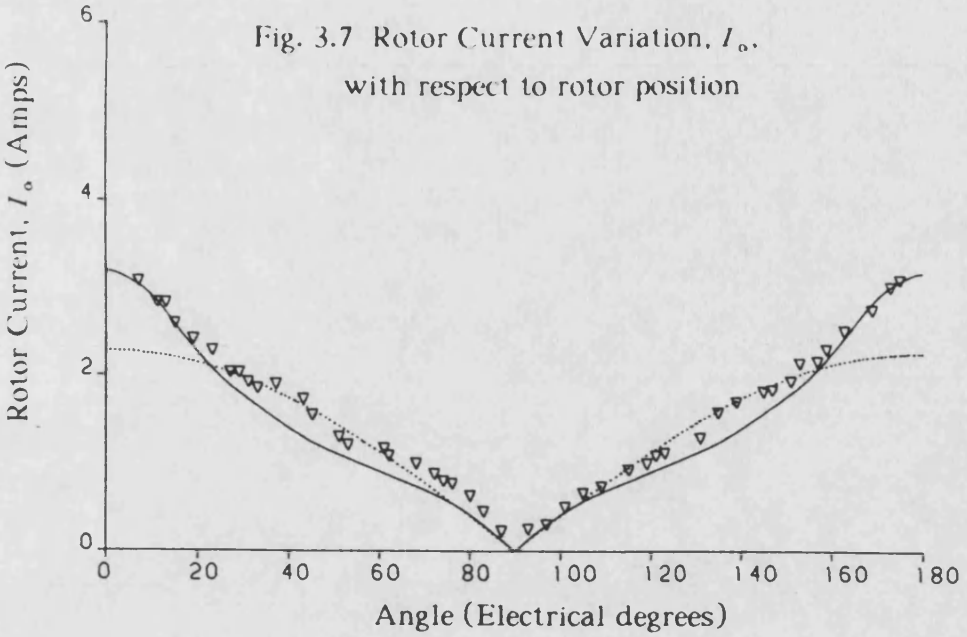

Fig. 3.7 Rotor Current Variation, I_α, with respect to rotor position

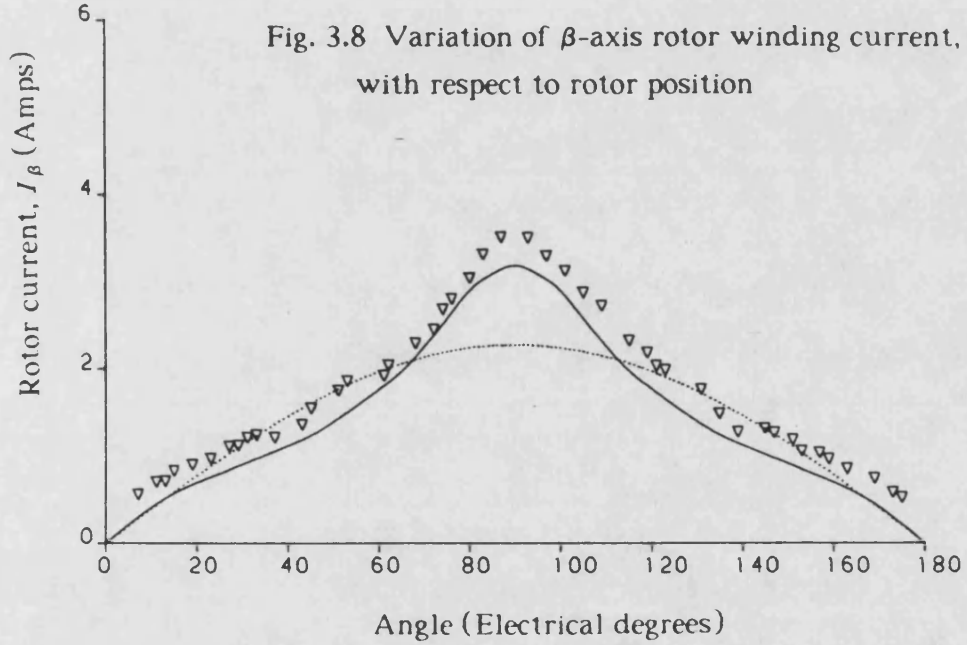

Fig. 3.8 Variation of β-axis rotor winding current, I_β with respect to rotor position

——— Predicted values

▽ ▽ ▽ Measured values

..... Predicted values for fundamental component of mutual inductances

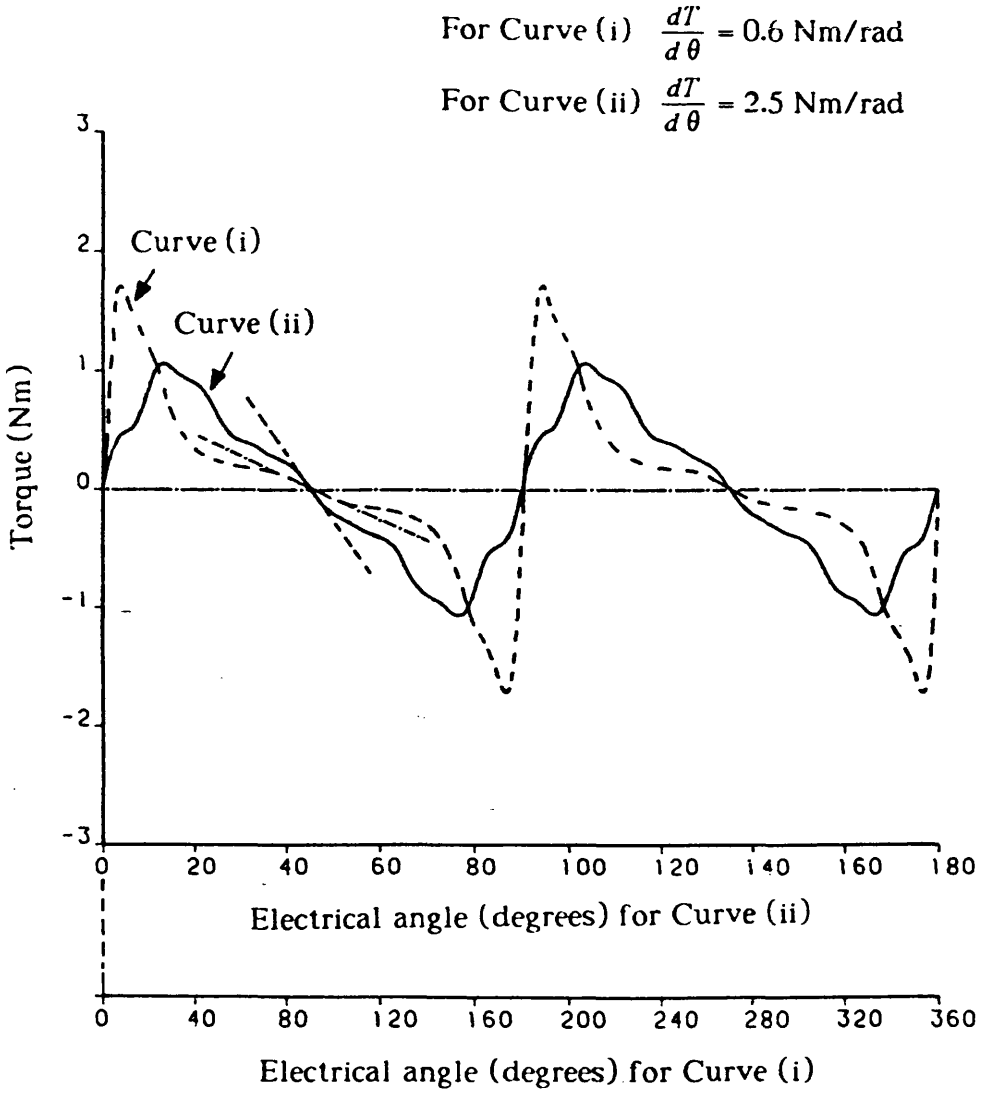

Fig. 3.9 Comparison of torque/angle characteristics between α and $\alpha\beta$-axes rotor

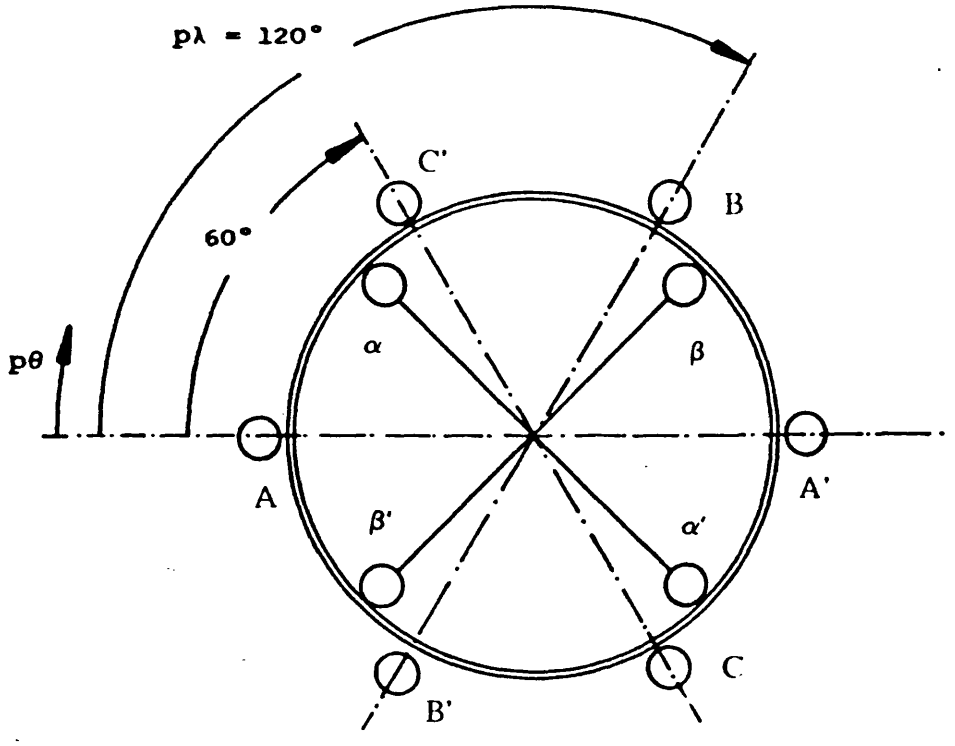

Fig. 3.10 2-pole, 3-phase induction stepping motor

A A'	A phase stator winding
B B'	B phase stator winding
C C'	C phase stator winding
α	α-axis rotor winding
β	β-axis rotor winding

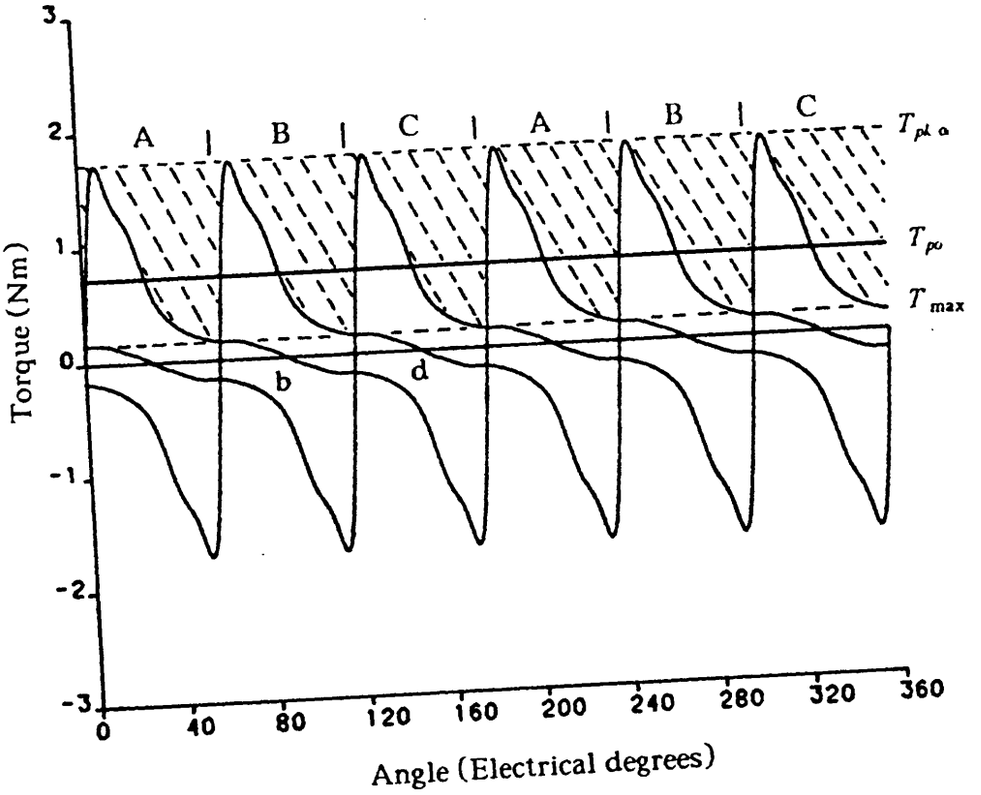

Fig. 3.11 Torque/angle curves for sequential excitation using α-axis rotor with one stator phase excited at a time

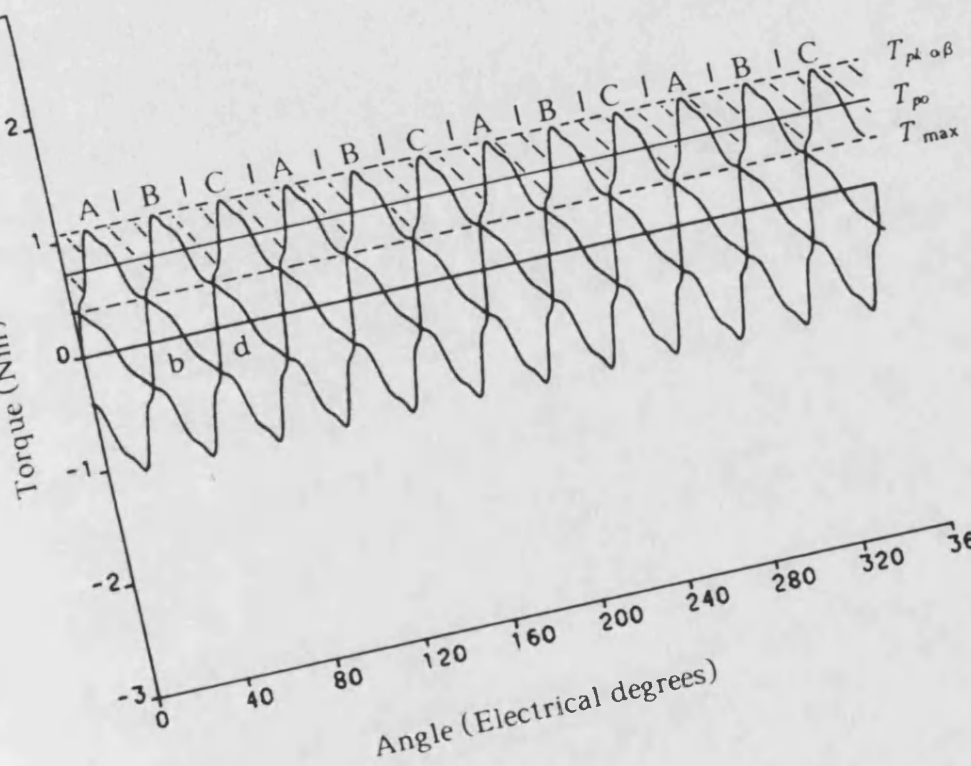

Fig. 3.12 Torque/angle curves for sequential excitation using $\alpha\beta$-axes rotor with one stator phase excited at a time

Fig. 4.1(a)

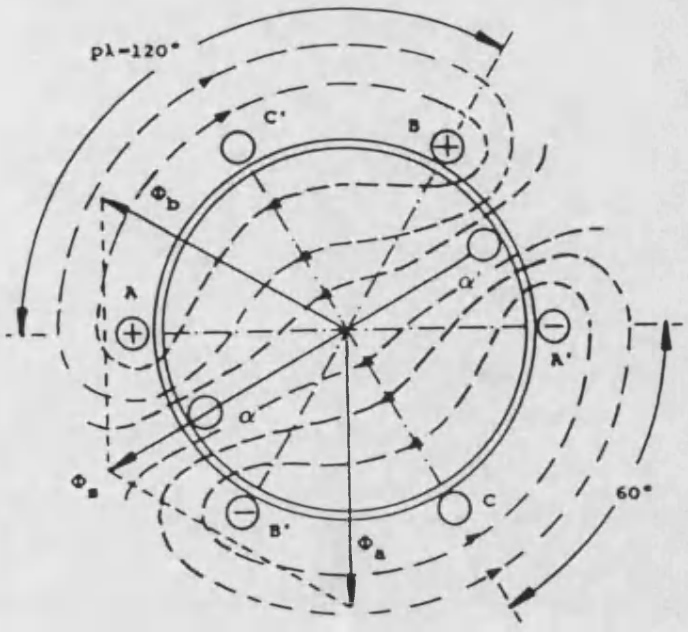

Fig. 4.1(b)

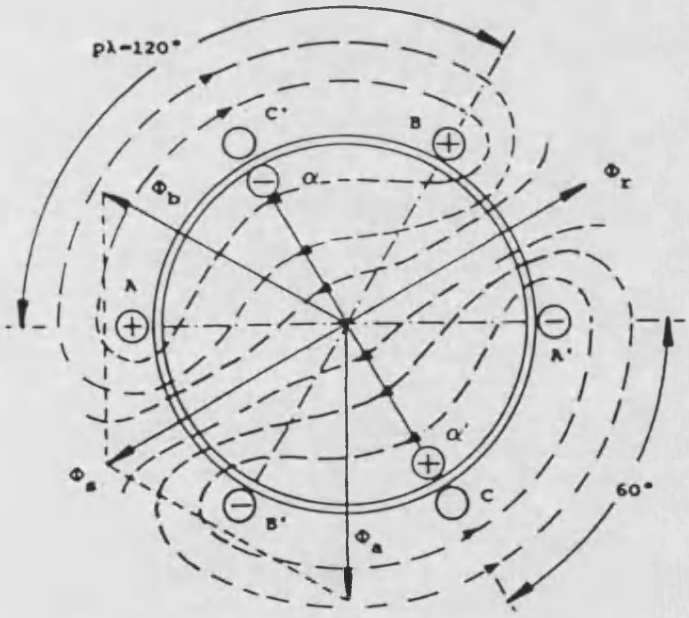

Fig. 4.1(a) α-axis rotor at minimum flux linkage position when A and B stator phases are excited

Fig. 4.1(b) α-axis rotor at maximum flux linkage position when A and B stator phases are excited

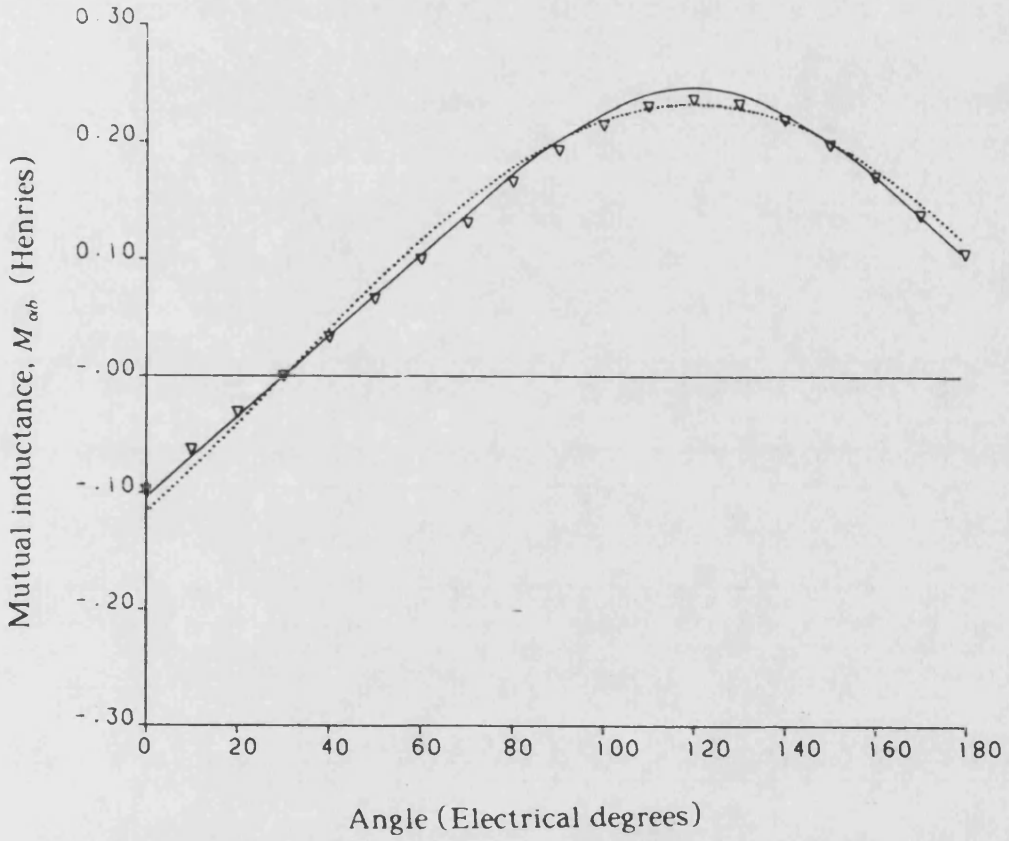

Fig. 4.2 Mutual inductance variation, M_{ab}, with respect to rotor position

——— Predicted values

▽ ▽ ▽ ▽ Measured values

..... Fundamental component of predicted values

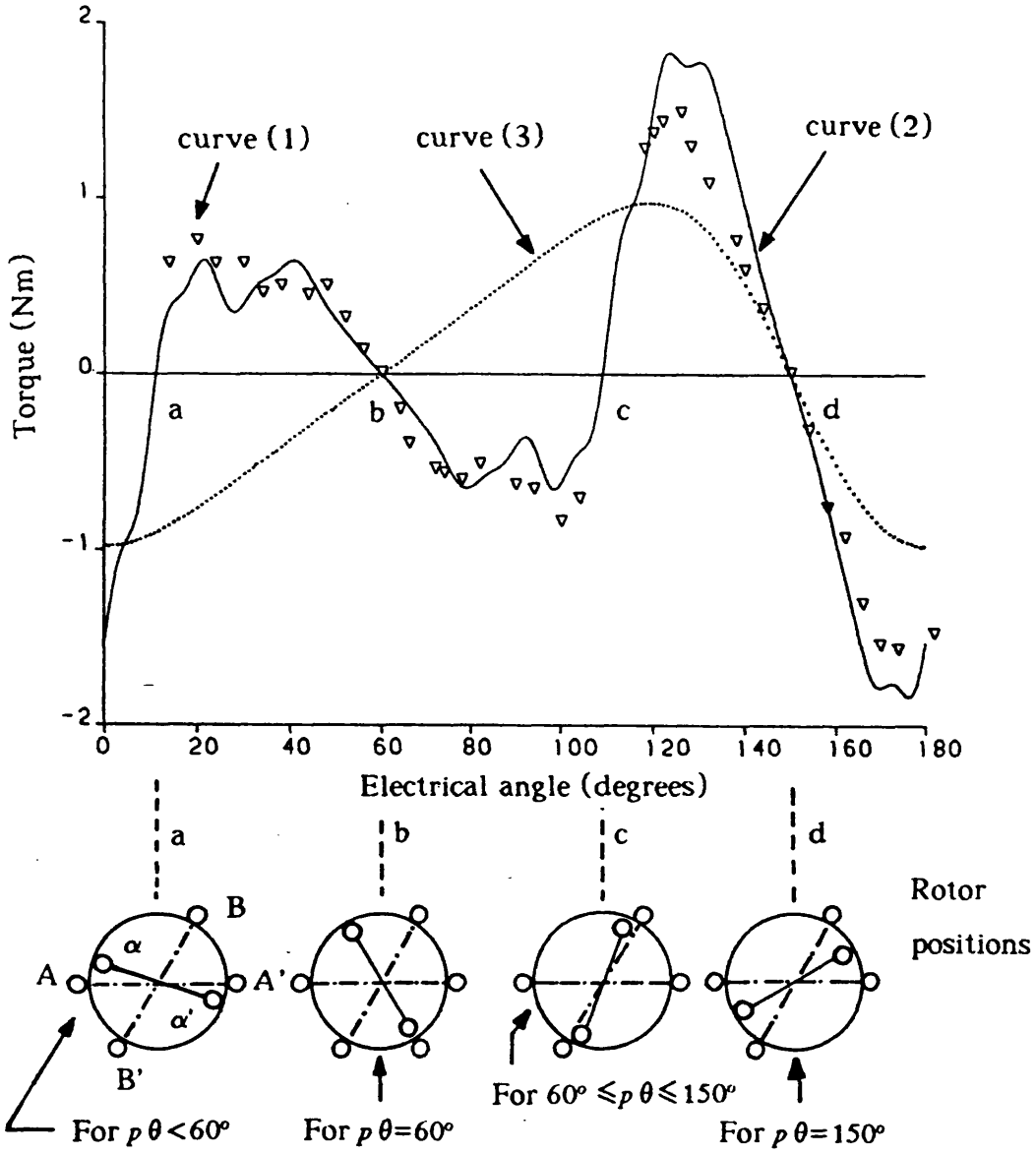

Fig. 4.3 Static torque/angle characteristics for α-axis rotor when A and B phases are excited

——— Predicted values

▽ ▽ ▽ ▽ Measured values

..... Predicted values for fundamental component of mutual inductances

Fig. 4.4 Variation of stator current, I_a with respect to rotor position

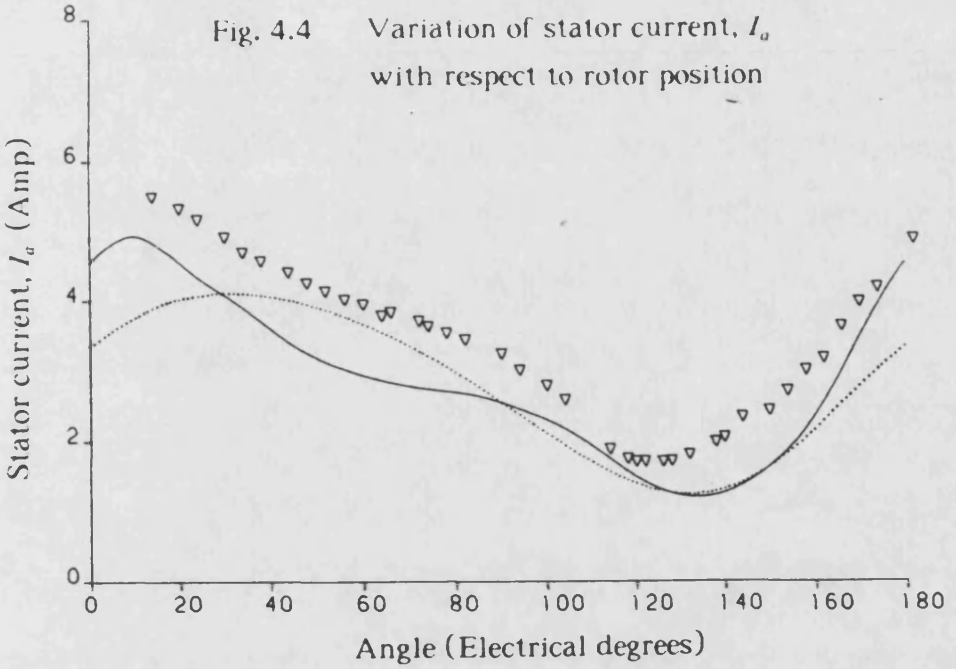

Fig. 4.5 Variation of stator current, I_b with respect to rotor position

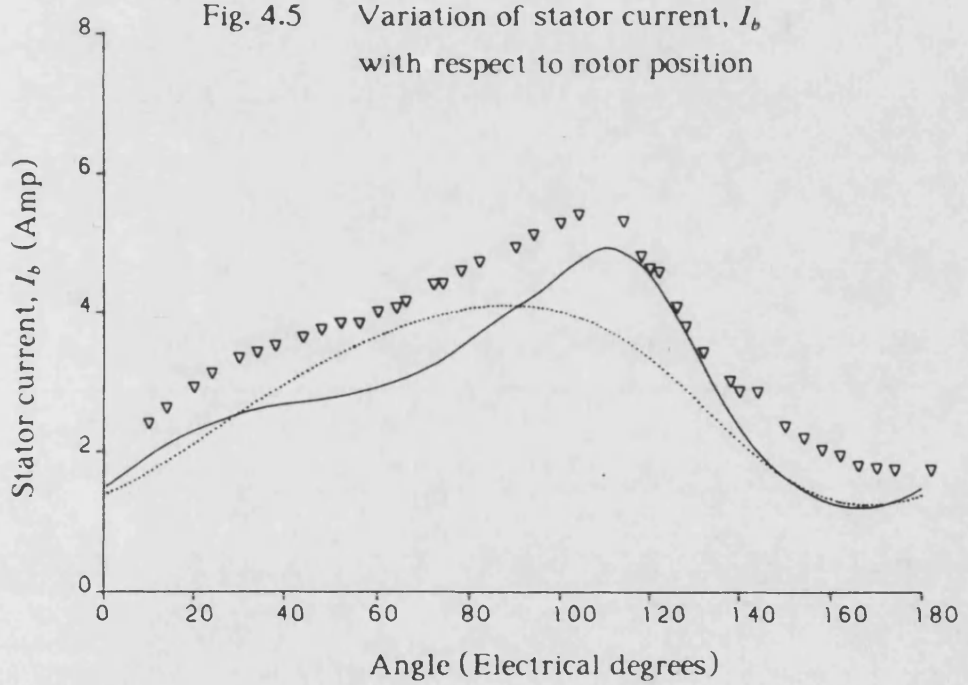

——— Predicted values

▽ ▽ ▽ Measured values

..... Predicted values for fundamental component of mutual inductance distribution

Fig. 4.6 Variation of rotor current, I_o with respect to rotor position for two-phase-on excitation using α-axis rotor

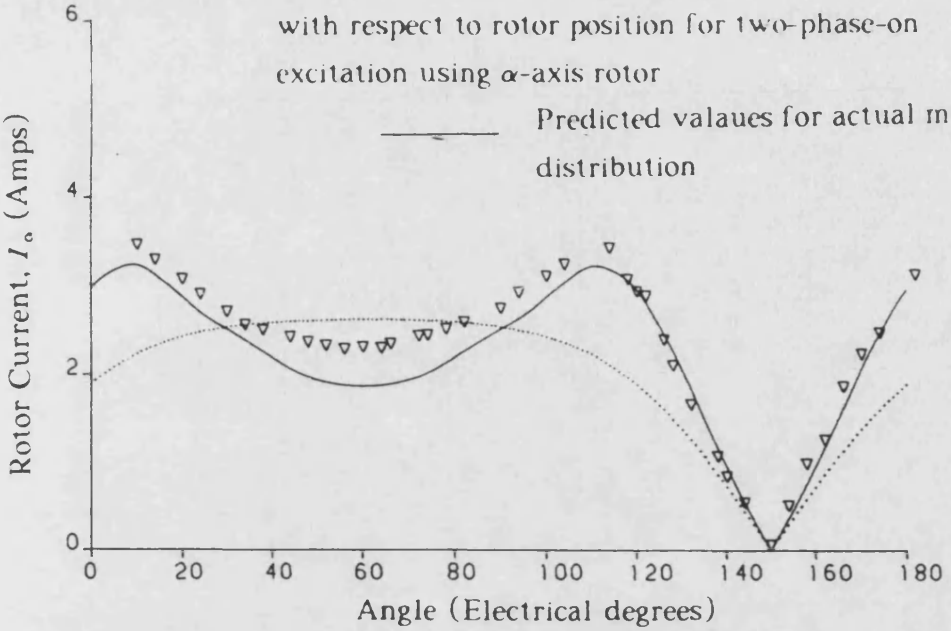

Fig. 4.7 Torque/angle characteristics for two-phase-on excitation of an α-axis rotor

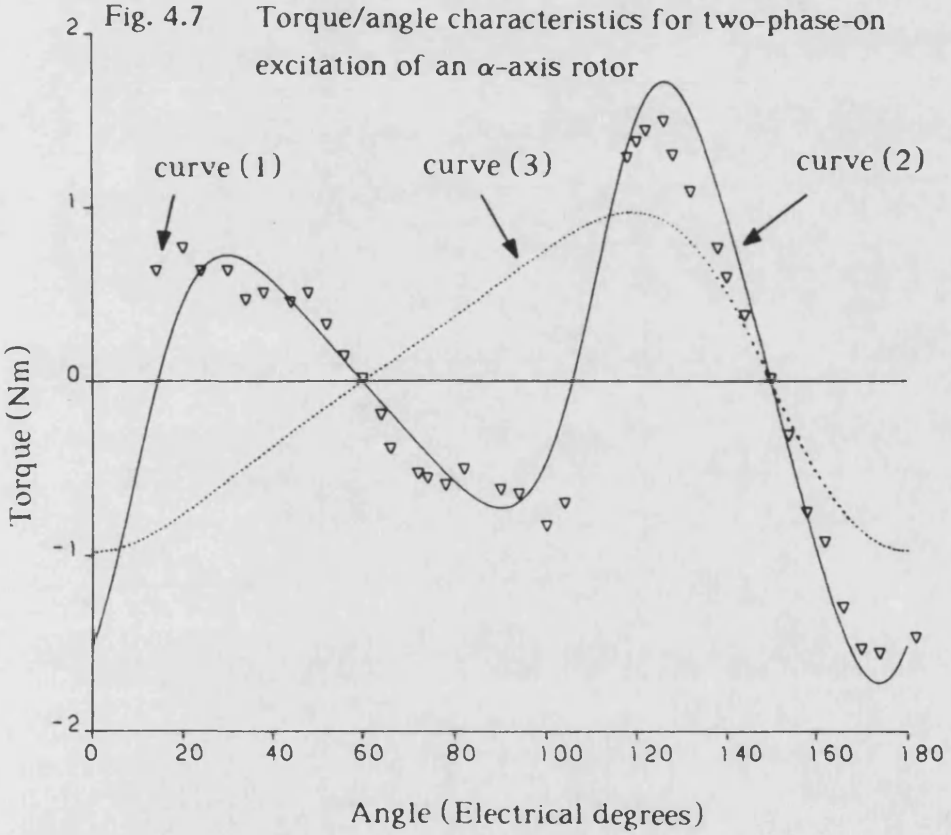

——— Predicted values for fundamental and third harmonic components

▽ ▽ ▽ ▽ Measured values

..... Predicted values for fundamental component of mutual inductances

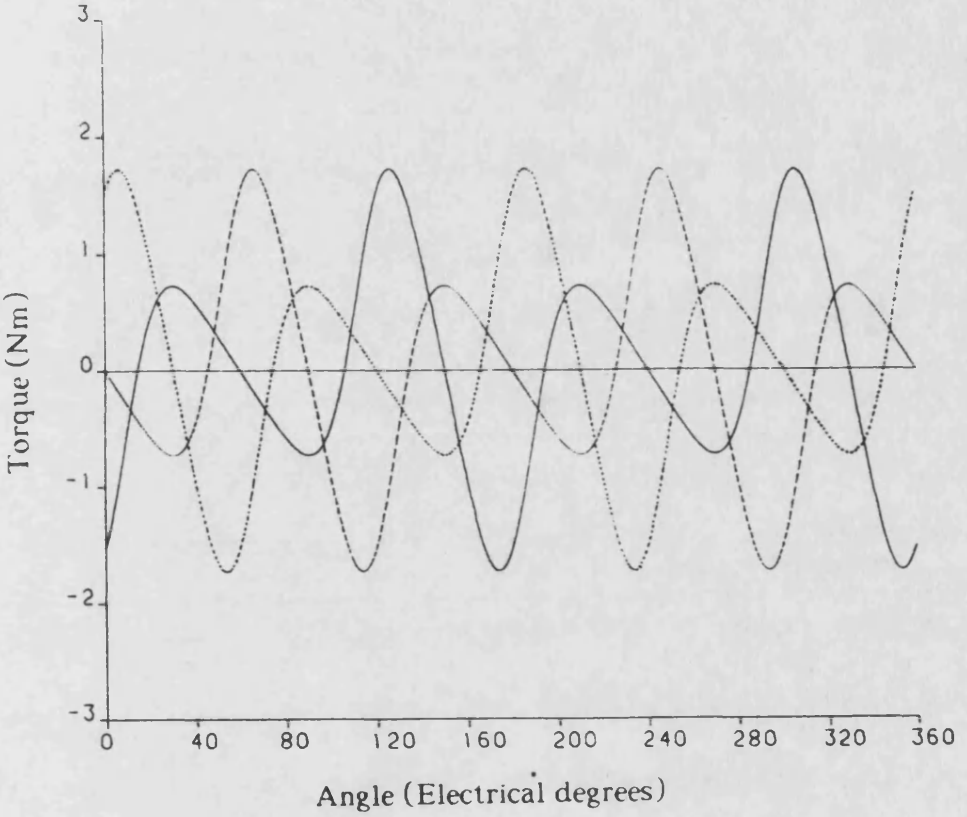

Fig. 4.8 Static torque/angle curves for sequential two-phase-on excitation using an α-axis winding rotor

——— When stator phases A and B are excited

- - - - - - - When stator phases B and C are excited

..... When stator phases C and A are excited

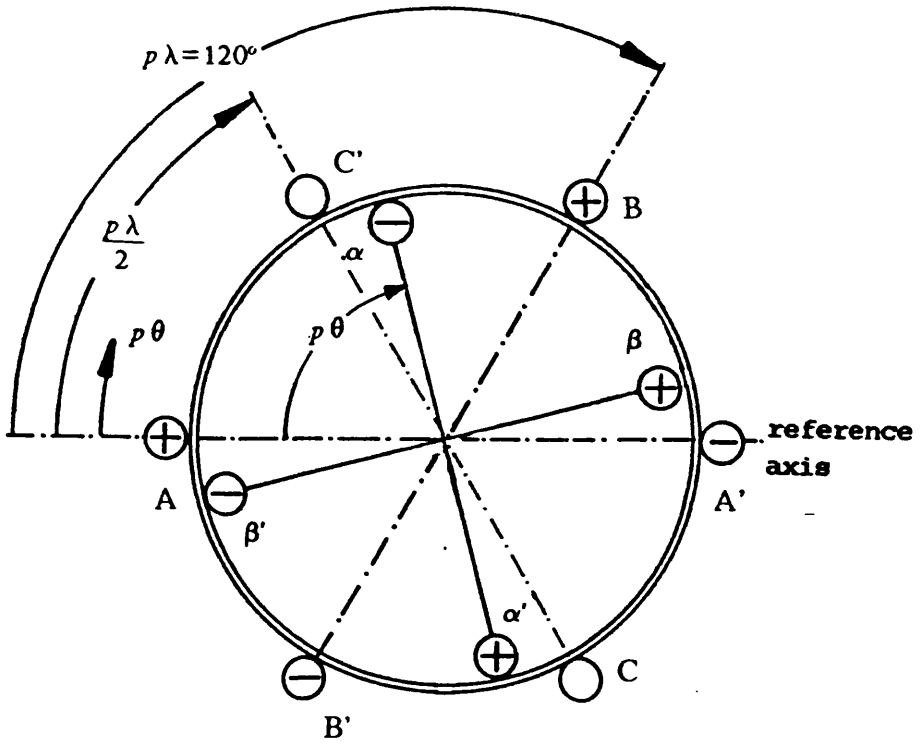

Fig. 4.9 2-pole, 3-phase induction stepping motor model with $\alpha\beta$-axes rotor for two-phase-on excitation

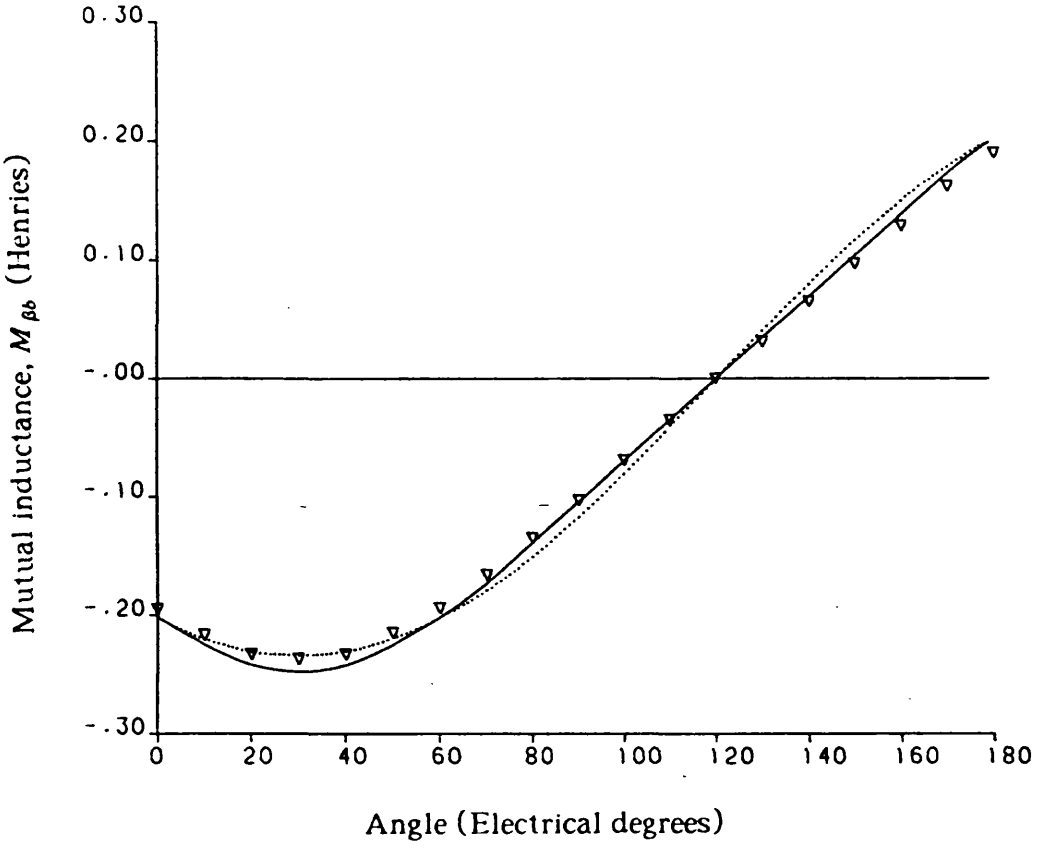

Fig. 4.10 Variation of mutual inductance, $I_{\beta b}$ with respect to rotor position

——— Predicted values

▽ ▽ ▽ Measured values

..... Predicted values for fundamental component

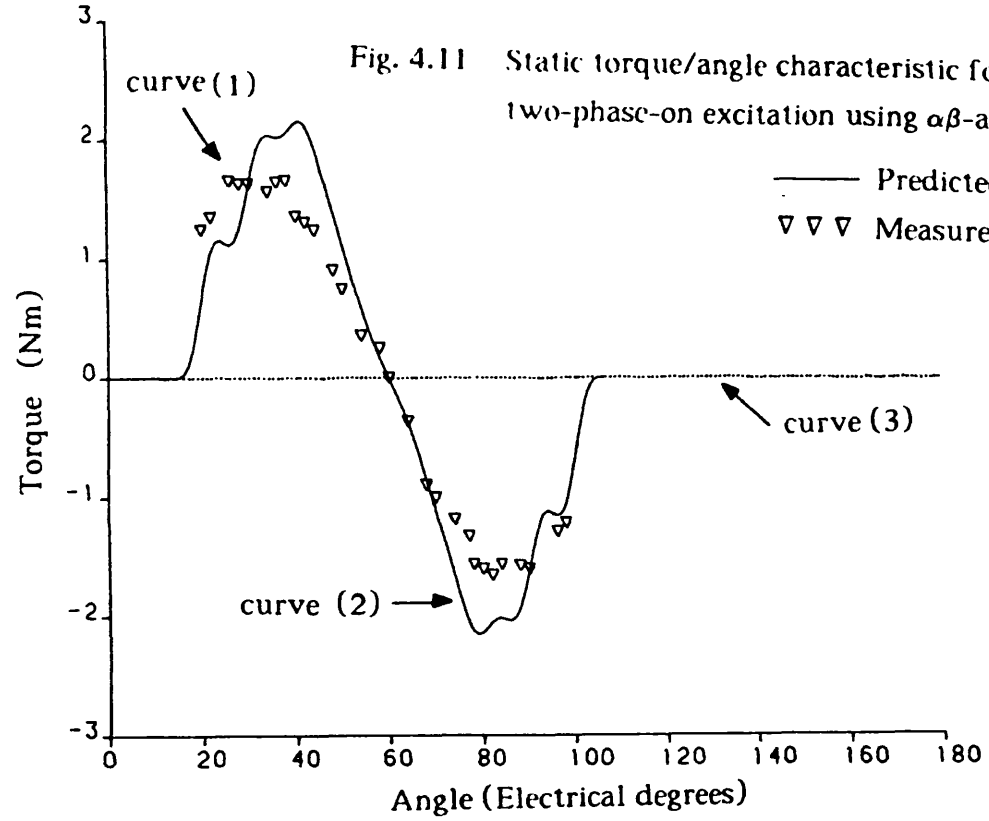

Fig. 4.11 Static torque/angle characteristic for two-phase-on excitation using $\alpha\beta$-axes rotor

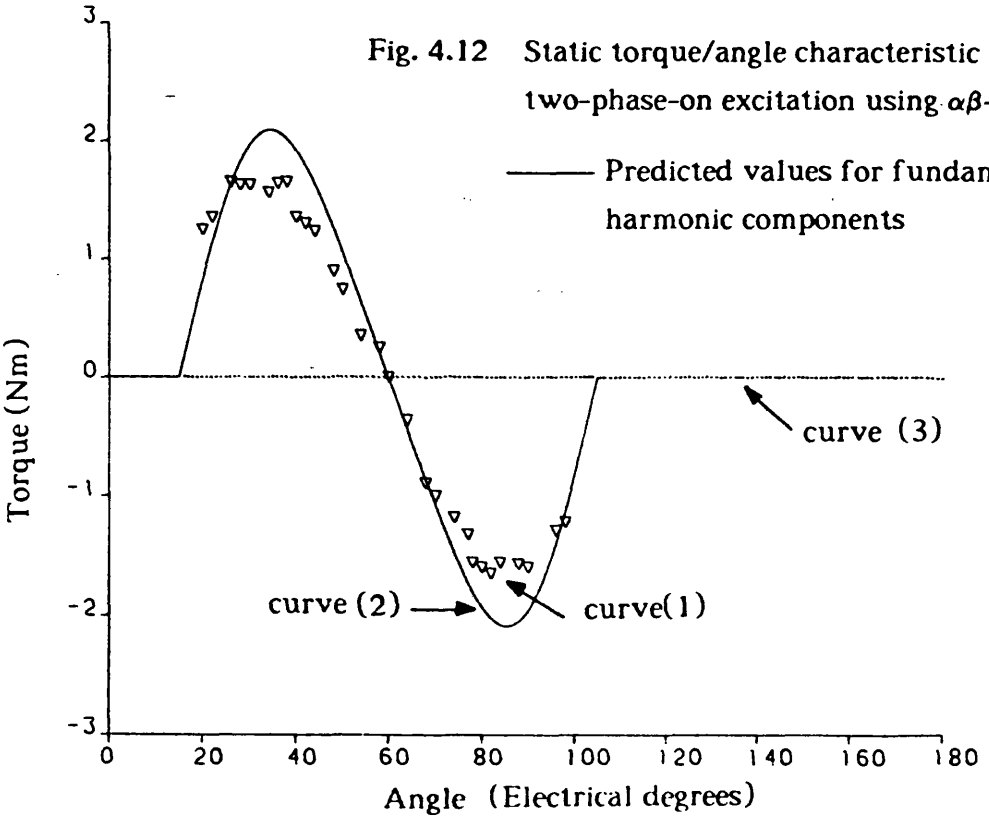

Fig. 4.12 Static torque/angle characteristic for two-phase-on excitation using $\alpha\beta$-axes rotor

Fig. 4.13 Variation of stator current, I_a with respect to rotor position

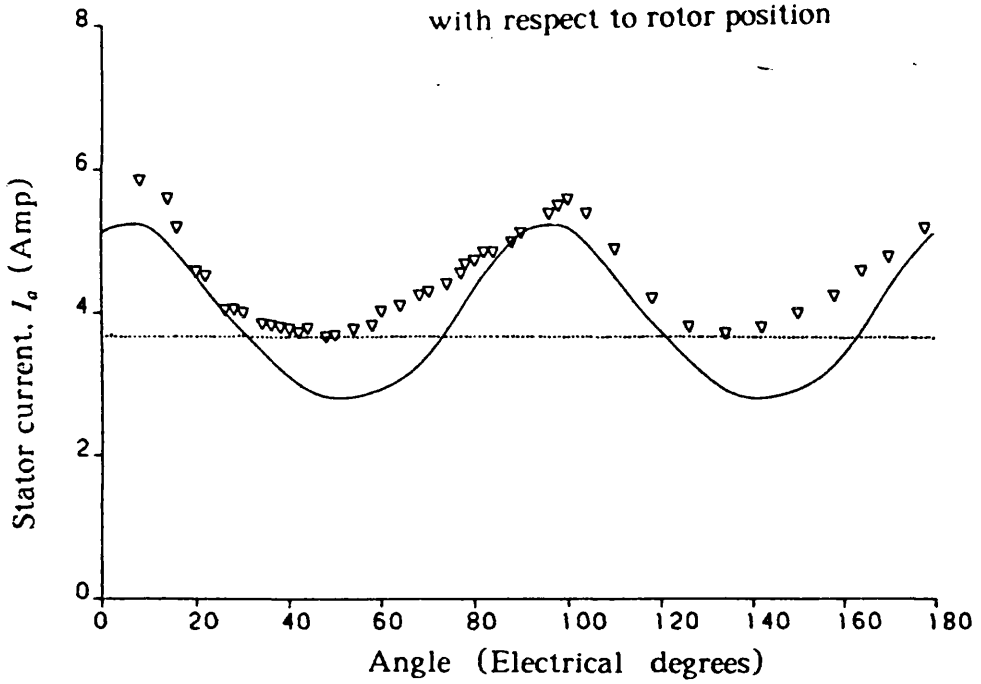

Fig. 4.14 Variation of stator current, I_b with respect to rotor position

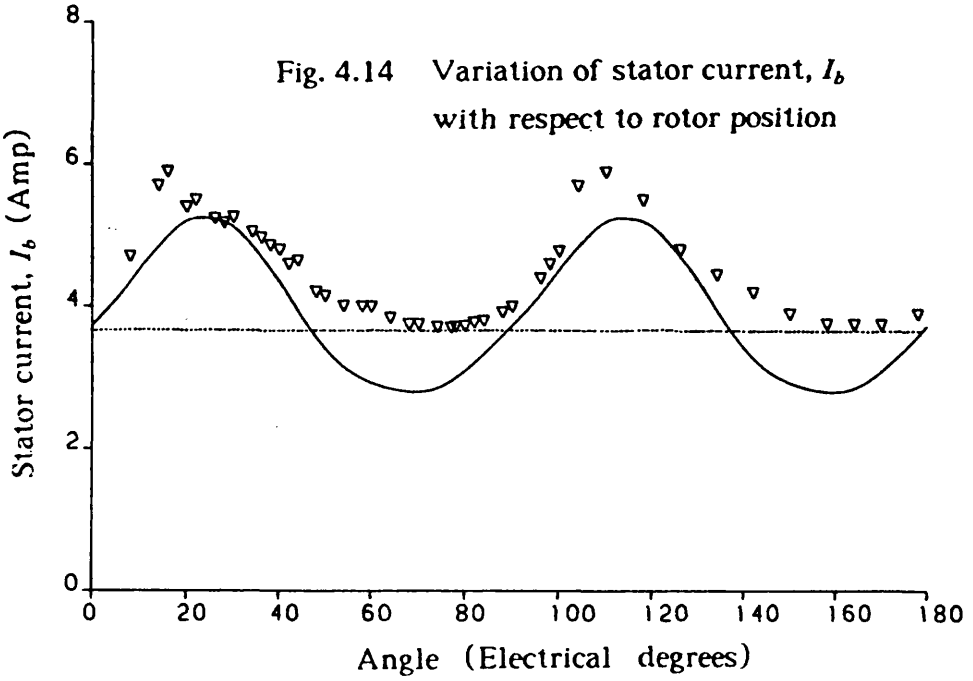

——— Predicted values

▽ ▽ ▽ Measured values

..... Predicted values for fundamental component of mutual inductances

Fig. 4.15 Variation of rotor current, I_α with respect to rotor position

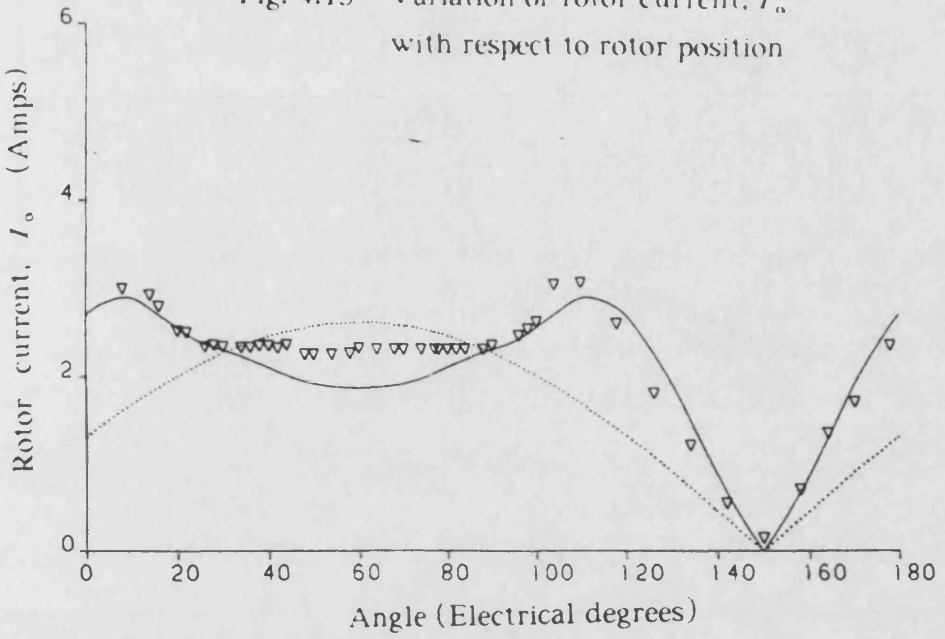

Fig. 4.16 Variation of rotor current, I_β with respect to rotor position

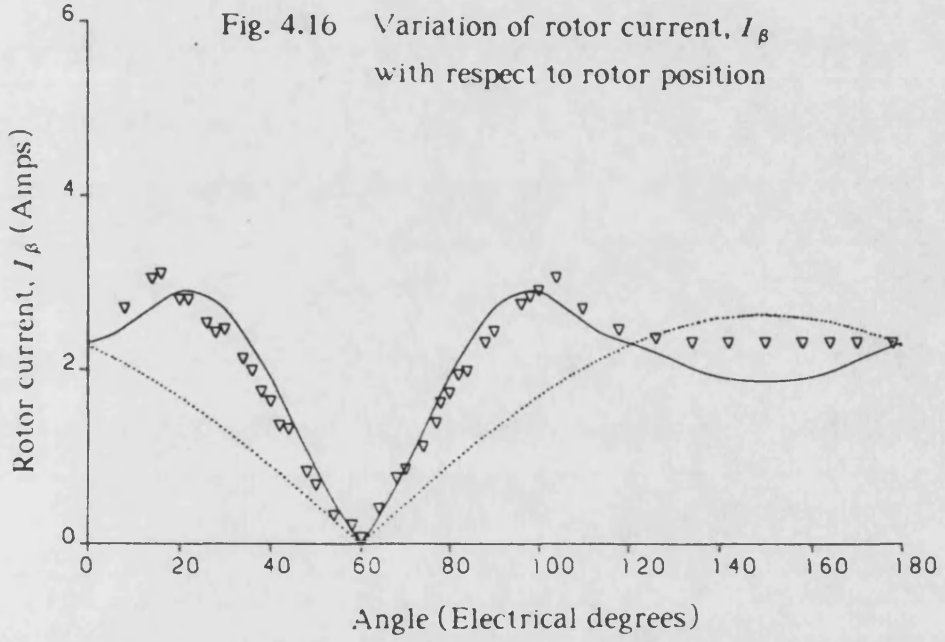

——— Predicted values

▽ ▽ ▽ Measured values

..... Predicted values for fundamental component

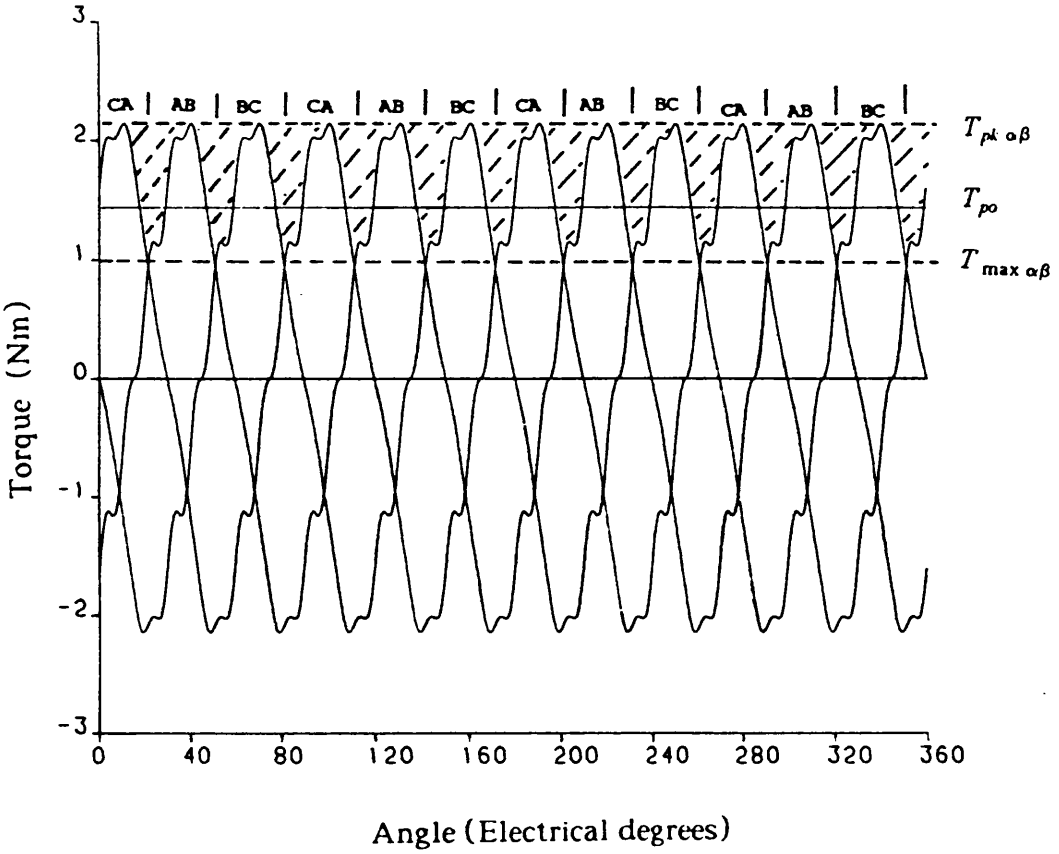

Fig. 4.17 Static torque/angle curves for sequential excitation of an $\alpha\beta$-axes rotor with two-phases-on at a time

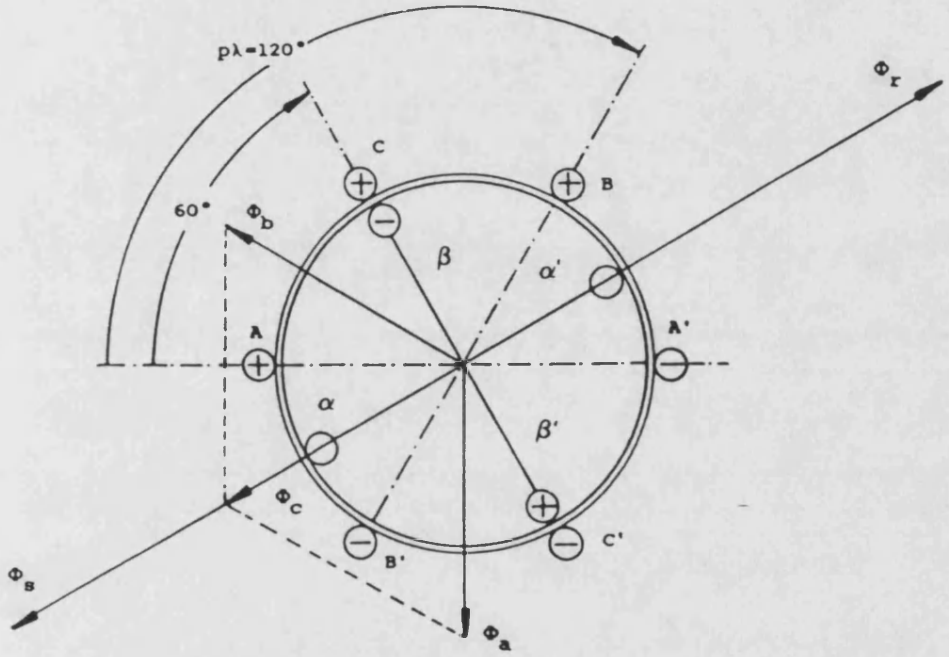

Fig. 4.18 Schematic diagram of the $\alpha\beta$-axes rotor for three-phase-on excitation showing various vectors

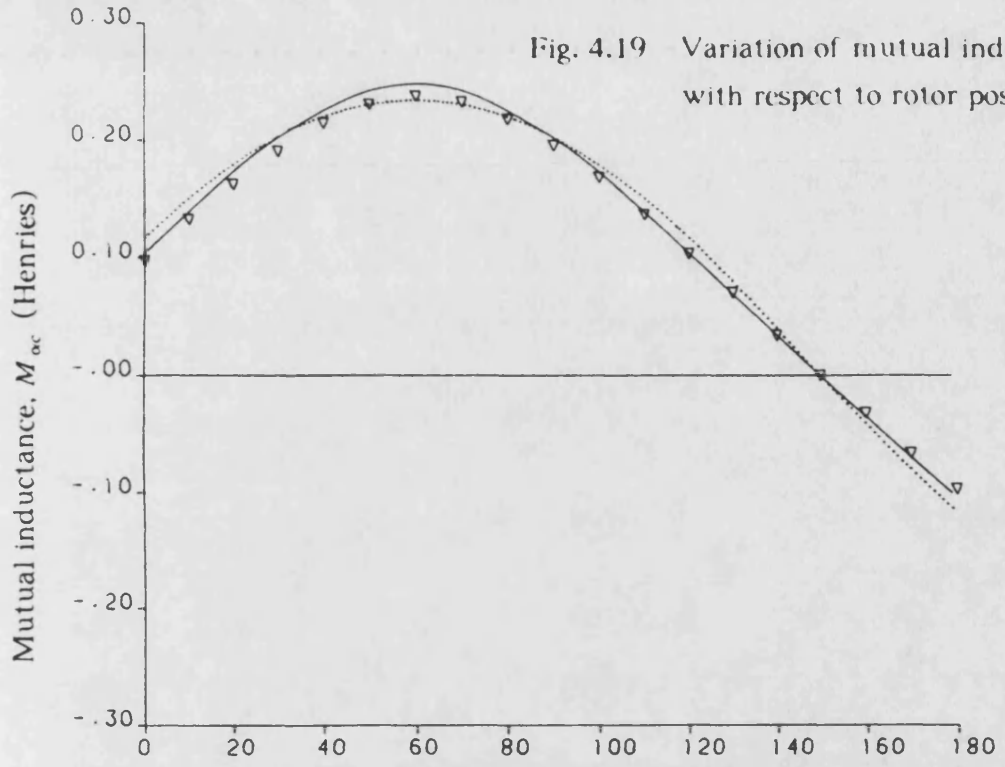

Fig. 4.19 Variation of mutual inductance, $M_{\alpha c}$ with respect to rotor position

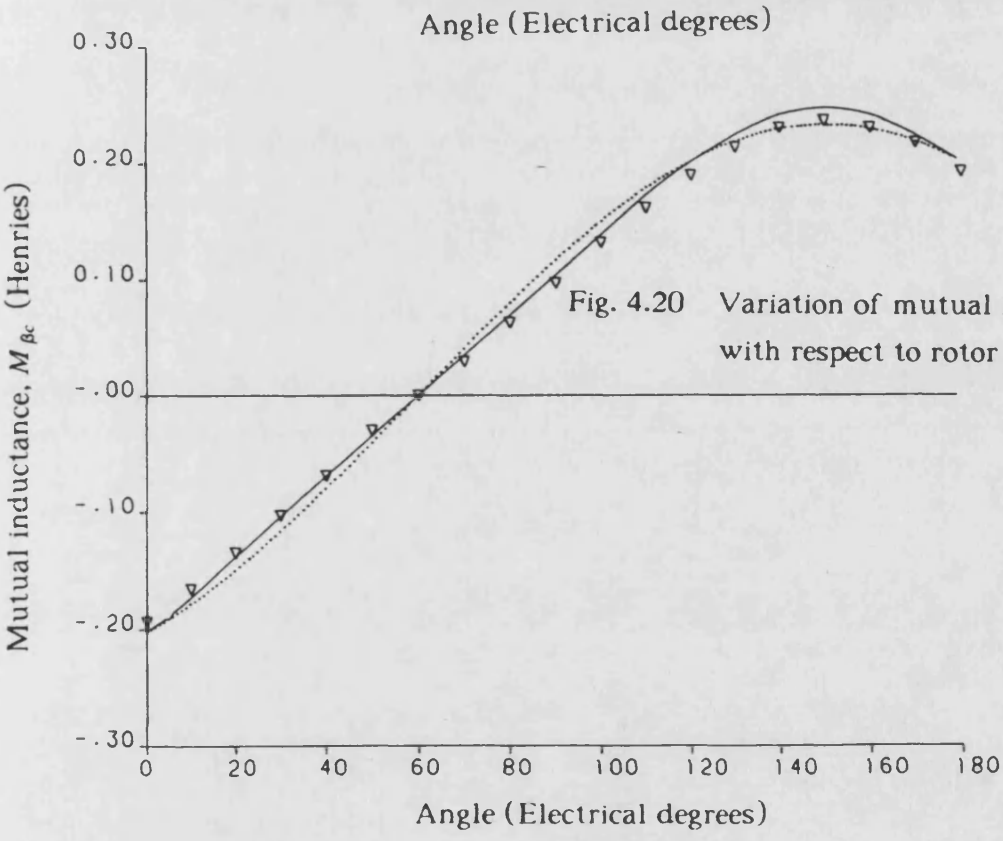

Fig. 4.20 Variation of mutual inductance, $M_{\beta c}$ with respect to rotor position

..... Fundamental component of predicted values

—— Predicted values

∇ ∇ ∇ Measured values

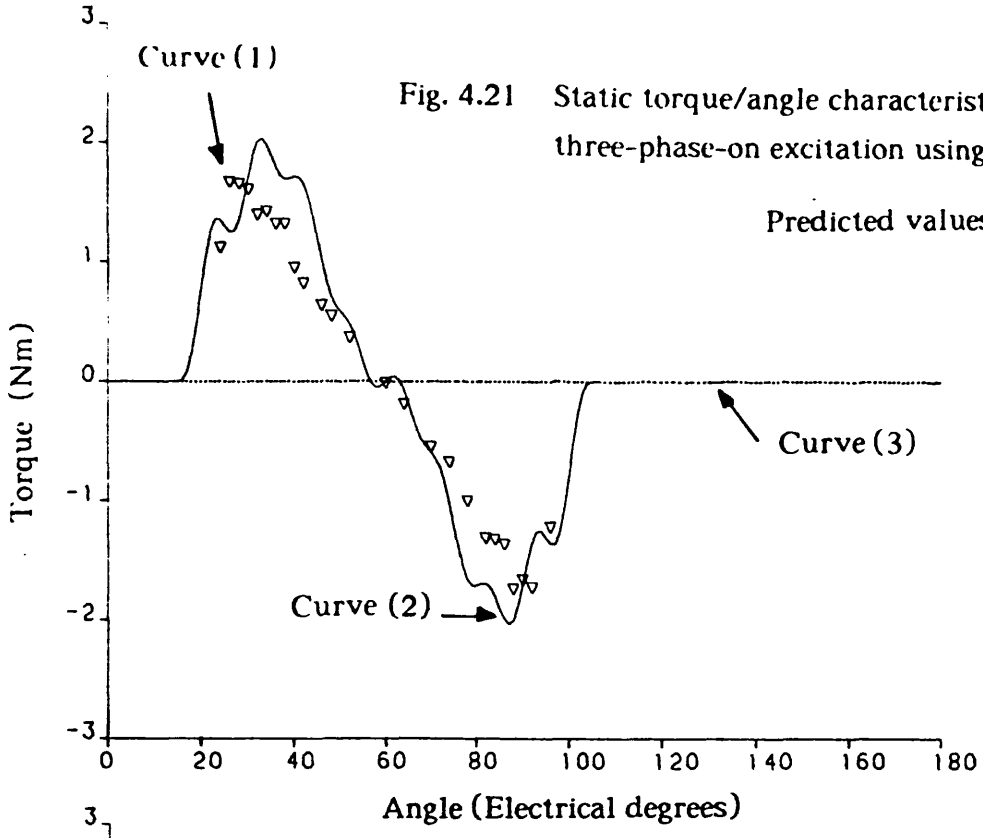

Fig. 4.21 Static torque/angle characteristics for three-phase-on excitation using an $\alpha\beta$-axes rotor

Predicted values

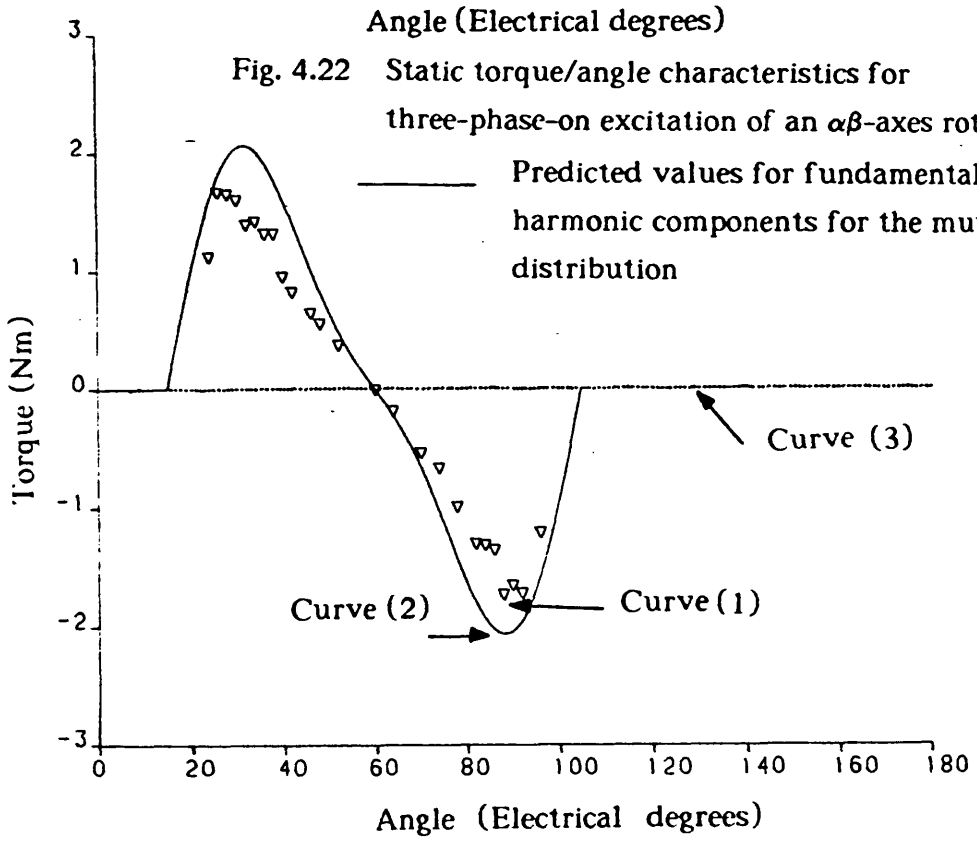

Fig. 4.22 Static torque/angle characteristics for three-phase-on excitation of an $\alpha\beta$-axes rotor

——— Predicted values for fundamental and third harmonic components for the mutual inductance distribution

..... · Predicted values for fundamental component of mutual inductances

▽ ▽ ▽ ▽ Measured values

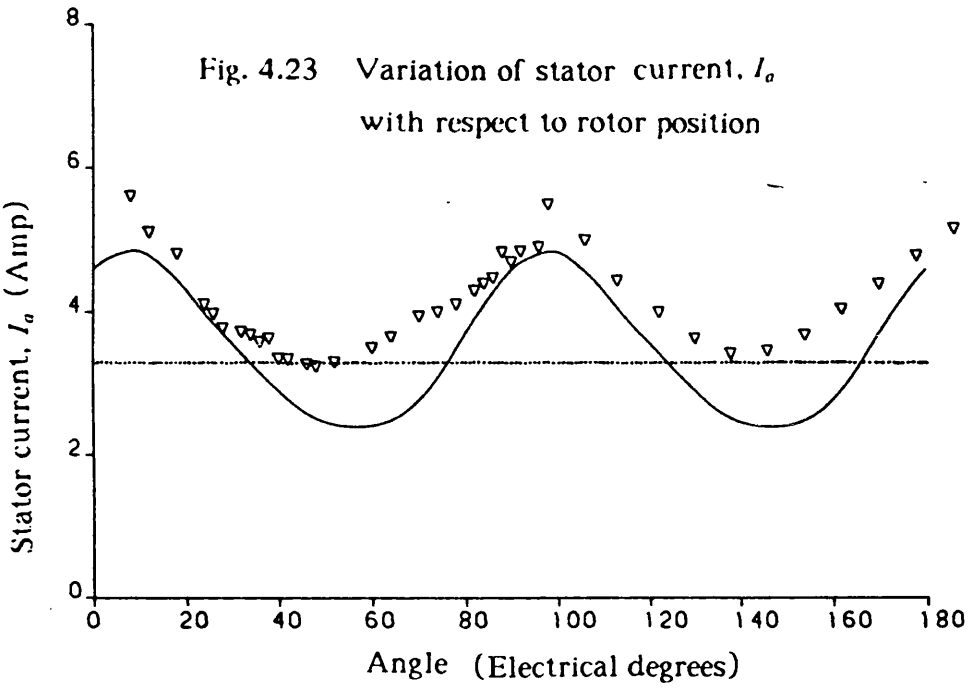

Fig. 4.23 Variation of stator current, I_a with respect to rotor position

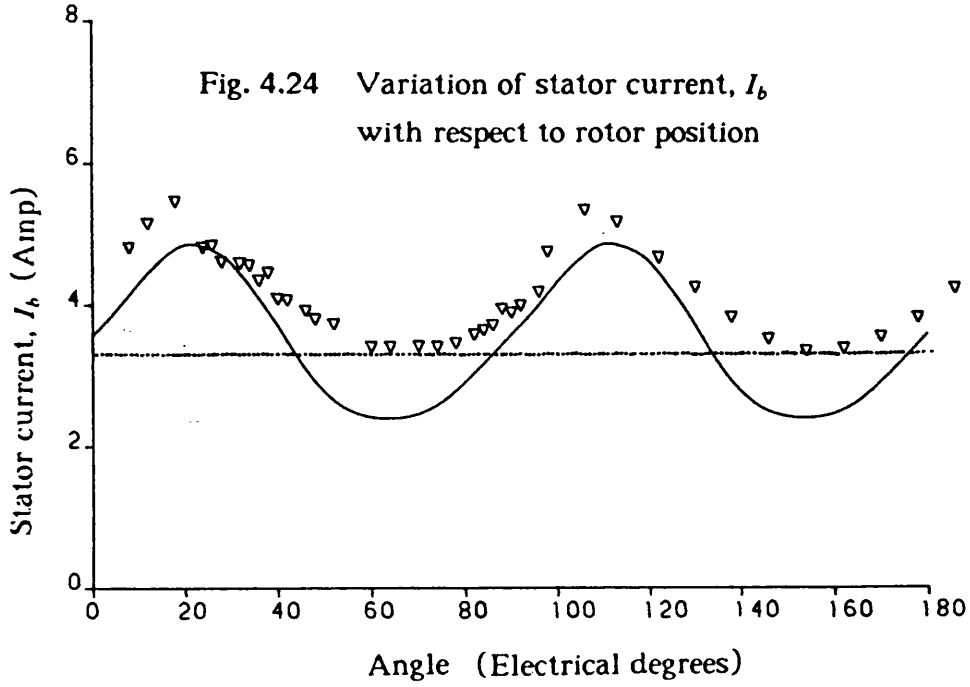

Fig. 4.24 Variation of stator current, I_b with respect to rotor position

——— Predicted values

▽ ▽ ▽ Measured values

..... Predicted values for fundamental component of mutual inductances

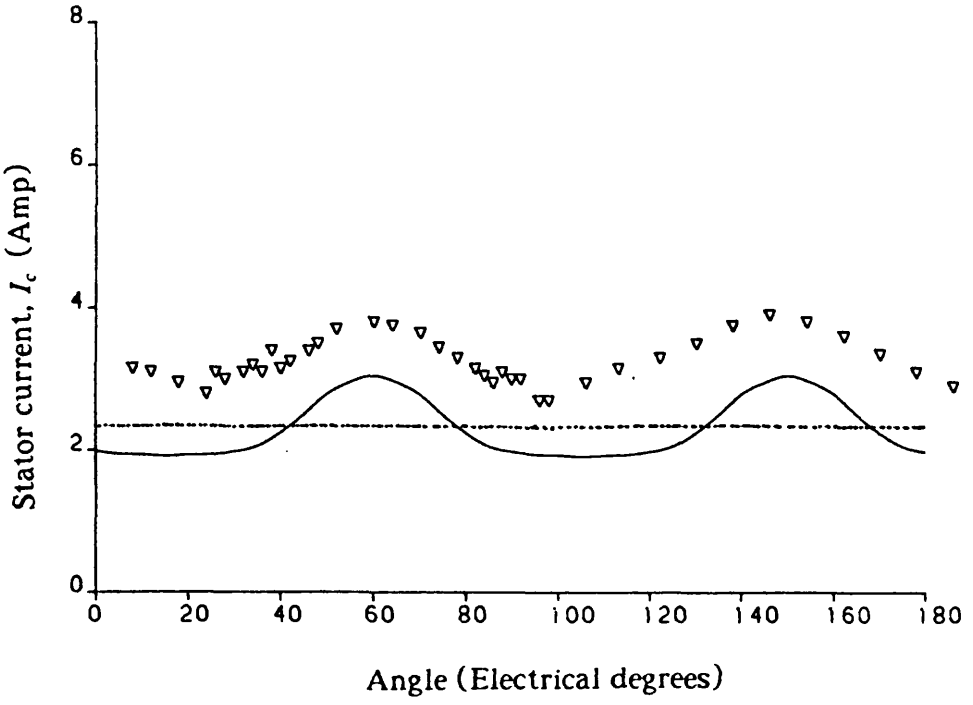

Fig. 4.25 Variation of stator current, I_c with respect to rotor position

——— Predicted values

▽ ▽ ▽ Measured values

..... Predicted values for fundamental component of the mutual inductance distribution

Fig. 4.26 Variation of rotor current, I_α with respect to rotor position

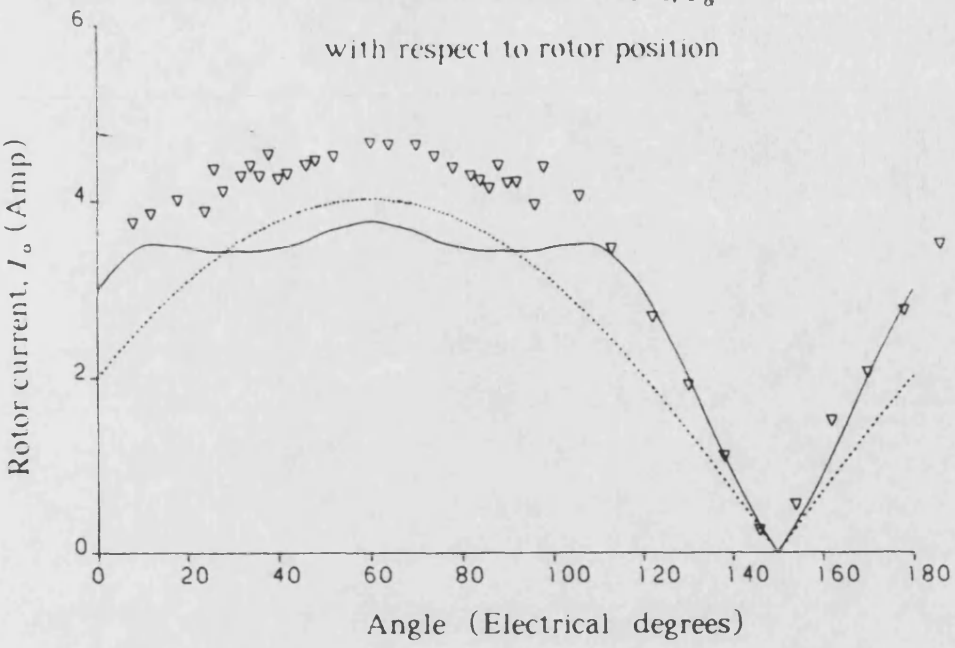

Fig. 4.27 Variation of rotor current, I_β with respect to rotor position

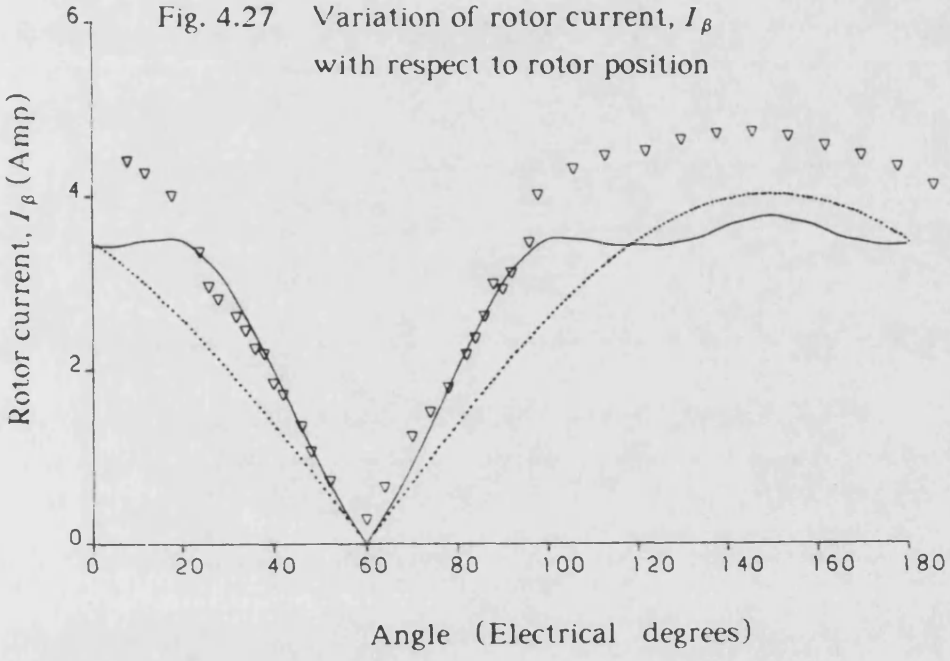

——— Predicted values

▽ ▽ ▽ Measured values

..... Predicted values for fundamental component of mutual inductances

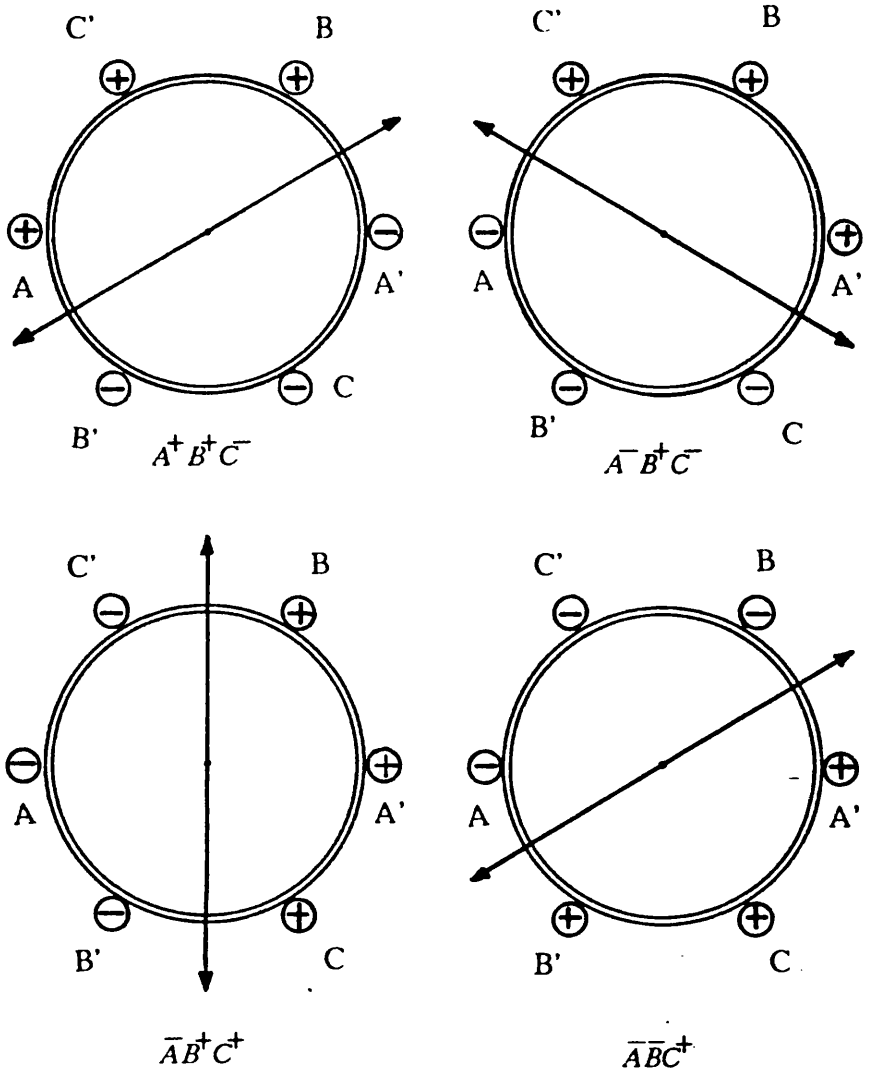

Fig. 4.28(a)Three-phase-on sequential excitation with the pattern

$$A^+B^+\bar{C} \rightarrow \bar{A}B^+\bar{C} \rightarrow \bar{A}B^+C^+ \rightarrow \bar{A}\bar{B}C^+$$

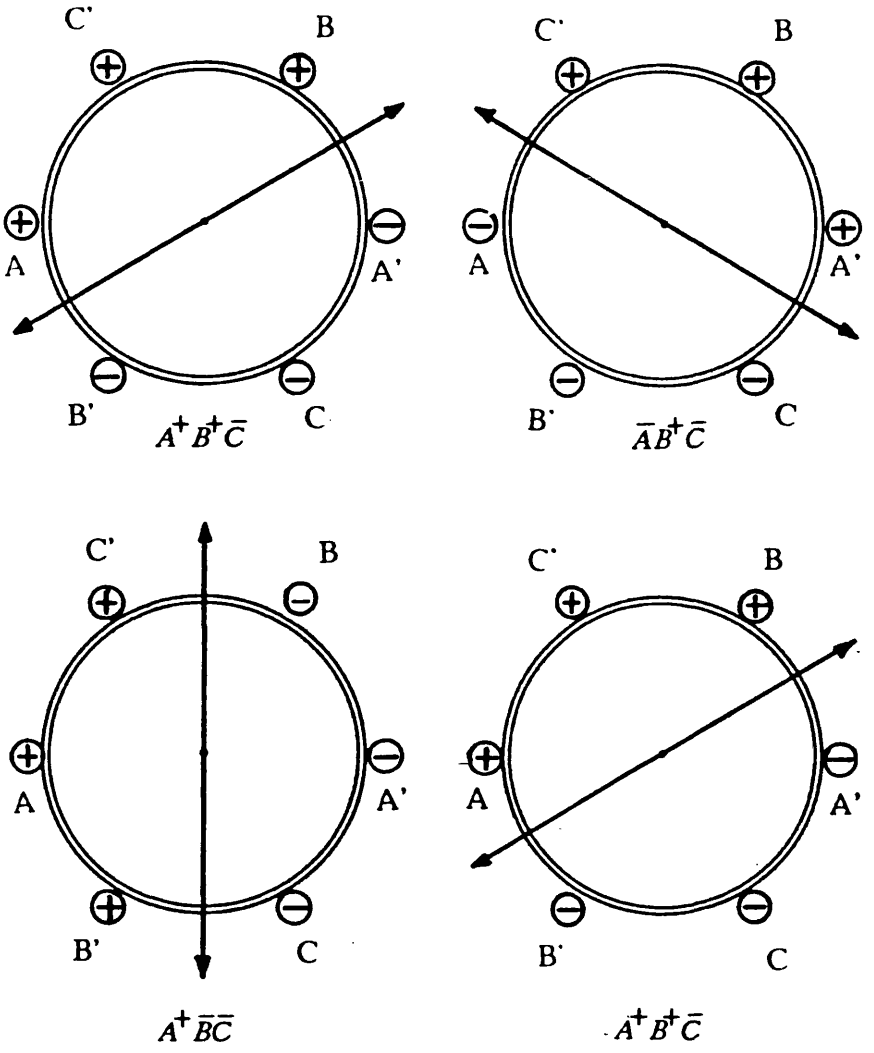

Fig. 4.28(b)Three-phase-on sequential excitation with the pattern

$$A^+B^+\bar{C}^- \rightarrow A^-B^+\bar{C}^- \rightarrow A^+\bar{B}\bar{C}^- \rightarrow A^+B^+\bar{C}$$

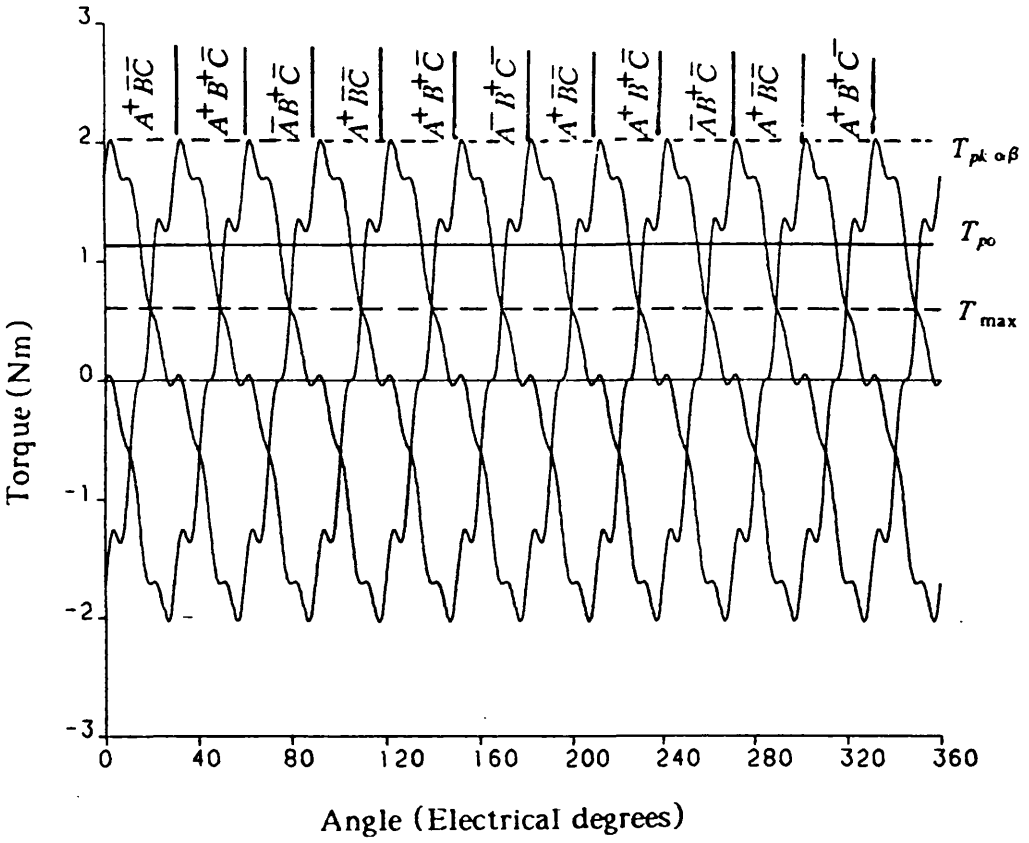

Fig. 4.29 Static torque/angle curves for three-phase-on sequential excitation

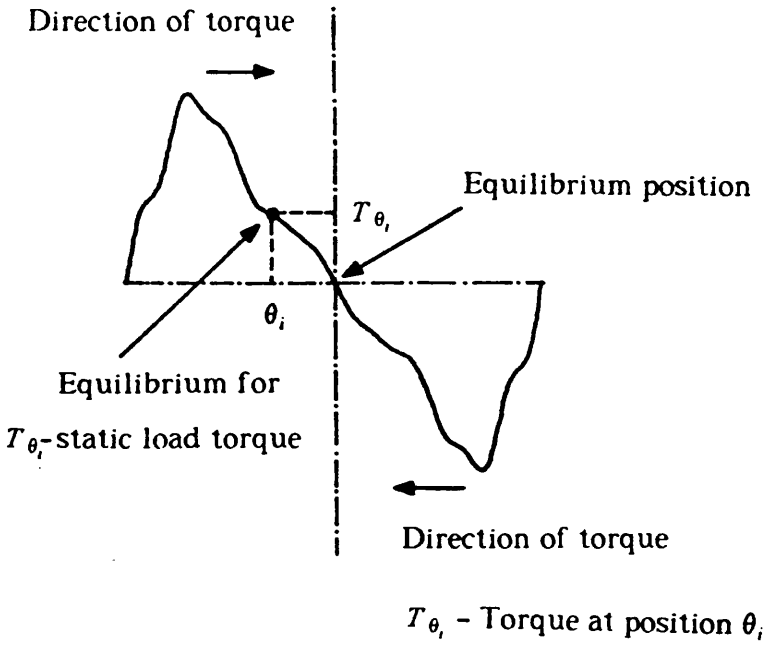

Fig. 5.1 Schematic diagram of the torque/angle characteristic at the equilibrium position

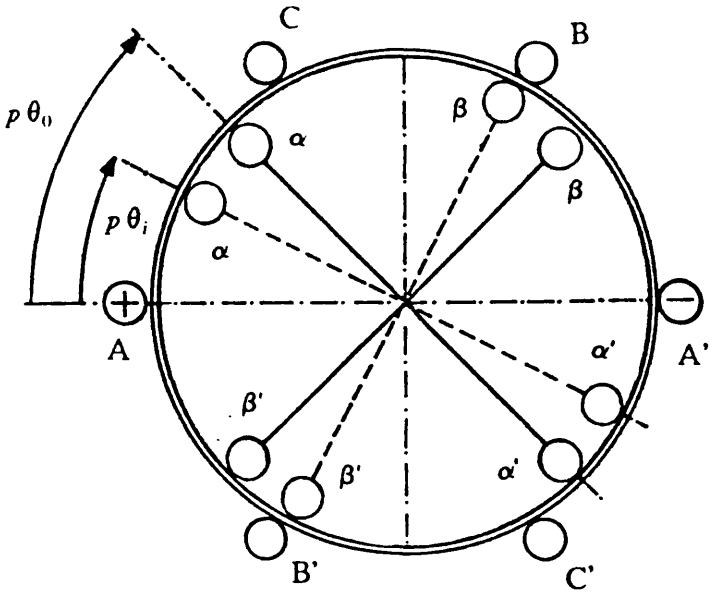

Fig. 5.2 Schematic diagram of the rotor representing the initial and final positions, $p\theta_i$ and $p\theta_0$, when A phase winding is excited

Fig. 5.3 Flow chart of computer programme for steady state solution

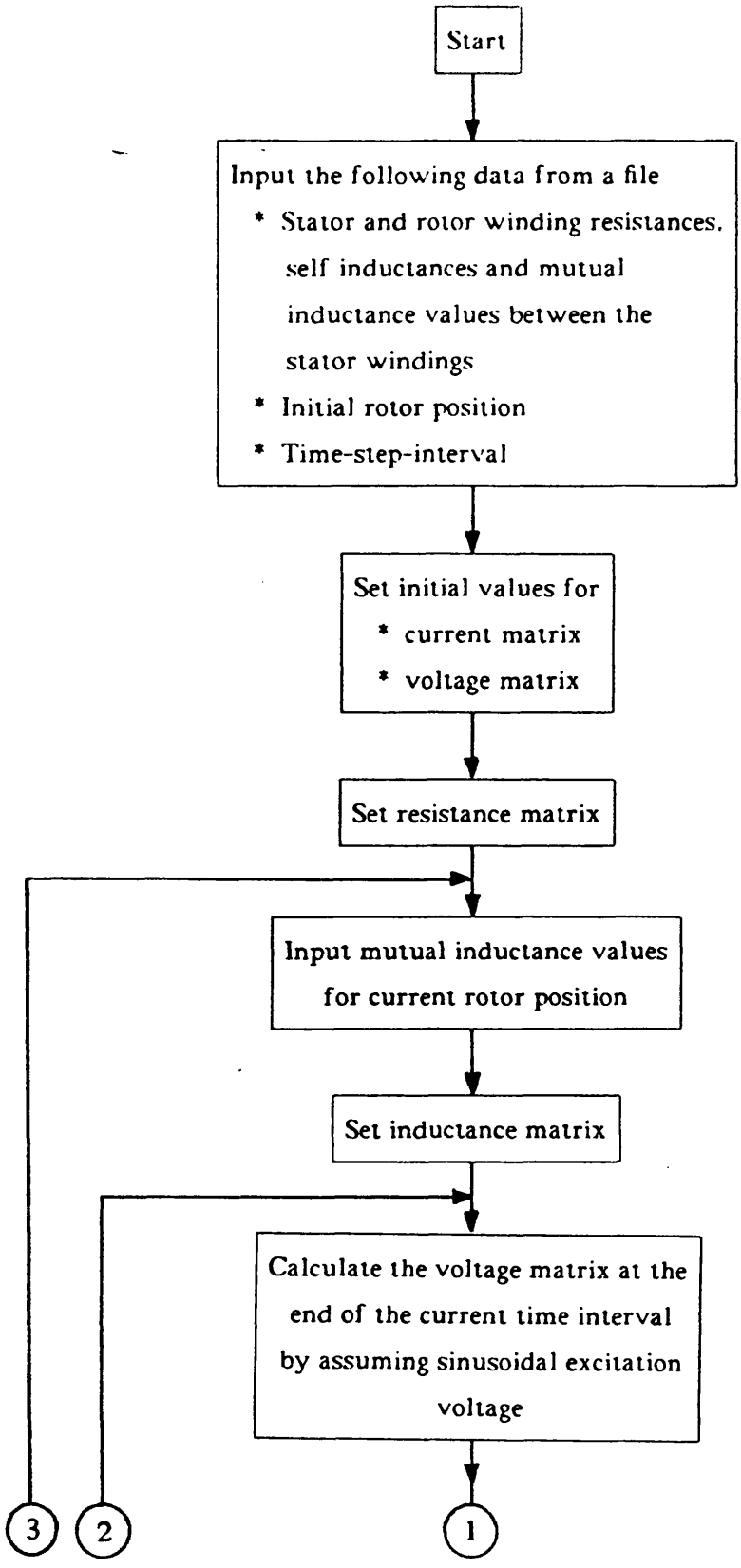

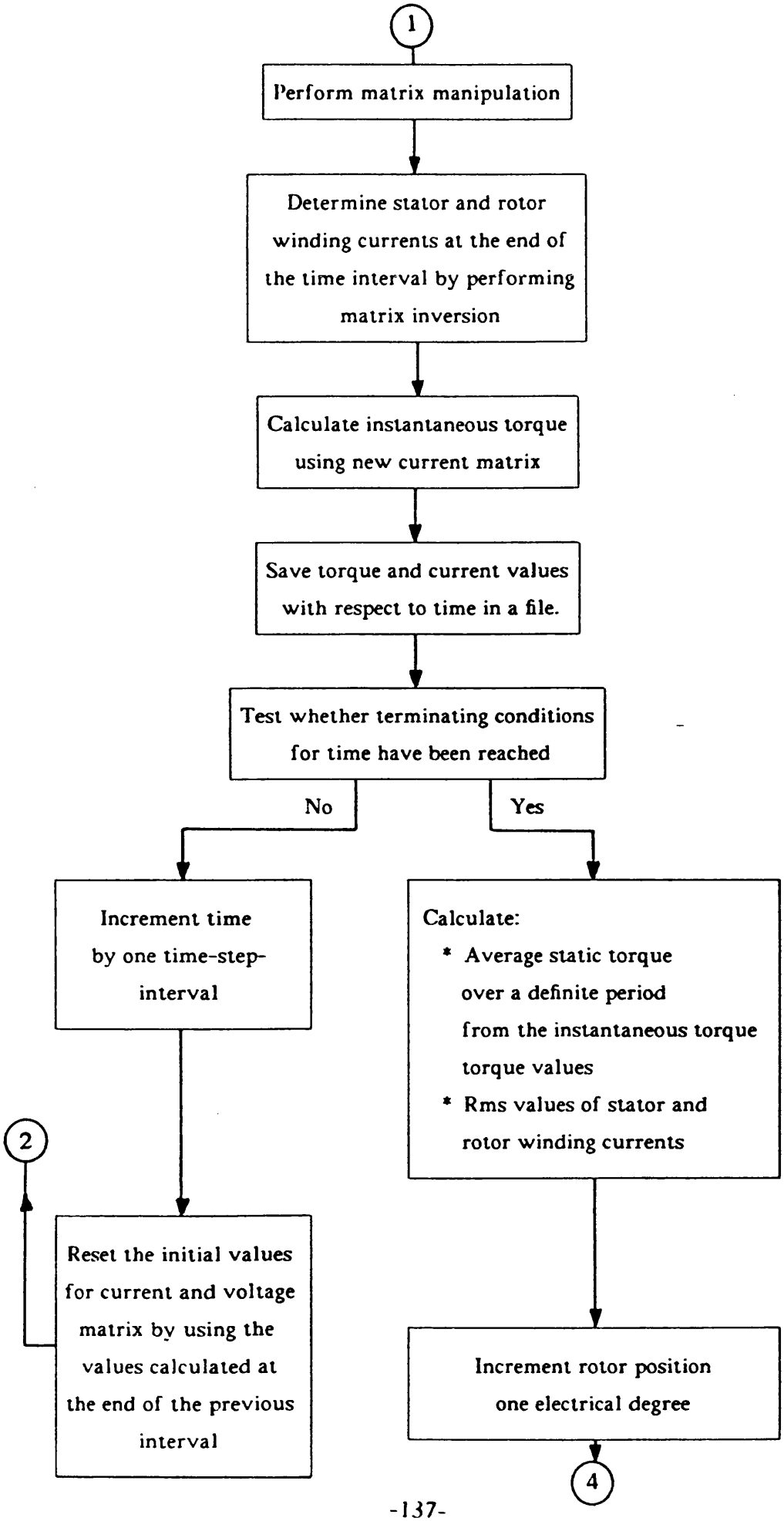
1
Perform matrix manipulation
Determine stator and rotor winding currents at the end of the time interval by performing matrix inversion
Calculate instantaneous torque using new current matrix
Save torque and current values with respect to time in a file.
Test whether terminating conditions for time have been reached
No
Yes
Increment time by one time-step-interval
Calculate:
* Average static torque over a definite period from the instantaneous torque torque values
* Rms values of stator and rotor winding currents
2
Reset the initial values for current and voltage matrix by using the values calculated at the end of the previous interval
Increment rotor position one electrical degree
4

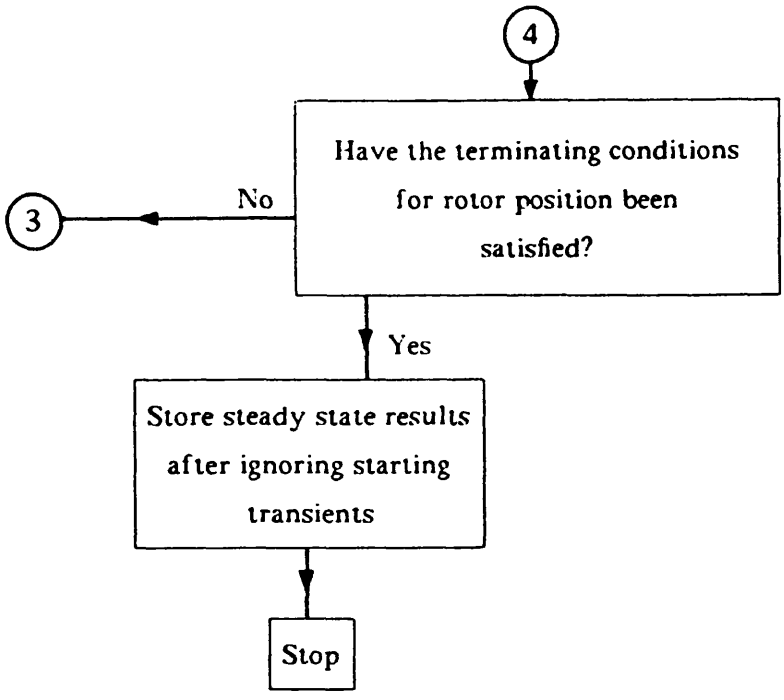
4
Have the terminating conditions for rotor position been satisfied?
No
3
Yes
Store steady state results after ignoring starting transients
Stop

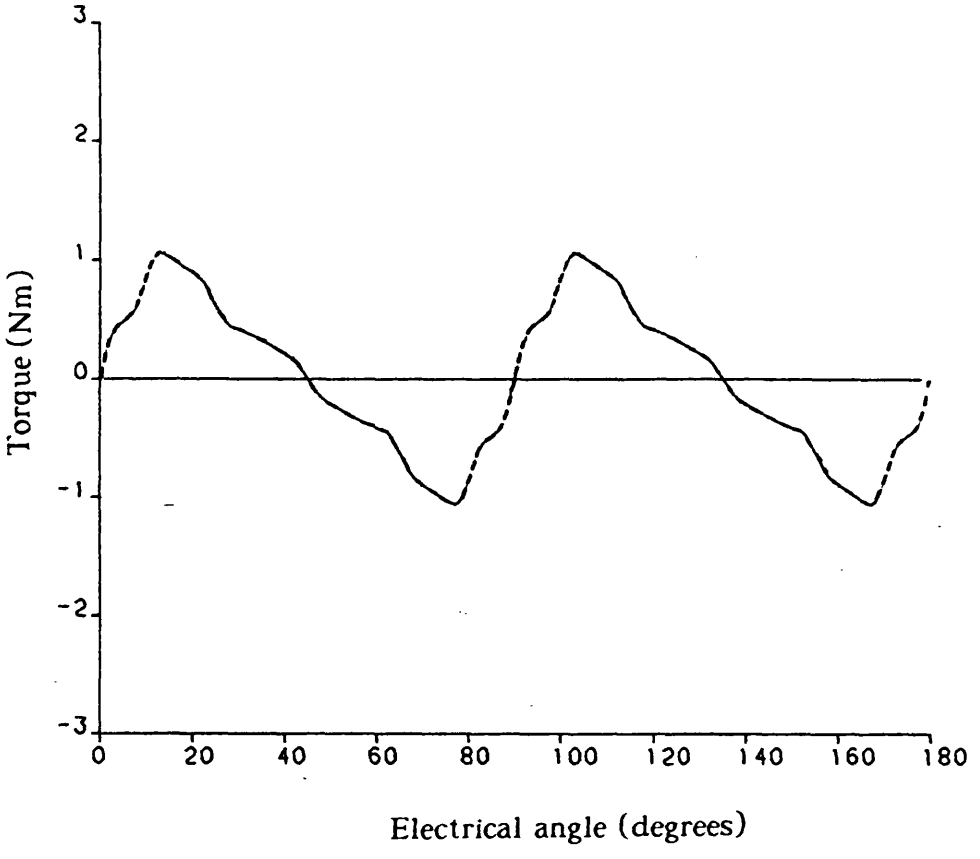

Fig. 5.4 Static torque/angle curves

_____ Predicted using analytical techniques

\- - - - - - Predicted using numerical techniques

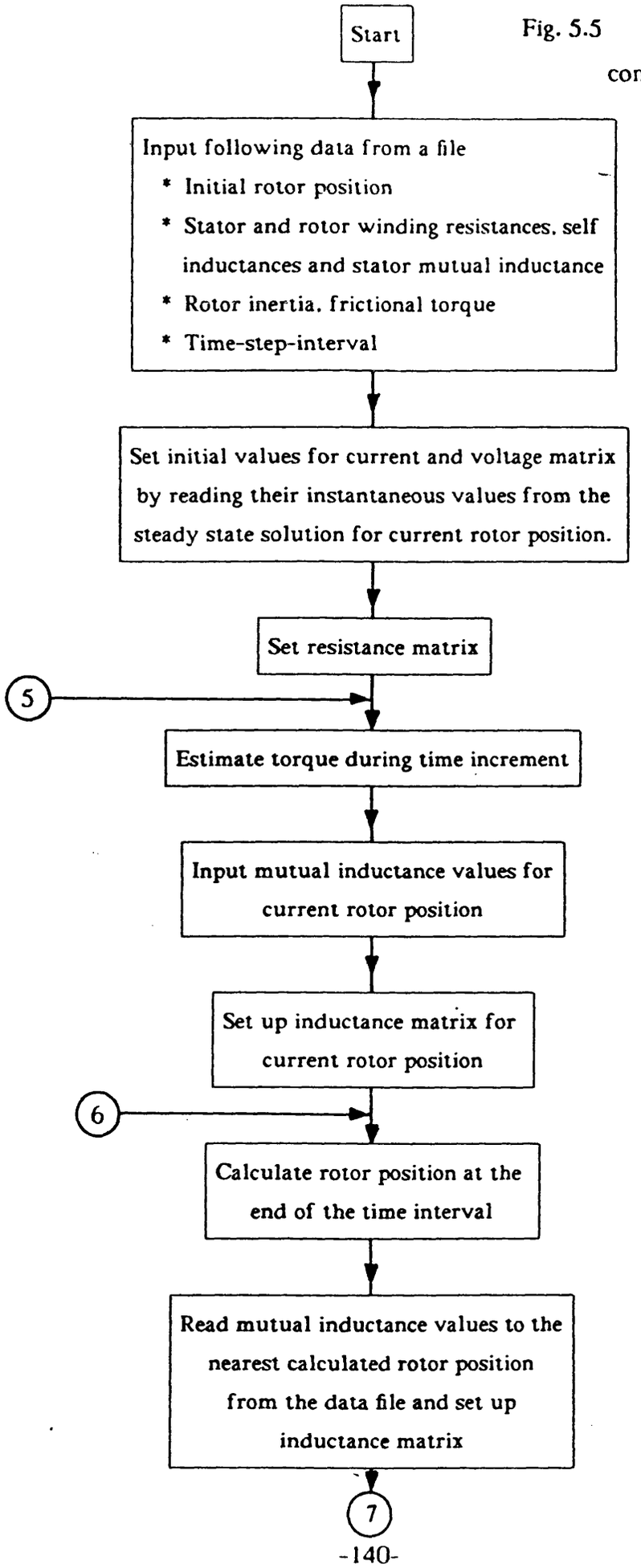

Fig. 5.5 Flow chart of the computer programme for transient solution

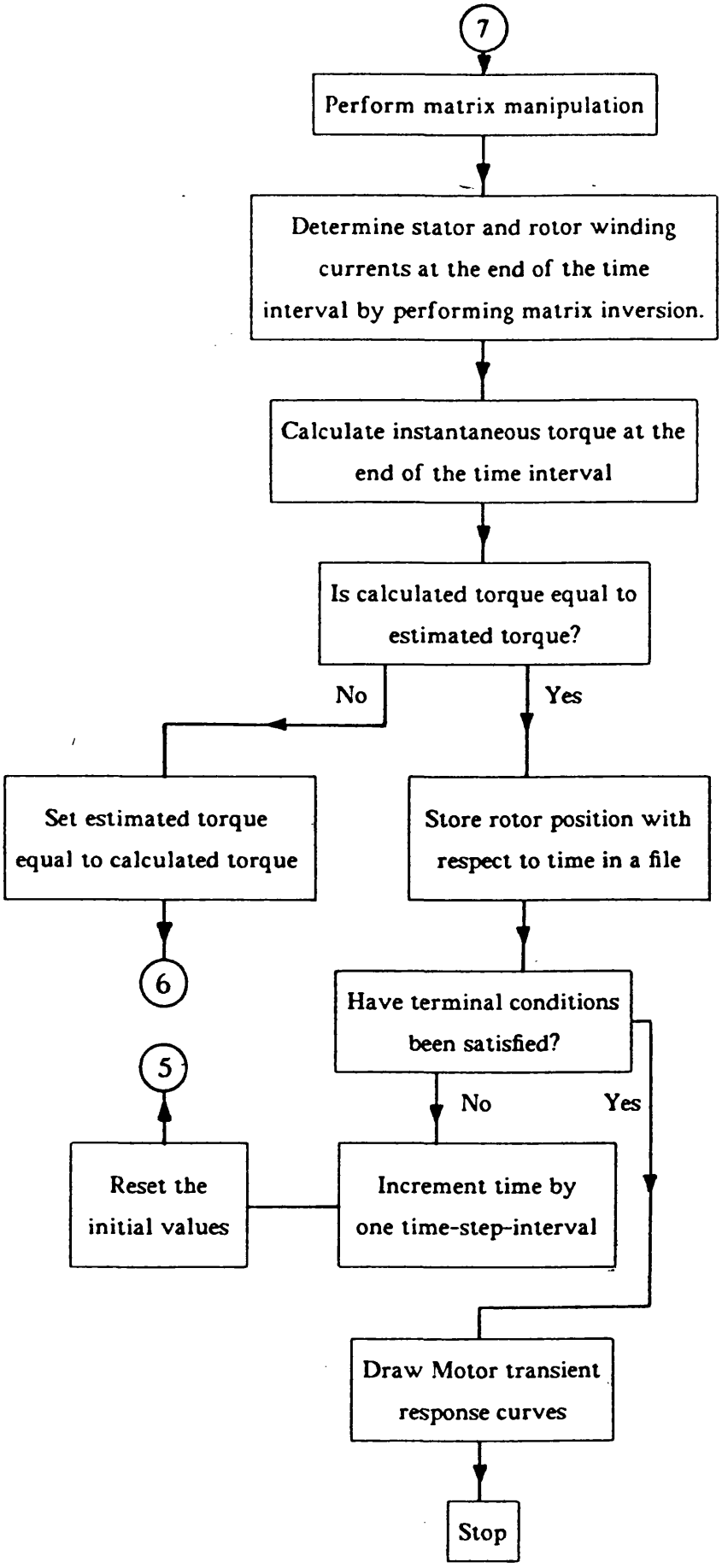
7
Perform matrix manipulation
Determine stator and rotor winding currents at the end of the time interval by performing matrix inversion.
Calculate instantaneous torque at the end of the time interval
Is calculated torque equal to estimated torque?
No
Yes
Set estimated torque equal to calculated torque
Store rotor position with respect to time in a file
6
Have terminal conditions been satisfied?
5
No
Yes
Reset the initial values
Increment time by one time-step-interval
Draw Motor transient response curves
Stop

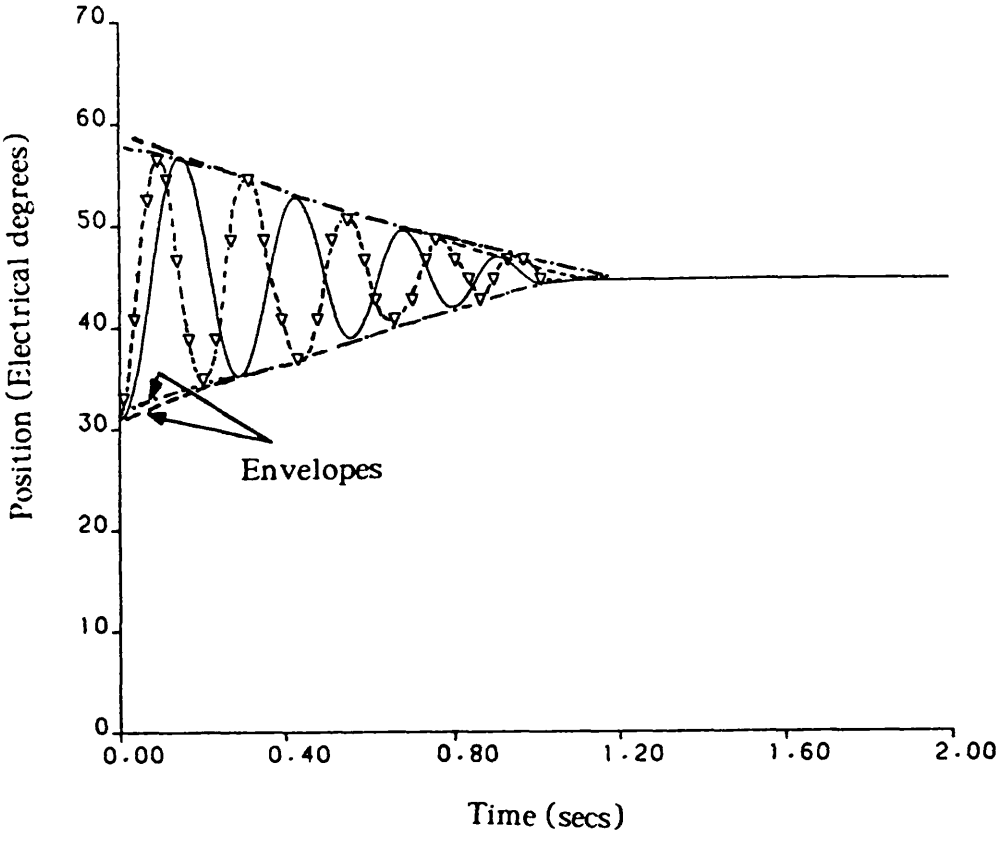

Fig. 5.6 Position response for one-phase-on excitation of an $\alpha\beta$-axes rotor

——— Predicted values

-▽- - -▽- Measured values

—·—·— Measured envelopes

– – – – – – Predicted envelopes

Fig. 5.7

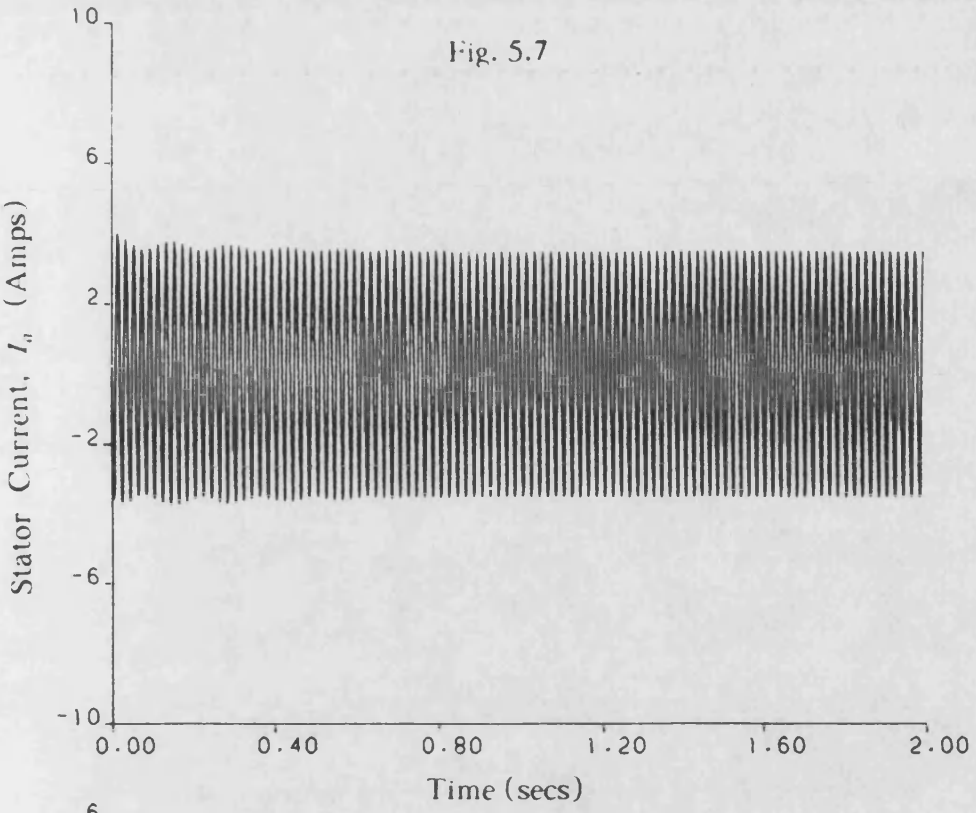

Fig. 5.8

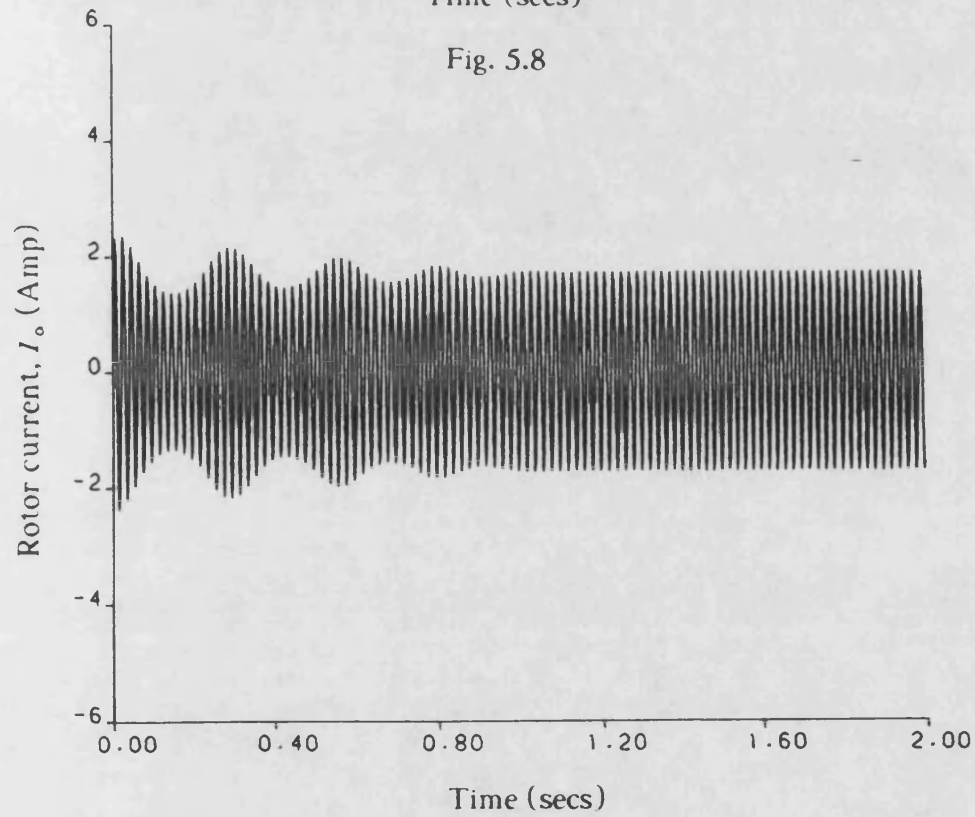

Fig. 5.7 Predicted stator current, I_a, variation with respect to time

Fig. 5.8 Predicted rotor current, I_a, variation with respect to time

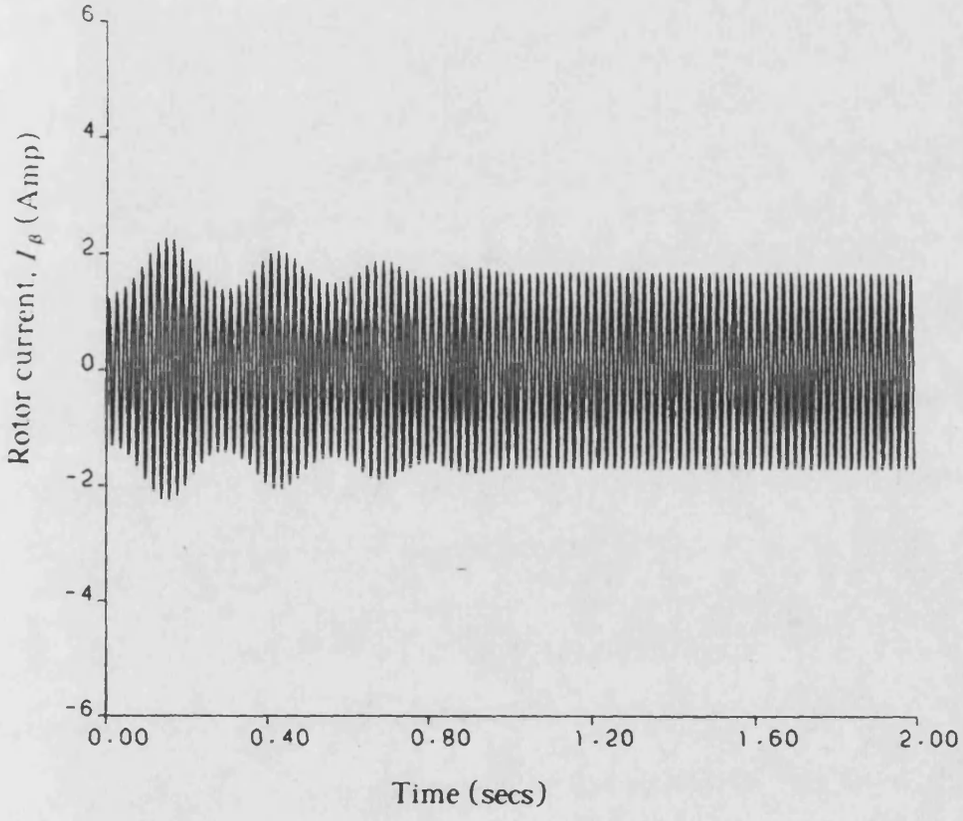

Fig. 5.9 Predicted rotor current, I_β variation with respect to time

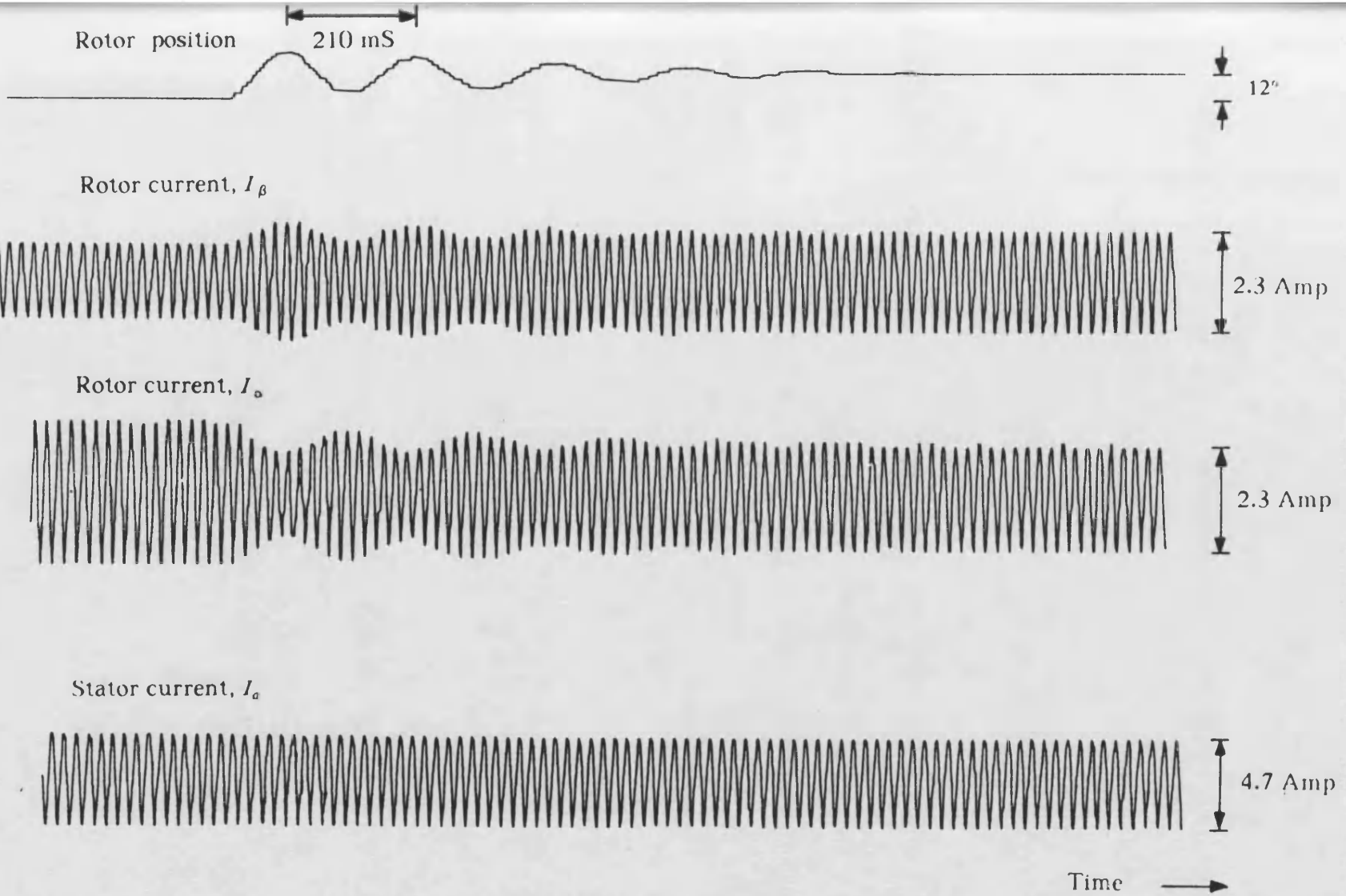

Fig. 5.10 Measured current oscillograms and position response

Fig. 5.11 Envelopes of the stator current, I_a oscillograms

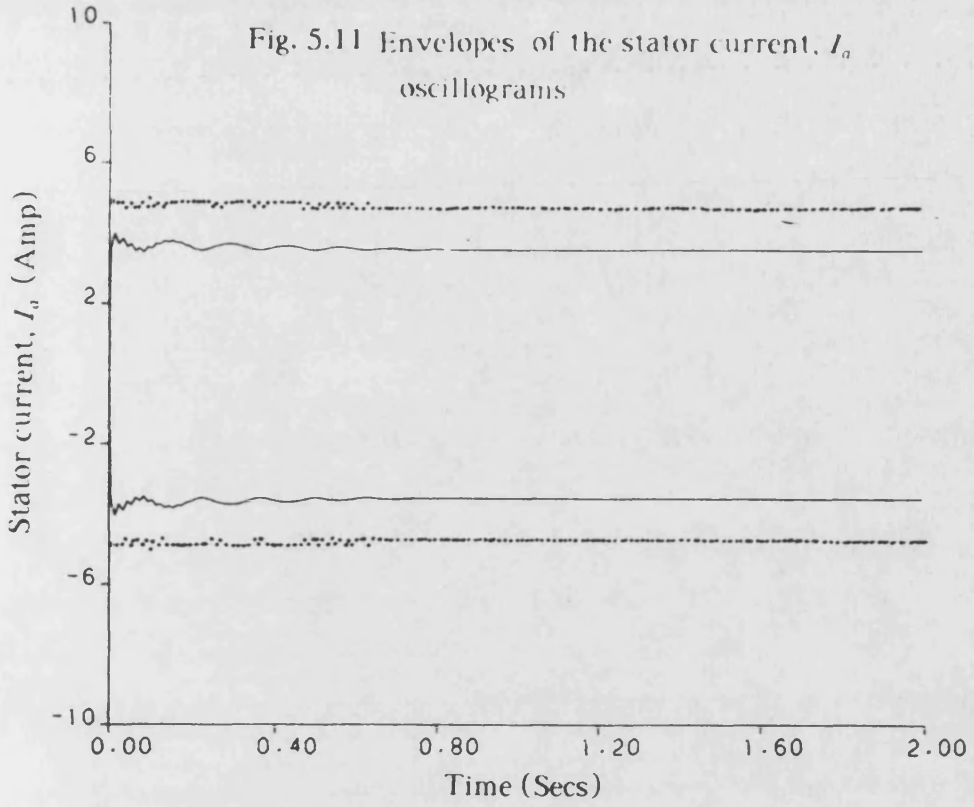

Fig. 5.12 Envelopes of the rotor current, I_a oscillograms

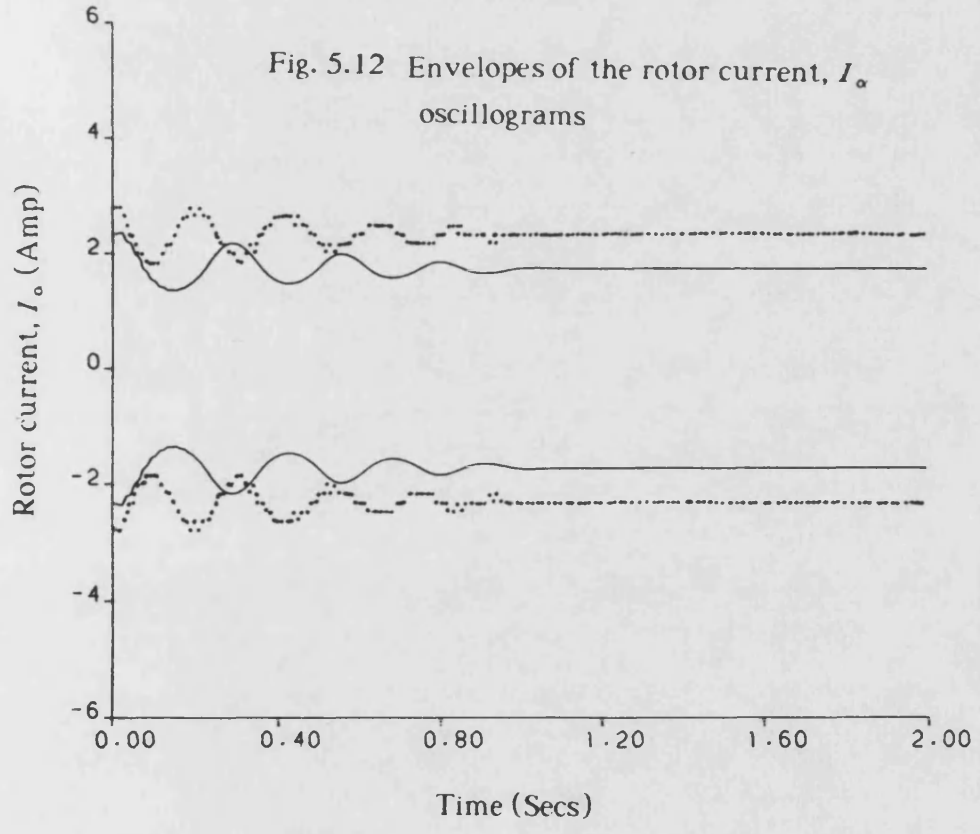

——— Predicted values

..... Measured values

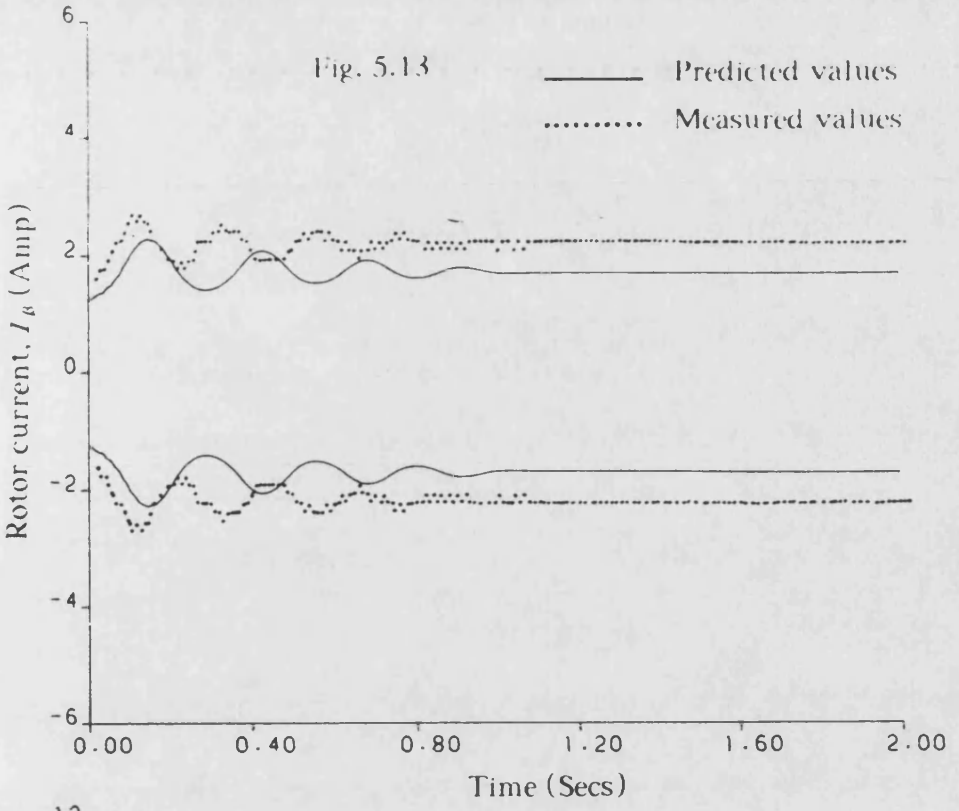

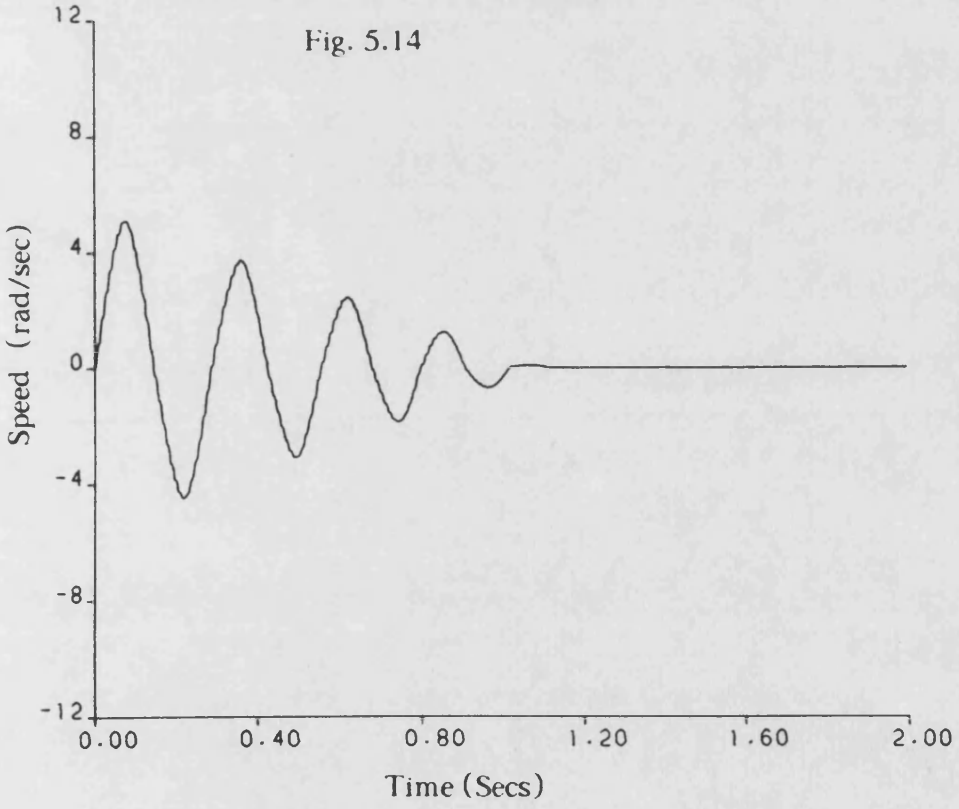

Fig. 5.13 Envelopes of the rotor current, I_β, Oscillograms

Fig. 5.14 Variation of rotor speed with respect to time

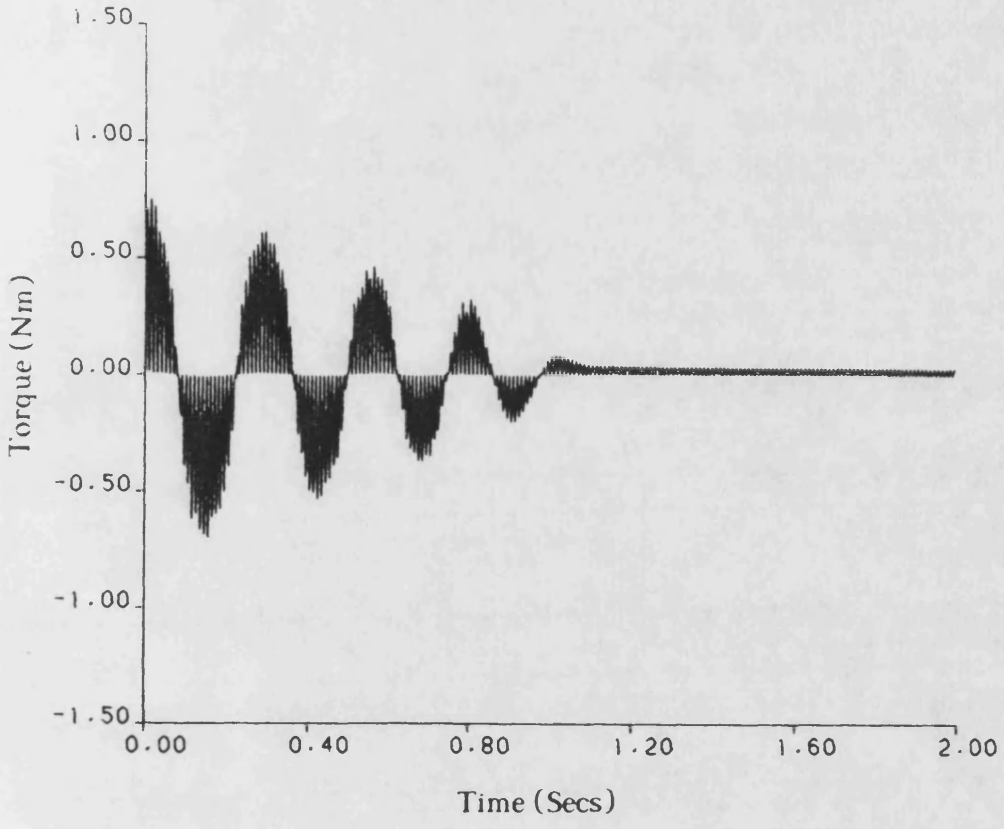

Fig. 5.15 Variation of pulsating torque with respect to rotor position

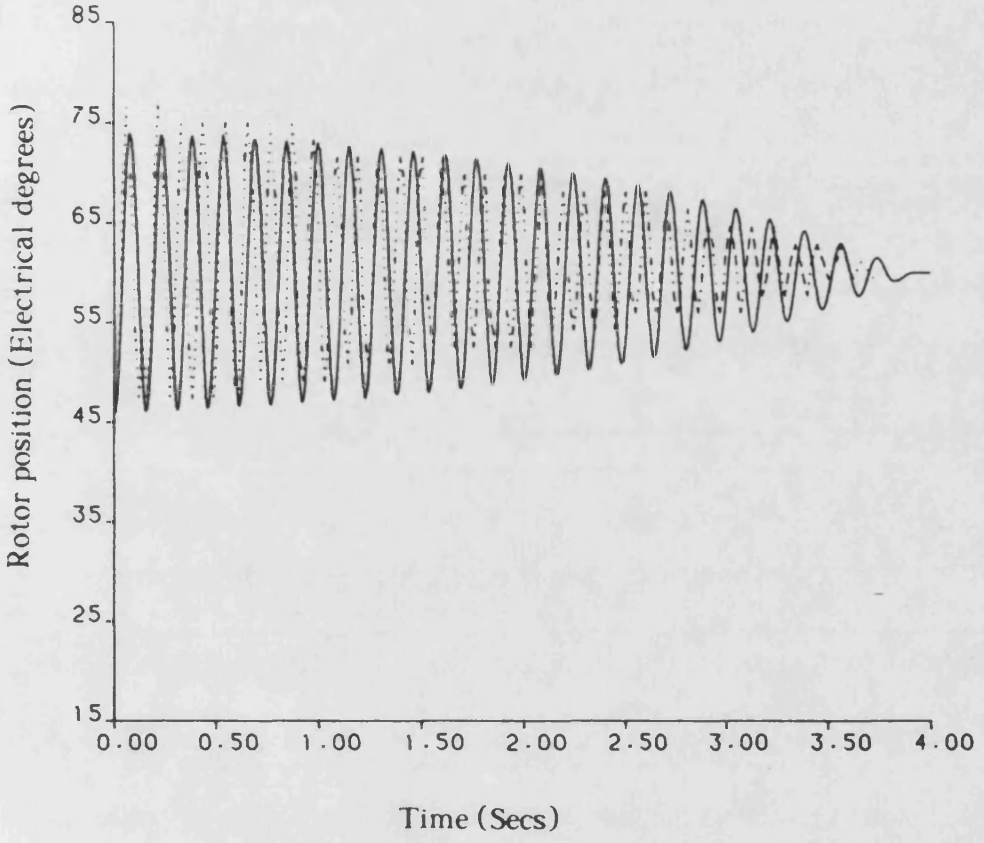

Fig. 5.16 Position response for two-phase-on excitation using $\alpha\beta$-axes rotor

_____ Predicted values

..... Measured values

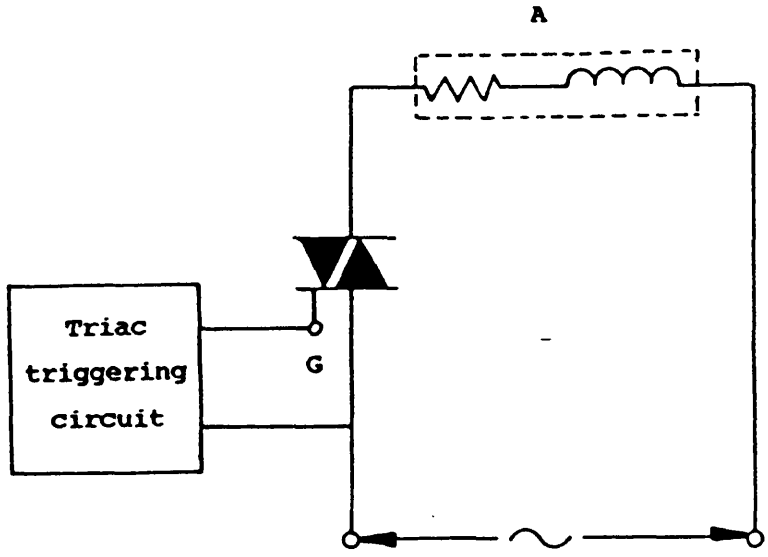

Fig. 6.1 A diagram representing the stator phase winding A in series with the triac

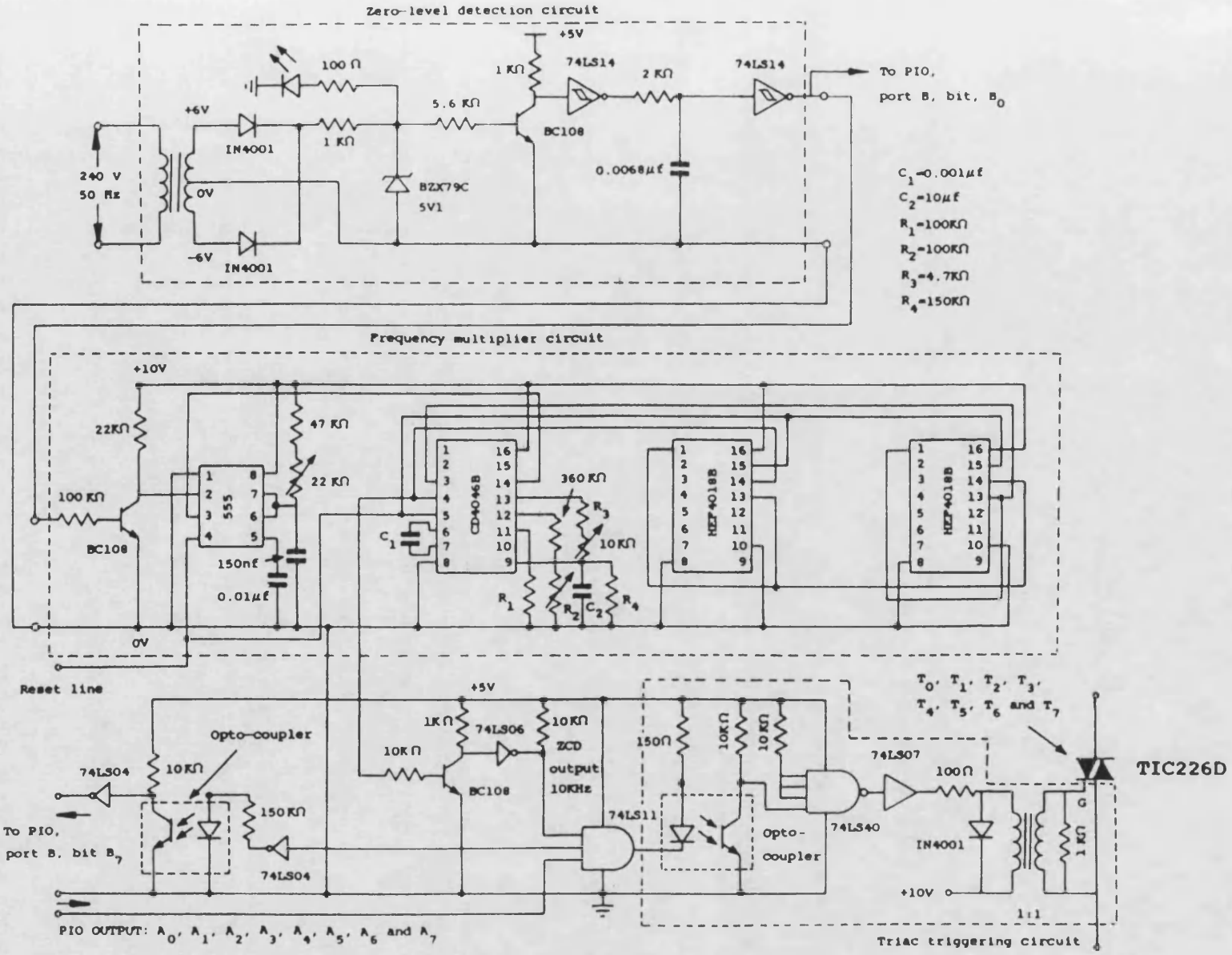

Fig. 6.2. Interfacing circuit between the microprocessor and triac

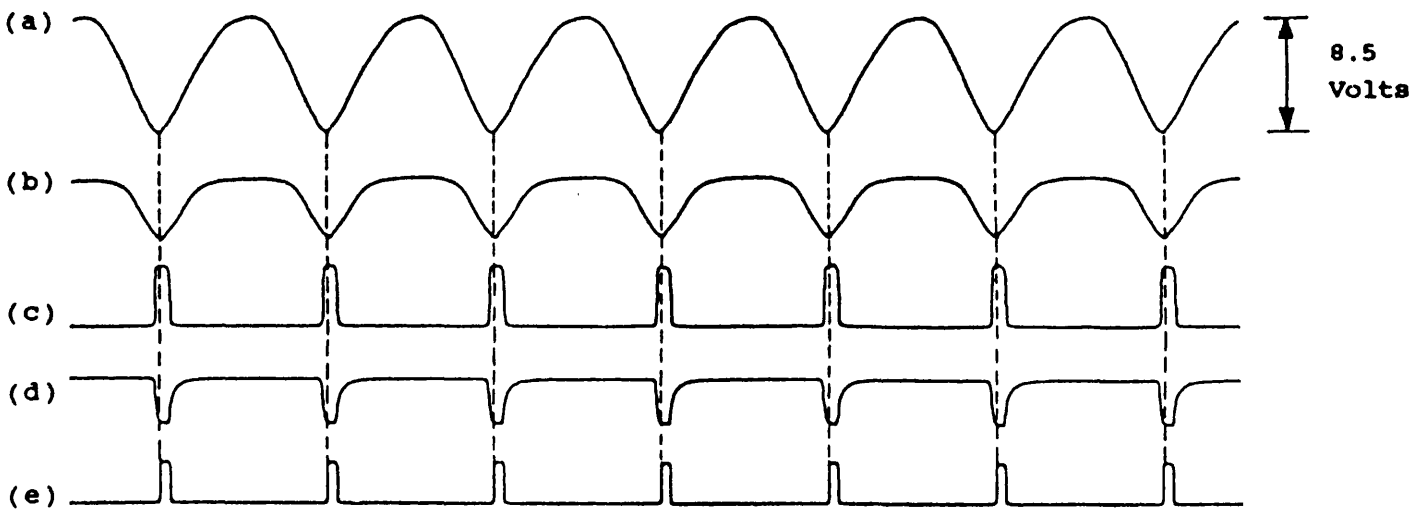

Fig. 6.3 Timing diagrams at various points in the zero-level detection circuit

(a) across the transformer secondary
(b) across the zener diode, BZX79C
(c) at the collector point of the transistor, BC108
(d) inverted signal across the capacitor 0.0068μf
(e) final output from the zero-level detector

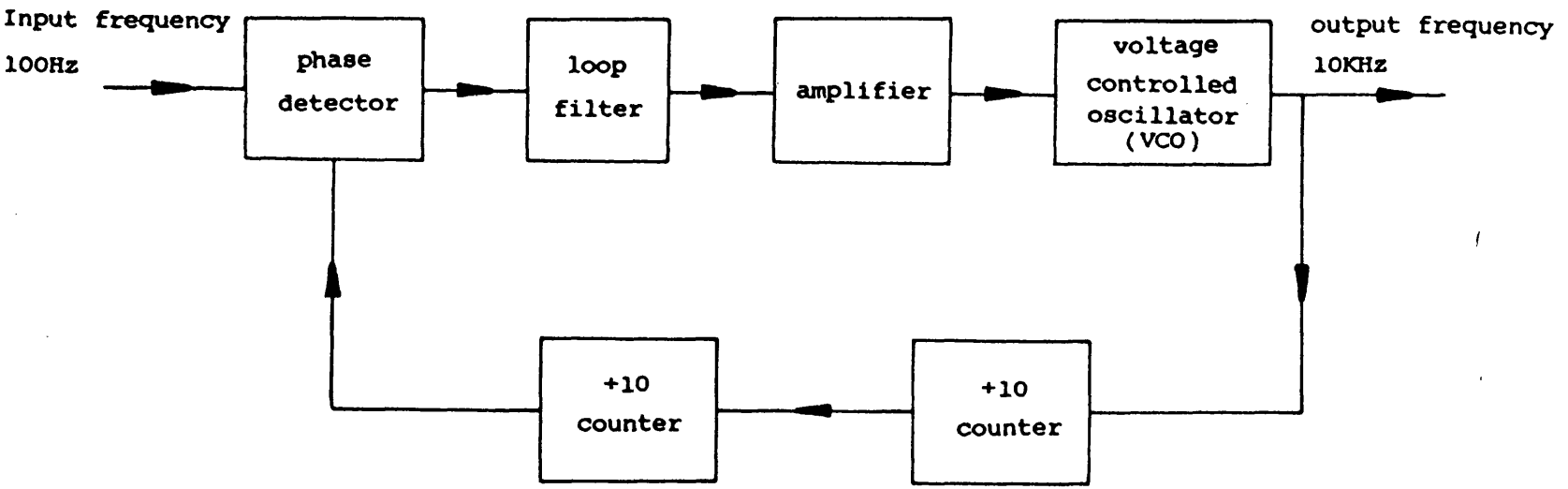

Fig. 6.4 Block diagram of frequency multiplier circuit
(timer, 555, is not included here)

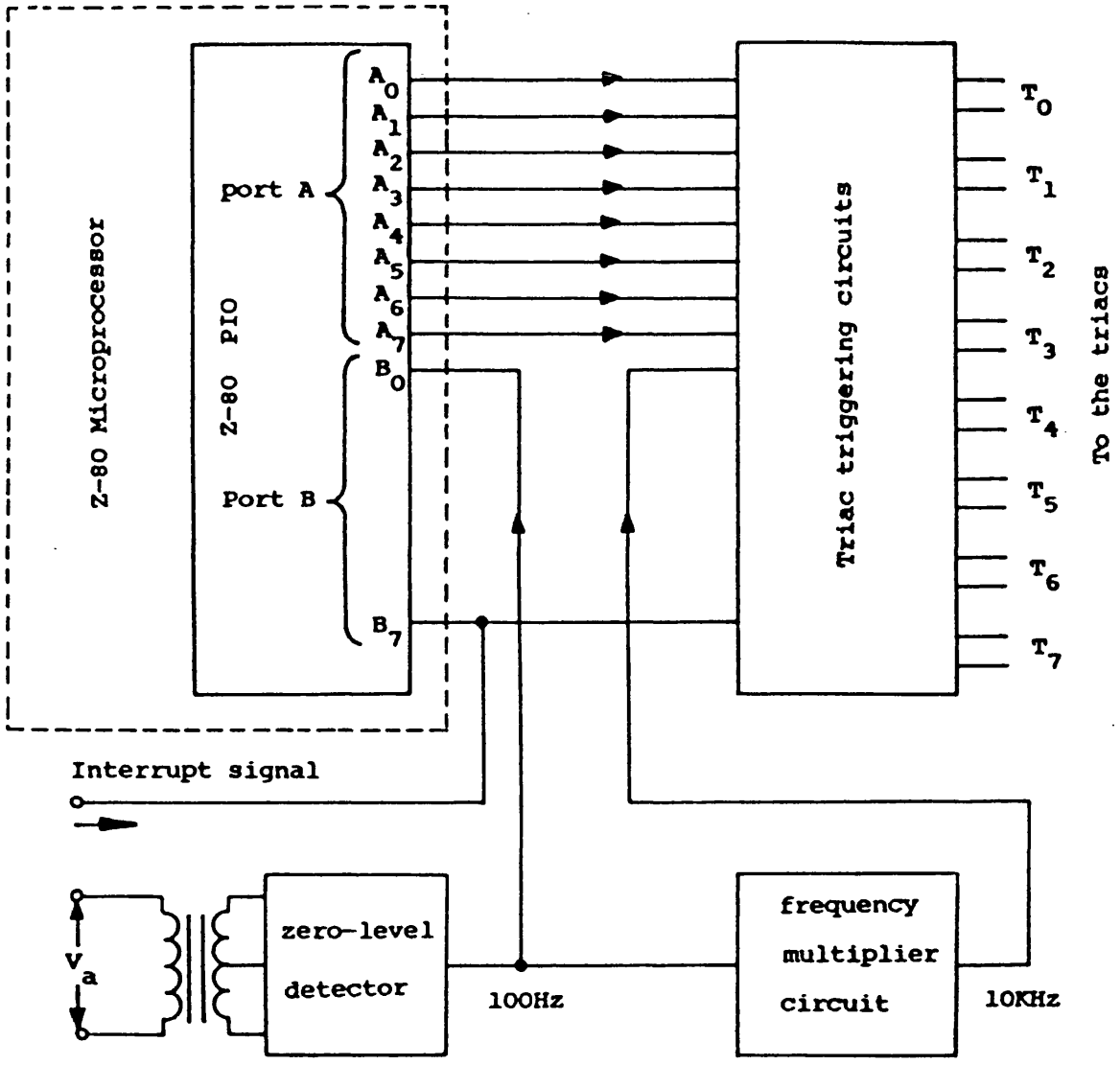

Fig. 6.5 Block diagram of the complete control system

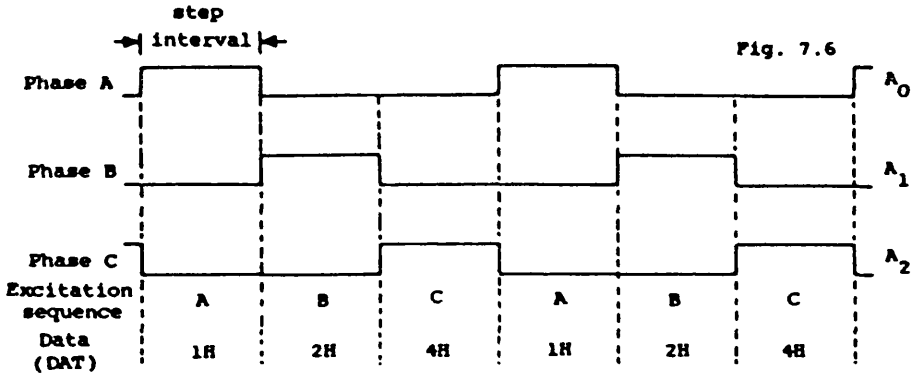

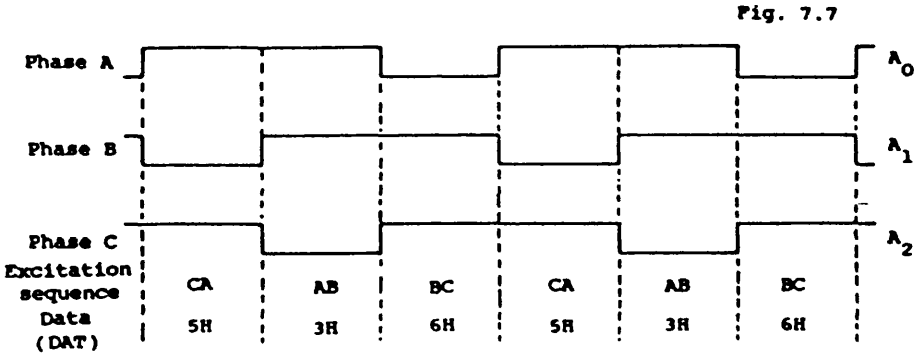

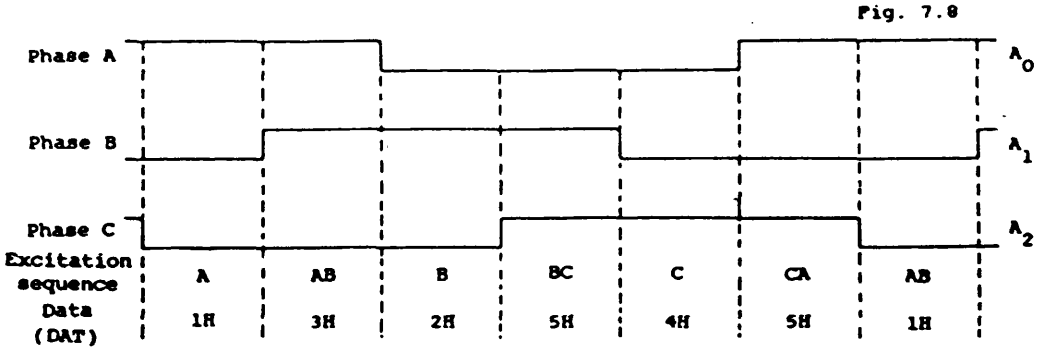

Fig. 6.6 Timing signals for one-phase-on operation

Fig. 6.7 Timing signals for two-phase-on operation

Fig. 6.8 Timing signals for half-stepping operation

Fig. 6.9 ALGORITHMS USED TO GENERATE THE SWITCHING SIGNALS

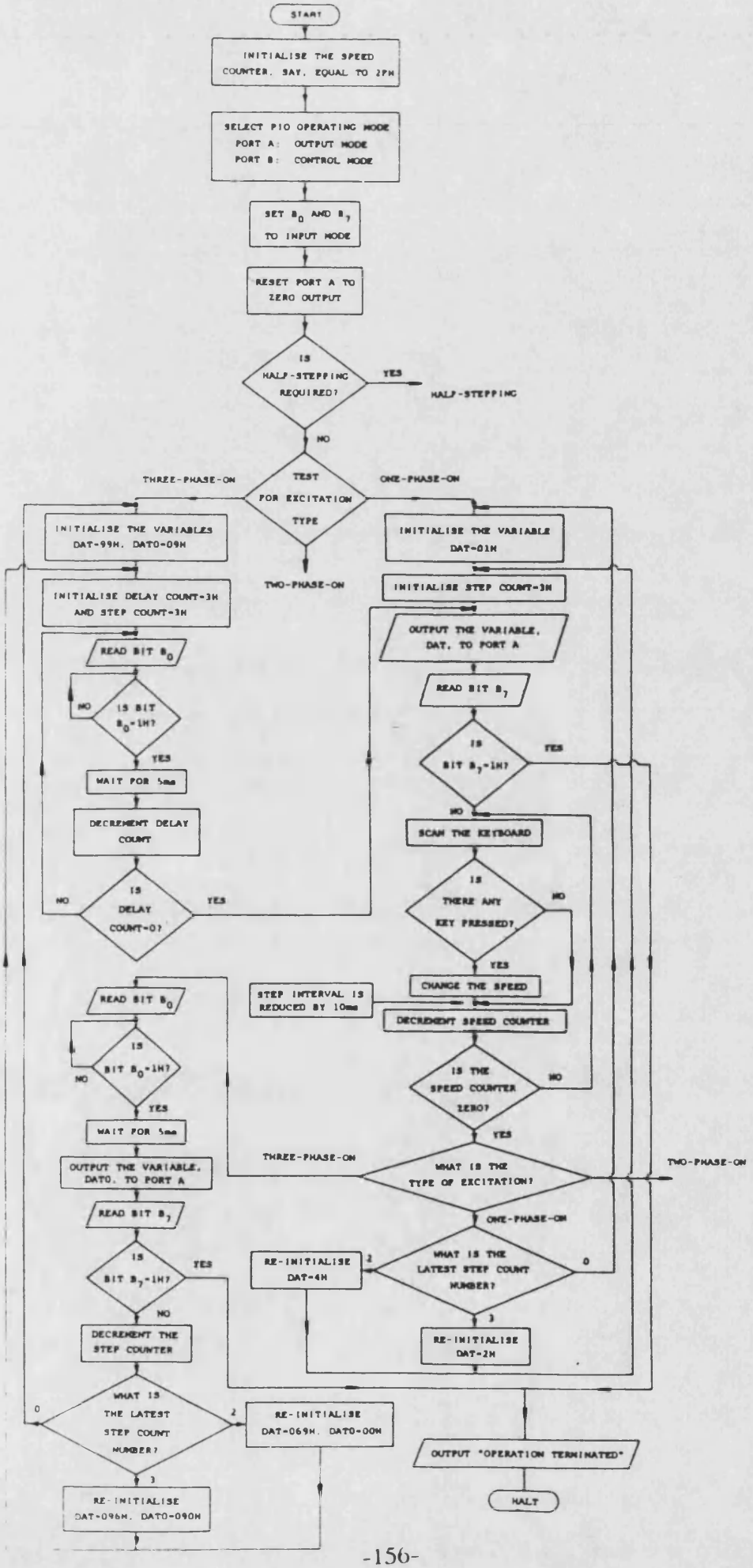

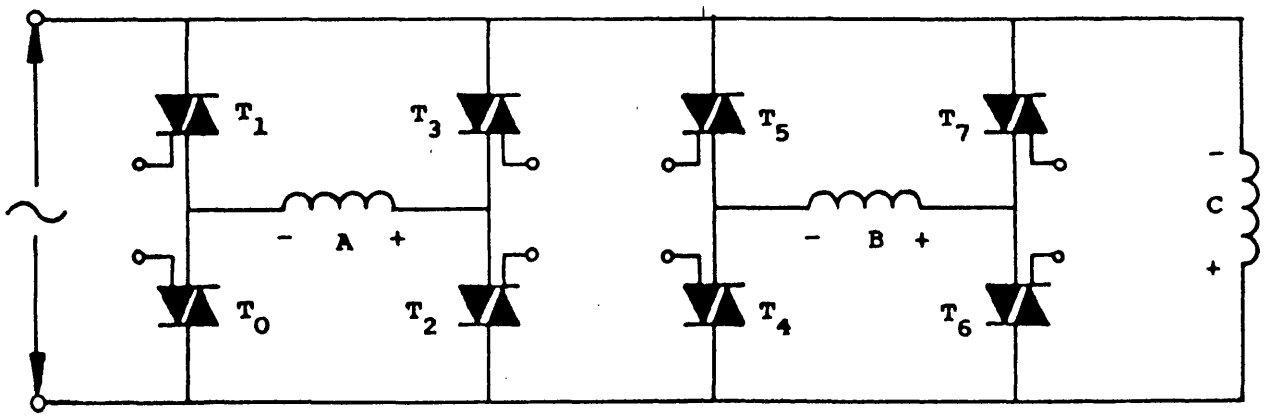

Fig. 6.10 Bridge connection of triacs for three-phase-on excitation

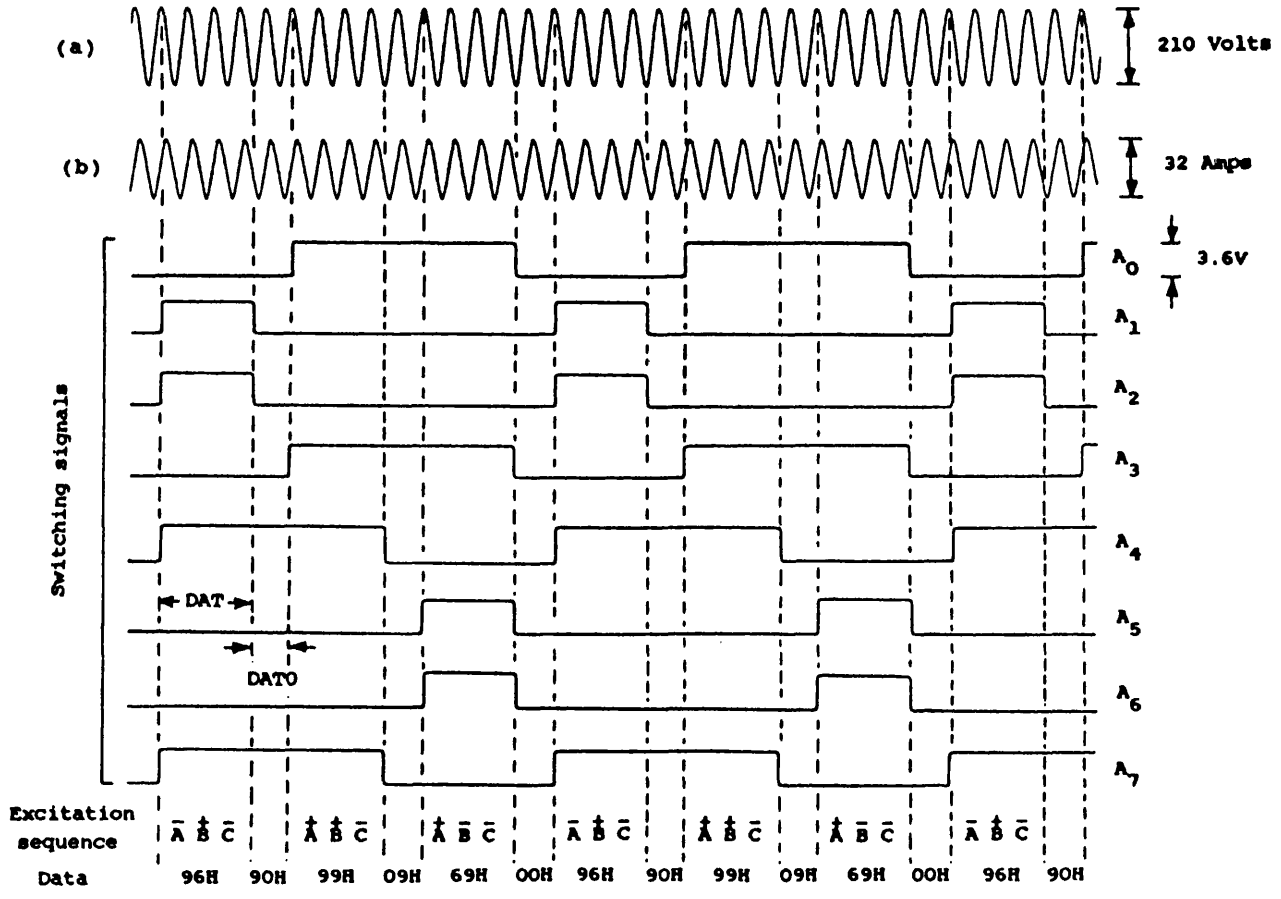

Fig. 6.11 Timing signals for three-phase-on excitation relative to: (a) the supply voltage and (b) the supply current

Fig. A.1(a)Connection diagram for open circuit test

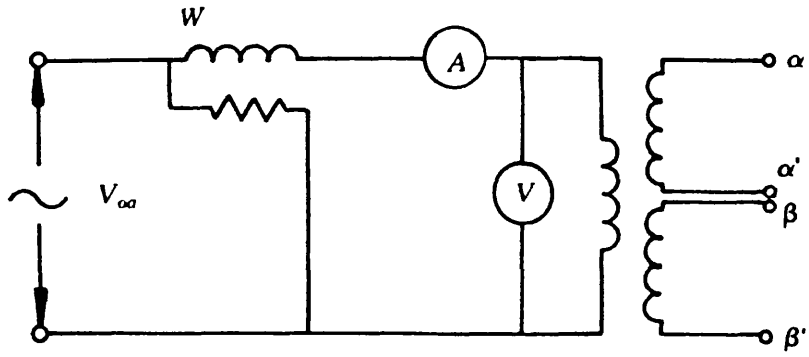

Fig. A.1(b)Equivalent circuit diagram for Fig. A.1(a)

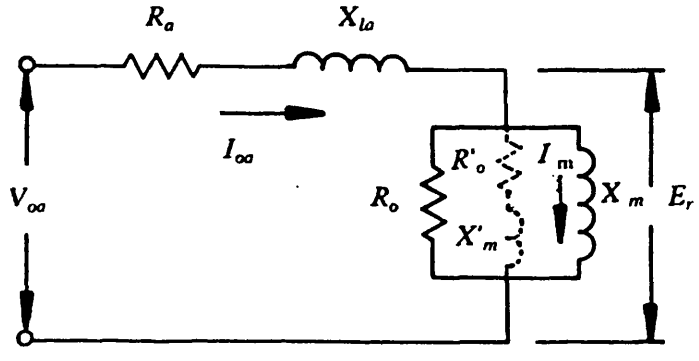

Fig. A.2(a) Connection diagram for short circuit test

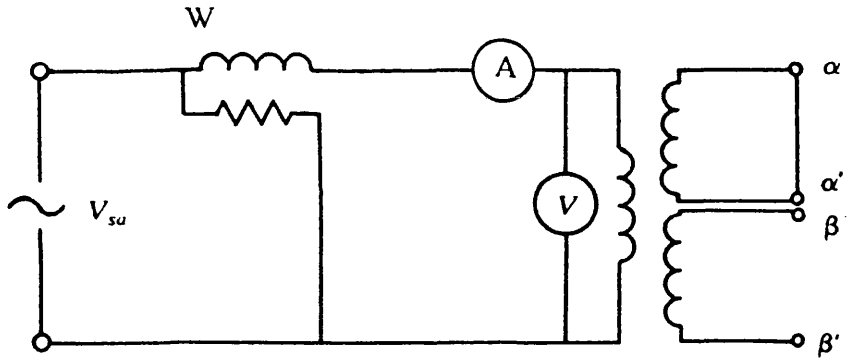

Fig. A.2(b) Equivalent circuit diagram for Fig. A.2(a)